

compass
one

PHASE B DOCUMENTATION

Released 08.06.2004



Preface

This book comprises the phase B documentation for the subsystem of the Compass-1 picosatellite. The work reflects the selection, comparison, trade-off and specification of the devices to be integrated into the specific subsystem in order to respond to the functionality requirements that evolved from the previous phase A study.

The overall time consumed by this project phase was about six month. Next to the detailed definition of each subsystem other things had to be accomplished as well. This includes the acquirement of equipment and tools, establishment of contacts to supplier and supporter, attendance of workshops and conferences, the homepage and much more.

As a result, the Compass-1 project additionally laid the way for such space research activities at the FH Aachen by providing a basic infrastructure and working environment to the students.

Rico Preisker

Oscar Moreno

Marco Hammer

Georg Kinzy

Jens Giesselmann

Robert Klotz

Ali Aydinlioglu

Sylwia Czernik

Cynthia Duda

Artur Scholz



2004-04-25

WBS410: Payload

Camera

Phase B: Detailed Definition

Author

Artur Scholz

FH Aachen, Germany



Scope

This paper documents the detailed definition of the camera payload for the COMPASS-1 spacecraft.

Contents

1. Hardware Definition	7
2. Software Definition	9
3. Budgets	9
3.1 Mass	9
3.2 Power Consumption.....	9
3.3 Volume.....	9
4. Conclusion.....	10
5. References	10

1. Hardware Definition

The camera module is defined as the payload and is the core item to fulfill the mission goal of capturing images from earth. The camera was defined very early in the project life cycle. The initial selection was to implement a commercially available C3188A device from Quasar Electronics [1], which has already been implemented into the “XI-IV” CubeSat and therefore proven its functionality in space conditions. In early meetings the whole project team came to the conclusion that a self-made construction of a camera module would be beyond our capabilities. This issue was raised because there are already lots more CMOS sensor devices on market that would top the C3188A features and also are less power consuming. Contacting Omnivision [2] (they manufacture the sensor chip on C3188A), we explained them our project and its intention as a technology demonstrator. We were told that the C3188A incorporates an Omnivision sensor of the 2nd generation and that this sensor family has already developed into the 4th generation. In addition the sensor is now offered as a complete camera module (OV7648FB Color CMOS VGA Camera Module, fig. 1.1), including a lens system and a flex cable.



Fig. 1.1: OV7648FB Camera Module

The module features:

- 326,688 pixels, VGA/QVGA format, 1/4" lens
- 10mm x 9mm x 6.89mm module size
- Flex cable connector
- 2.5V operation, low power dissipation
- I²C interface
- Function controls (Exposure control / Gamma / Gain / White balance / Color matrix / Color saturation / Hue control / Windowing)
- Operational: -10°C to 70°C

Its key specifications are shown in fig. 1.3.

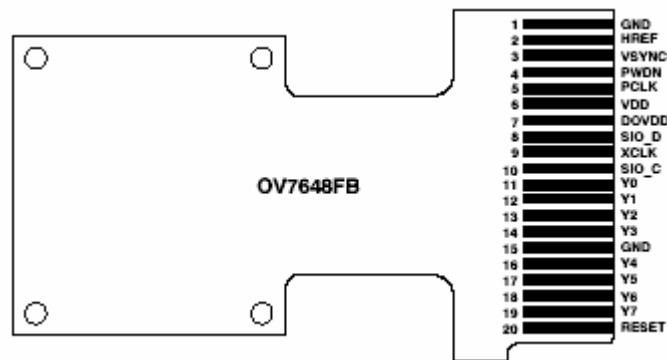


Fig. 1.2: Pinout diagram of OV7648FB

Array Size	VGA	640 x 480
	QVGA	320 x 240
Power Supply	Core	2.4V to 2.6V DC
	I/O	2.25V to 3.6V DC
Power Requirements	Active	40 mW
	Standby	25 μ W
Output Formats (8-bit)		<ul style="list-style-type: none"> • YUV/YCbCr 4:2:2 ITU-656 • Raw RGB Data
Lens Size		1/4"
Maximum Image Transfer Rate	VGA	30 fps
	QVGA	60 fps
Min. Illumination (3000K)	f1.2	< 1 lux
	f2.8	< 5 lux
S/N Ratio		46 dB (AGC off, Gamma=1)
Dynamic Range		> 48 dB (due to 8-bit ADC limitation) 62 dB for internal signal
Scan Mode		Progressive
Exposure Time		523 to 1 line period (at selected frame rate)
Gamma Correction		0.45/1.0
Pixel Size		5.6 μ m x 5.6 μ m
Dark Current		30 mV/s
Fixed Pattern Noise		< 0.03% of $V_{PEAK-TO-PEAK}$
Image Area		3.6 mm x 2.7 mm
Package Dimensions		10mm x 9mm x 6.89mm

Fig. 1.3: Key Specifications of OV7648FB

The camera has a small flex cable as indicated for input and output. Since the camera will be mounted on the lower side of the CubeSat (facing earth) another cable will be used to connect it to the main board. To do so, a small PCB is going to be engineered, on which a FHX connector from JST [3] is mounted as can be seen in fig. 1.4. Its pins are tracked to bigger pads, on which Teflon cables are soldered that refer the signals towards the main board. On side of the main board an adequate connector will be mounted.

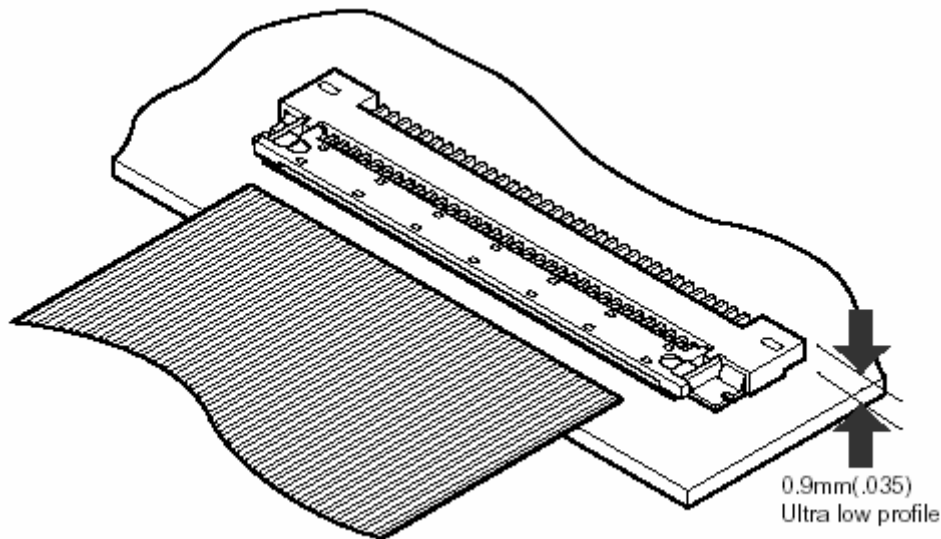


Fig. 1.4: FHX Connector

2. Software Definition

The chip integrates a various registers to allow total control of the image outcome. The settings are accessible via the I²C interface (SIO_C and SIO_D).

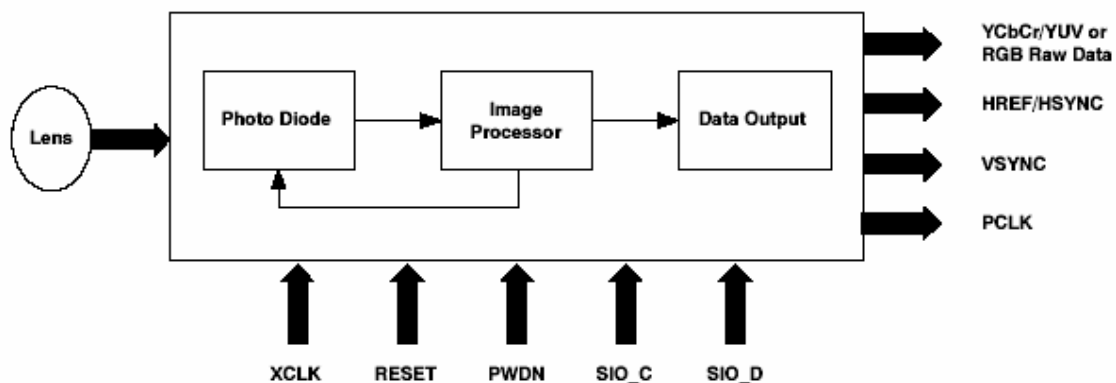


Fig. 2.1: Functional Block Diagram

3. Budgets

3.1 Mass

The mass for the camera module is below 5g, which is an excellent figure for a CubeSat payload.

3.2 Power Consumption

According to the datasheet the chip consumes 40mW when active. This is well inside the boundaries set in the previous phase.

3.3 Volume

The module is very small in size, about 9mm x 8mm x 7mm. This yields to a volume of 504mm³. The requirement was to stay below 40mm x 40mm x 20mm.

4. Conclusion

The payload camera module corresponds to the requirements and has the capability to fulfill the mission objectives. The interconnections and interfaces were established on a logical level and have to be translated onto physical level in the next phase. Careful and iterative testing of software and hardware will ensure a reliable system for the satellite.

5. References

- [1] www.quasarelectronics.com
- [2] www.ovt.com
- [3] www.jst.com



2004-05-28

WBS420: ADCS

Attitude Determination and Control System

**Phase B Documentation
Subsystem Definition**

Authors

Jens Giesselmann
(ADCS Subsystem Supervisor)

&

Ali Aydinlioglu
(ADCS Subsystem Engineer)

University of Applied Sciences Aachen, Germany



Scope

This paper documents the definition activities leading a sophisticated on-board navigation system for the 'Compass-1' spacecraft, i.e. the Attitude Determination and Control System (ADCS). This documentation is part of an overall subsystem development documentation. It is based on the results of the preceding preliminary design phase (Phase A) results and will be the reference for further development activities within the Compass-1 project. This Phase B document is meant to be a complete documentation of the definition effort, such that the need to refer to the preliminary documentation is avoided whenever possible.

This document is sectioned into three parts. They deal with the theoretical analysis, hardware definition and selection and flight software considerations as preparation for the following development phase (Phase C/D).

The first part constitutes a deeper analytical reflection on the spacecrafts dynamics, which have been discussed in the preliminary study to a shorter extend, and its implications for the further design of the ADCS. In the second part, the detailed definition of the system's hardware will be performed in a comprehensive manner. Whenever applicable, the hardware selection is evaluated on the basis of trade-offs and the critical comparison of components.

Contents

1.	Introduction	16
2.	The magnetic Control Law of Compass-1	17
2.1	The Challenge of magnetic Control	17
2.2	The Control Law	19
2.3	Slewer	21
2.4	Detumbler	21
2.5	Attitude Determination Problems	22
2.6	Selection of Reference Frames	23
3.	The Simulation Tool	25
3.1	Modeling the external environment	28
3.1.1	The Geomagnetic Field	28
3.1.2	The Gravity Gradient	30
3.1.3	Solar Pressure Torque	31
3.1.4	The Aerodynamic Torque	31
3.2	Simulation Objectives	32
4.	Hardware Interfaces	33
5.	The Magnetic Torquers	33
5.1	Design Constraints	33
5.2	Investigation of the Helmholtz coil configuration	34
5.3	Design Preliminaries	35
5.4	The Coil Driver	37
5.4.1	The H-Bridge (HB)	37
5.4.2	The Low Pass (LP)	38
5.4.3	The Current Sensor	38
6.	The GPS System	39
6.1	The Phoenix Receiver	39
6.1.1	Mechanical Specification	40
6.1.2	Electrical Specification	41
6.1.3	Antenna Interface	41

6.1.4	Interface Data Protocol.....	41
6.1.5	Environmental Characteristics	41
6.2	GPS Antenna.....	42
6.2.1	Product Comparison.....	42
7. The Magnetometer	45
8. The Sun Sensors	47
9. The Digital PCB Thermometer	50
10. The Controller Core of the ADCS	51
10.1	Microcontroller Unit (MCU)	51
10.2	Digital Signal Processor.....	55
10.2.1	Introduction	55
10.2.2	Component Selection	56
10.2.3	The DSP56300 Family.....	56
11. System Budget Estimation	59
11.1	Mass Budget.....	59
11.2	Power Budget.....	60
12. The ADCS Flight-Software	61
12.1	Modes of Operation	61
12.1.1	Boot procedure/Detumbling.....	61
12.1.2	Control Mode	63
12.1.3	Safe Mode	63
12.2	Communication between ADCS and CDHS	65
12.2.1	The I ² C Data bus	65
12.2.2	The Command Codes (CC).....	65
12.2.3	The Status Codes.....	66
13. Conclusions	67
14. Outlook on future development challenges	67
15. References	68

Abbreviations

ADCS	Attitude Determination and Control System
CC	Comand Code
CDHS	Command and Data Handling
CoM	Center of Mass
COTS	Commercial-off-the-Shelf
CPU	Central Processor Unit
DLR	Deutsches Zentrum für Luft- und Raumfahrt
DSP	Digital Signal Processor
DTU	Denmark Technical University
ECI	Earth Centered Inertial
EPS	Electrical Power System

GPS	Global Positioning System
HB	H-Bridge
IGRF	International Geomagnetic Reference Field
IIC	Inter-Integrated-Circuit
LEO	Low Earth Orbit
LP	Low Pass
LVLH	Local Vertical Local Horizontal
MCU	Microcontroller Unit
MIC	Microelectronics Institute
MOEMS	Micro-Opto-Electro-Mechanical System
PCB	Printed Circuit Board
SC	Status Code
STR	Structures and Mechanisms

Introduction

The Attitude Determination and Control System is a very demanding system in many ways. First of all, a mathematical concept has to be established. Then, the hardware is being built around a single mathematical equation, the control law. In no other subsystem design it becomes more obvious than in dynamics related spacecraft systems like the ADCS: the hardware is the carrier of the software, which is the theoretical concepts translated into a numerical solution. And the ADCS hardware truly is complex and diverse. But a diverse hardware does not only complicate all the associated hardware developments, it might also lead to infeasibility of the entire system. The system budgets are tight; the biggest enemy of the system design for a pico-satellite is the lack of sufficient electrical power.

During a precursor to the preliminary design review it has been deliberated how to reduce the system's complexity without compromising the stated subsystem mission requirements.

During this brainstorming session it became clear that there is no simplification justified in order to create an autonomous magnetic control system which ought to be the overall requirement of the design.

But apart from the technical obstacles, a different issue plays a significant role, dealing with the design environment of the project. Since this is a student project, timing is of the essence. The overall complexity of the system puts a remarkable pressure on the small ADCS group. Not all of the group members can commit their full time on the development. The system is planned to be finished (and launched) in the first half of 2005. Despite the fact that the ADCS is perhaps the most demanding system of all Compass-1 subsystems, differences between completion times must be kept minimal. These constraints lead to an important notion with regard to the system design: the system is designed to be clean and simple! No ‘fancy stuff’, no parallel main frame computation, no back-up of a back-up. The ever underlying question during the system definition must be: ‘What do we really need here, and how are we going to achieve it?’ There is always room for future improvement. For now, we want to demonstrate for the first time, that active magnetic control is within the realm of possibility on a pico-satellite spacecraft. No more, no less.

The magnetic Control Law of Compass-1

The Challenge of magnetic Control

In the preliminary system design of Compass-1 [1], it has been decided to implement a purely magnetic control onto the spacecraft bus. Hence, the magnetic torquer is the only actuating device for the purpose of attitude control of the satellite. Three flat coils are mounted orthogonally onto the outward panels of the cube. The orthogonal orientation of the individual coils enables to generate a nearly arbitrary magnetic dipole moment vector (control vector) in the spacecraft. This is achieved by invoking a current through the turns of the individual coils. Depending on the currents, three orthogonal vector components are contributed by the three coils.

$$\vec{m} = \begin{pmatrix} m_x \\ m_y \\ m_z \end{pmatrix}; \quad m_{x,y,z} = n_i \cdot I_i \cdot A_i, \quad i = 1,2,3 \quad (1)$$

The orientation of the vector is theoretically arbitrary, but the magnitude is not. It is restricted by the maximum current that is supplied to the coil driver and depends mostly on the inherent resistance of the coil.

The artificially generated control field interacts with the local geomagnetic field and produces a control torque. Simply speaking, the control vector will produce a torque that is directed in such a way that the control vector alligns itself with the local vector, very similar to a dampened compass needle (, the little brother of Compass-1). Mathematically, the produced control torque follows as

$$\vec{T}_m = \vec{m} \times \vec{B} \quad (2)$$

Hence, **the control torque is always perpendicular to the geomagnetic vector and the control dipole vector.**

The magnetic control of a spacecraft is complicated in nature. The reason for the difficulties lies in the cross product in equation 2. A magnetic control moment produced in the coils does not generate a torque, which is linearly dependent of the input to the torquer. This, however, is a basic assumption of the classical automatic control theory.

The basic feedback control scheme of figure 1 illustrates how the controller (for derivative and integral action being zero) generates a control signal as a linear function of the difference between the demanded variable value and the actual variable value (also called the error). This control signal (it may be a voltage for instance) is then translated into an actuator response, i.e. a torque. This actuator response then alters the plant's (e.g. a satellite) state, which is then again compared with the demanded state via the (negative) feedback loop. This simple but effective feedback loop is an example of a pitch control using reaction wheels for torque generation. Considering only the pitch axis, i.e. the principal y-axis, a control signal would drive the spin rate of the reaction wheel, which would react to the changing voltage input governed by its inert dynamical behavior. This behavior can be accurately modelled by means of Laplace transformed transfer functions, generating a torque output, which is ultimately (in the quiescent steady-state condition) a linear function of the control signal, independent of the current state of the spacecraft (e.g. pitch angle). And furthermore, the generated torque is a pure pitch torque. Under certain mathematical assumptions and to keep the example simple no other torque components are being produced.

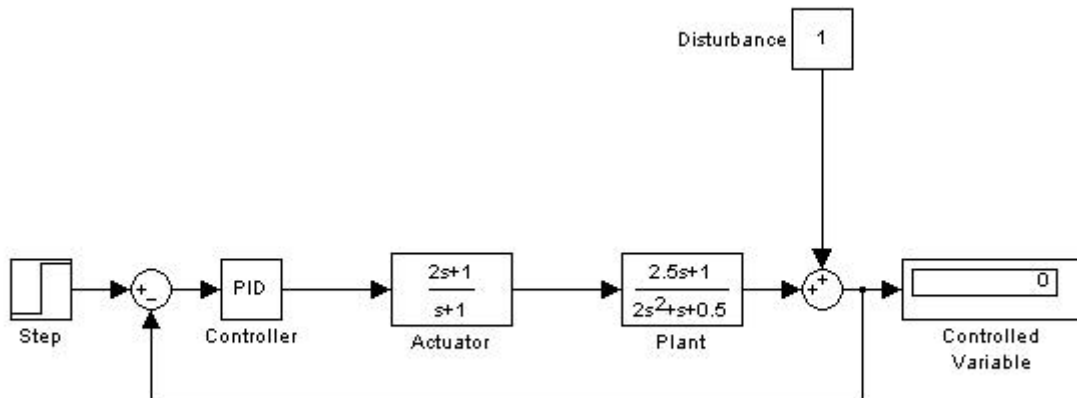


Figure 1: An example of a simple negative unity feedback control loop; note that this is not the actual control scheme of Compass-1

Coming back to the magnetic control of Compass-1, the situation is completely different, forcing the design to incorporate a very different control strategy. The torque that can be produced by the coils is strongly dependent of the current state of the vehicle, i.e. the produced torque level is dependent of the control signal and the current attitude, **and** it is never possible (apart from some rare exceptions) to generate a torque in a defined general direction (e.g. body-y-direction for pitch control).

This hypothesis can be discussed mathematically. Rewriting equation 2 in a different but equivalent form of a set of linear equations yields

$$\begin{pmatrix} T_x \\ T_y \\ T_z \end{pmatrix} = \begin{bmatrix} 0 & -m_z & m_y \\ m_z & 0 & -m_x \\ -m_y & m_x & 0 \end{bmatrix} \cdot \begin{pmatrix} B_x \\ B_y \\ B_z \end{pmatrix} \quad (3)$$

The determinant of the matrix is always zero, hence the matrix is singular. The set of linear equations cannot be generally solved for \mathbf{m} . I.e., there is no general solution for a set of magnetic moments of the three coils (m_x , m_y , m_z) to produce a defined torque with a given geomagnetic vector \mathbf{B} . This is a trivial observation when thinking about the nature of magnetic interaction. As stated before in equation 2 the resulting mechanical torque can **only** be perpendicular to the geomagnetic field vector. Trying to solve the set of equations for a general torque orientation violates this constraint. This is a serious problem for the magnetic control of a spacecraft.

Literature tends to tackle this problem by incorporating at least one reaction wheel on one of the three axes [2]. Due to the simplicity of the behavior of reaction wheels described above the modified set of equations suddenly does become solvable, hence the problem is resolved. However, this is not an option for Compass-1. Proposing the use of a reaction wheel at this stage of the system engineering would dramatically delay the progress of the development. As pointed out in the preliminary study [1] the state of miniaturization of such devices is not yet sufficiently matured. This would require the design team to develop a device of high complexity which would add a significant amount of risk (and cost) to the mission. As a side note, other CubeSat teams faced the same problems and initiated the development of a customized reaction wheel, which had to be stopped due to technical problems as the project proceeded.

The solution, the attitude control system of Compass-1 has to head for is a compromise solution which will decrease the efficiency of the control concept without violating the overall requirement of autonomous controllability.

The Control Law

The previous section outlined the physical limitations of magnetically controlled spacecrafts. This section will develop the control concept as a compromise between efficiency and system engineering considerations.

It has been comprehensively shown, that it is impossible to produce mechanical torque components parallel to the local geomagnetic field vector. For high efficiency control, however, it is often desirable to generate considerable torque components in this direction.

The vector in which the torque must be generated can be most easily described by the principal euler axis. The euler axis is the general axis within the spacecraft about which a rotation has to occur in order to turn the satellite from an actual attitude into a desired attitude. Any vector \mathbf{a} can be expressed in the satellite frame and in the target frame as \mathbf{a}_S and \mathbf{a}_T , respectively, in the following way:

$$\vec{a}_S = A_S \cdot \vec{a} \quad (4.a)$$

$$\vec{a}_T = A_T \cdot \vec{a} \quad (4.b)$$

Combining the two equations 4.a and 4.b yields

$$\vec{a}_S = A_S \cdot A_T^{-1} \cdot \vec{a}_T = A_S \cdot A_T^T \cdot \vec{a}_T = A_E \cdot \vec{a}_T \quad (5)$$

If the components of two noncollinear vectors \mathbf{a} are identical in both the satellite frame (S) and the target frame (T), then it is obvious that these frames coincide and that the satellite body axes have reached the desired target attitude in space. At this point the matrix A_E (called the direction cosine error matrix) becomes the unity matrix.

The principal euler axis can now be calculated as the (real) eigenvector associated with the eigenvalue $\lambda = 1$ of the error matrix A_E . Note that every error matrix has at least one eigenvalue $\lambda = 1$.

Still, the principal euler axis of rotation, now known, does not lie within the plane perpendicular to the geomagnetic field vector \mathbf{B} . Here is where the compromise is introduced to the control concept. Since it is not possible to generate the torque about the euler axis \mathbf{a} , it must be transformed in such a way, that the torque can be produced about the new axis of rotation \mathbf{a}_\perp , which is then perpendicular to the plane defined by the normal vector \mathbf{B} . What has to be done, is to project the principal euler axis onto the \mathbf{B} plane. First, the vector is being projected onto \mathbf{B} to form a new vector \mathbf{a}' :

$$\vec{a}' = \frac{(\vec{B} \cdot \vec{a})}{|\vec{B}|^2} \cdot \vec{B} \quad (6)$$

To get the projection onto the \mathbf{B} plane, the vector component in the direction of \mathbf{B} (i.e. vector \mathbf{a}') must be subtracted from the euler axis as in equation 7.

$$\vec{a}_\perp = \vec{a} - \vec{a}' = \vec{a} - \frac{(\vec{B} \cdot \vec{a})}{|\vec{B}|^2} \cdot \vec{B} \quad (7)$$

This vector has one very handy property: it is perpendicular to \mathbf{B} . The magnetic moment vector \mathbf{m} generates a torque \mathbf{T} that is aligned with \mathbf{a}_\perp , as long as \mathbf{m} is set to be perpendicular to \mathbf{B} . That means that all vectors are perpendicular to each other and the cross product becomes commutative. Due to the described constraint of $\mathbf{a}_\perp = \mathbf{T}$, the magnetic moment \mathbf{m} can be calculated as

$$\lambda \cdot \vec{m} = \vec{a}_\perp \times \vec{B} = \vec{T} \times \vec{B}, \quad \lambda \in R_0 \quad (8)$$

Equation 8 describes how the \mathbf{m} vector must be oriented in order to create a rotation which is as close to the desired euler rotation as possible. The control action, hence the actual control law is governed by the principal euler angle α , i.e. the angle by which the spacecraft has to be rotated about the principal euler axis in order to achieve the desired attitude. The principal euler angle can be calculated as

$$\alpha = \cos^{-1} \left(\frac{1}{2} \cdot \left(\sum_{i=1}^3 a_{Eii} - 1 \right) \right) \quad (9)$$

Unfortunately this equation does only allow for a computation of the absolute value of the euler angle as can be seen by the inverse cosine function in equation 9. A functional control law, however, requires the knowledge of the direction in which to rotate the satellite. This information is not carried by the euler axis either. Up to date, finding a closed form mathematical solution is an unresolved problem yet. However, numerical methods have been successfully applied within the simulation software tool described in the following section.

The control law handles the principal euler angle only, i.e. the control action is based on the principle euler angle as opposed to a set of three attitude euler angles. This reduces the

computational burden. The controller will incorporate a constant gain and a derivative gain only, such that the final non-linear control law can be written as

$$\vec{m} = \left(K_p \cdot \alpha + K_D \cdot \frac{d\alpha}{dt} \right) \cdot (\vec{a}_\perp \times \vec{B}) \quad (10)$$

As mentioned before, this is a constrained control approach which allows for control about an axis which can be located on a plane only. This implies that there is always one axis within the spacecraft which cannot be controlled at a given time. This would be a dramatic drawback if the geomagnetic field was a static entity. Fortunately it is not. During one polar orbit, the \mathbf{B} vector flips twice, hence constantly altering the uncontrolled axis over time. Since the control action will be performed over a prolonged period of time the overall controllability is maintained.

The above description of the attitude control concept is particularly useful for large attitude maneuvers but can be applied to small corrections as well. Special attention, however, has to be paid to the computational burden of the control algorithm and possible singularities. Simplifications like the non-singularity quaternion description have to be investigated and implemented into the final flight software.

Slewer

The slow control law is not intended to differ from that of the regular control mode. The way the control law is designed it is capable of handling slew maneuvers as well as keeping the spacecraft on-station during ADCS normal mode.

Detumbler

The control law of the detumbler differs from the normal and slew mode control law. This is due to the fact, that the detumbling is a critical phase of the mission. If the spacecraft cannot gain control, all other mission objectives, i.e. establishment of a communication link and controlled image taking, will be severely impacted. No risks should be taken by incorporating high-end control algorithms, which might be subject to failure. However, of greater concern than the complexity of the control action is the power demand during the phase of detumbling. The detumbler should work with minimal sensor requirements and little computational overhead such that a large portion of available electrical power (1000mW peak) can be routed to the actuators. It is reasonable to expect that the detumbling phase is the most torque demanding phase of the mission.

The ultimate goal of the detumbler is to decrease the rotational kinetic energy of the satellite from a maximum expected energy to a more moderate rotational state which can then be controlled by the more accurate normal control law. The (rotational) kinetic energy of a rigid body is defined as

$$E_{rot} = \vec{\omega}^T [I] \vec{\omega} \quad (11)$$

The maximum expected tumbling rate is

$$\vec{\omega}_{\max} = \begin{pmatrix} 0.1 \\ 0.1 \\ 0.1 \end{pmatrix} \text{rad} / \text{s}$$

The detumble algorithm shown in detail in the following has been successfully implemented on many spacecraft before Compass-1. The detumbler requires the information acquired by the magnetometers only! All other sensors are off-line during detumbling.

$$\text{Decreasing the kinetic energy during detumbling means } \vec{\omega}^T \cdot \vec{T}_c < 0 \quad (12)$$

$$\text{The control torque from the magnetic interaction is } \vec{T}_c = \vec{m} \times \vec{B}, \quad (13)$$

$$\text{such that condition 12 equivalently means } \vec{\omega}^T \cdot (\vec{m} \times \vec{B}) < 0. \quad (14)$$

With the genral rules cross product manipulation

$$\vec{a}^T \cdot (\vec{b} \times \vec{c}) = \vec{c}^T \cdot (\vec{a} \times \vec{b}) \text{ and } \vec{a} \times \vec{b} = -(\vec{b} \times \vec{a}) \quad (15)$$

the condition can be rewritten as

$$-\vec{\omega}^T (\vec{B} \times \vec{m}) < 0 \text{ or } \vec{m}^T \cdot (\vec{\omega} \times \vec{B}) < 0 \quad (16)$$

This inequity can be solved by expanding equation 16 with a scalar gain C

$$\vec{m} = C \cdot (\vec{\omega} \times \vec{B}) \quad (17)$$

With the main assumption of the change of the magnetic field vector being a result of the rotation of the spacecraft only, it finally becomes the detumbling control law

$$\vec{m} = C \cdot \dot{\vec{B}}. \quad (18)$$

This control law requires the measurement and derivative of the magnetic field vector only. Detumbling is considered to be finished when the rate of change of the magnetic field is below a certain threshold value for an extended period of time. This is the abort condition which will be implemented in the flight software.

Attitude Determination Problems

The normal control algorithm as well as the slew procedure require the unambiguous attitude determination from two linearly independent measured base and computed reference vectors. These vectors are obtained from the measurement of the local geomagnetic field and the sun direction using magnetometers and sun sensors and the computation of a reference geomagnetic vector and sun vector in the local frame of reference. Apart from hardware/software malfunctions, there are several situations in which the determination of the actual attitude is impossible. These are:

1. the sun is obstructed by either the satellite body or the Earth
2. the sun is located in the ‘dead zone’ of the detector configuration
3. the measured base vectors are (near-)collinear
4. the reference vectors are (near-)collinear

The first point addresses the effect of temporary obstruction of the line-of-sight from the sun sensors to the sun. In other words, the invisibility of the sun for the sensors. Due to the configuration of the sensors (see hardware section for details) a body-induced self-obstruction can be excluded. But the obstruction due to the Earth is not the least negligible. The shadow conditions the spacecraft is subject to are called *umbra* and *penumbra*. According to the information from the TCS group, the analytical calculation of the time frames for each conditions yields 60.52min solar (63%) and 35.38min umbra (34%) including a few seconds of penumbra in between. There is no need to be more specific; the exact solar/umbra fraction depends on the exact orbital characteristics and will change as the mission proceeds. But the irregular change of solar conditions raises the question of how the ADCS operation will cope with this problem. It is obvious that with respect to a highly autonomous system operation the ADCS must detect an umbra situation in-situ without any additional external information. At this stage, it seems most reasonable to achieve that with the sun sensors. How exactly the sensor will behave under the lack of a high-magnitude light source cannot be easily predicted (due to the specific sensor principle) but will be one of the objectives during the sun sensor component level test in phase C/D.

Another scenario in which the sun vector is not determinable is when the sun is currently located in the ‘dead zone’ of the sensors. The dead zone will be discussed in a later section.

If the two measured vectors, i.e. magnetic field vector and sun vector, are (near-) collinear, the attitude cannot be determined unambiguously, hence the control law cannot perform. Although this issue must be taken into consideration during the software design, this will not state a huge problem for the system operation. The vectors will eventually (after a few minutes the most) become linearly independent again. The emerging software requirement is to detect possible numerical over-/underflows, before initiating further parts of the algorithm. The same is true for the last point of the above list.

Selection of Reference Frames

The frames of reference have been selected in consistency with literature sources to avoid confusion. In total four frames are defined for the purpose of attitude parametrization. These frames are:

- Earth Centered Inertial Frame (ECI, J2000)
- Orbital/Local Frame (LVLH)
- Body Frame
- Principal Axes Frame

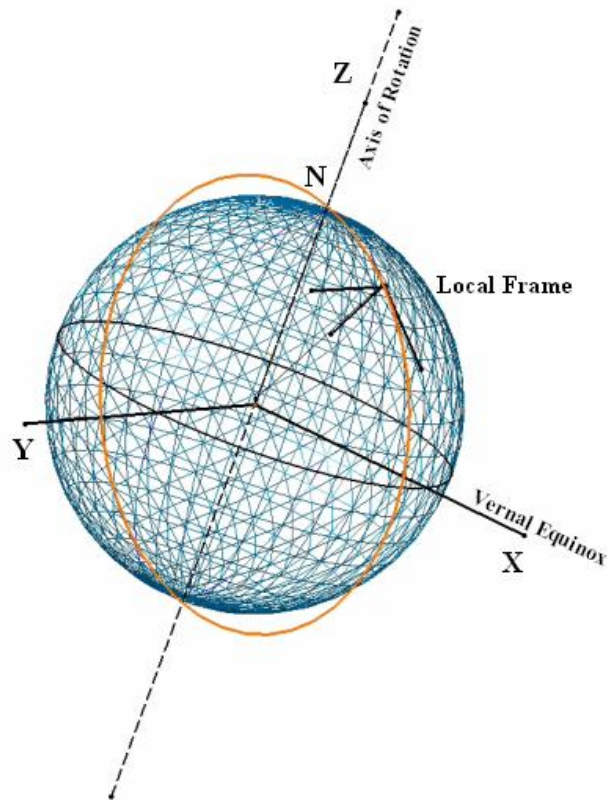


Figure 2: The frames of reference: The ECI (Earth Centered Inertial Frame, cartesian) with the local frame

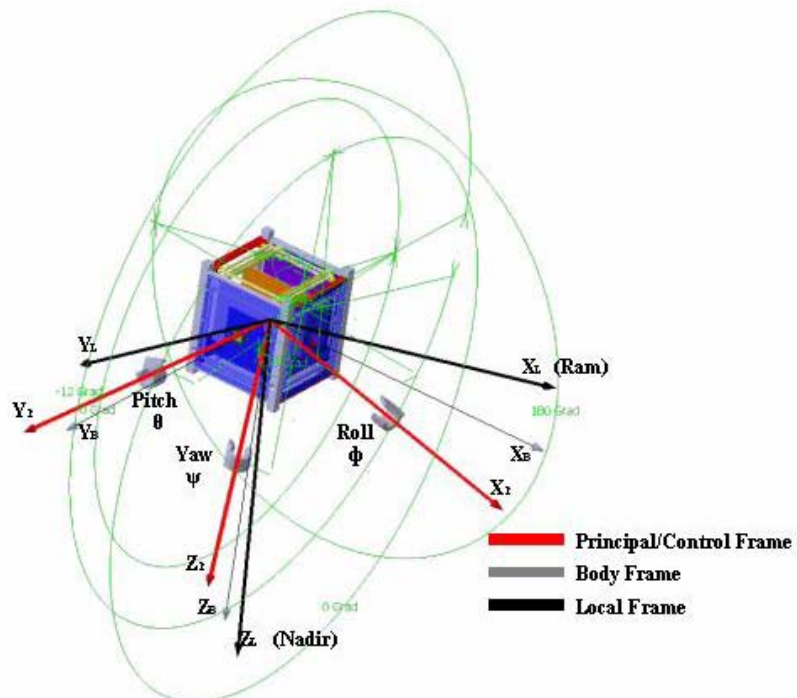


Figure 3: The frames of reference: The principal frame and the body frame and their relation to the local frame; displayed euler angle directions are positive

Earth Centered Inertial Frame (ECI). The ECI Frame (sometimes referred to as the J2000 frame) is an inertial frame originating in the Earth's center of mass. The x-axis points towards

the vernal equinox (2000), the z-axis passes through the geographic north pole and the y-axis completes the right-hand orthogonal frame of reference.

Geodetic Frame (Lat/Lon). The geodetic frame is a non-inertial frame fixed to the Earth's rotation. Also, the coordinates are spherical; a location described in the geodetic frame is expressed by 2 angles and a radius distance from the Earth's center of mass. The angles are usually referred to as latitude and longitude, the radius often given in terms of an altitude above the Earth's surface.

Orbital Frame (LVLH). The Local Vertical Local Horizontal (LVLH) or Orbital Frame or Local Frame defines a right-hand orthogonal frame with its origin in the spacecraft's center of mass (CoM). The z-axis points towards the Earth's CoM, the y-axis is parallel to the normal of the orbital plane and the x-axis is codirectional with the satellite's vector of velocity.

Body Frame. The axes of the Body Frame are aligned with the normals of the satellite's side panels. They coincide in the body's geometrical center.

Principal axes frame. The principal axes (of inertia) can be found by linear transformation starting from the body frame. The angles of rotation into this frame are iteratively updated by the structures subsystem as configurational changes are performed. In this stage of analysis, the body frame and the principal frame are considered to be identical!

The Simulation Tool

For reasons of design flexibility it has been decided to develop a comprehensive attitude simulation tool in the Matlab/Simulink environment tailored to the analysis demands of the ADCS on Compass-1. This section shall not go into great detail of the various programming issues faced during the tool development. A detailed documentation can be found in reference [3]. However, some features of the tool should not remain unmentioned. In particular, the enhancements of the analytical means of the preliminary phase and the definition phase should be noted. Furthermore this section states the assumptions made in the analysis. Since the quality of an investigation of a system is always limited by the assumptions made, considerable effort has been spent to decrease the level of deviations from the reality whenever reasonable.

To maintain a systematic approach in developing the required software several functional modules were defined and integrated into a single complete software solution step by step.

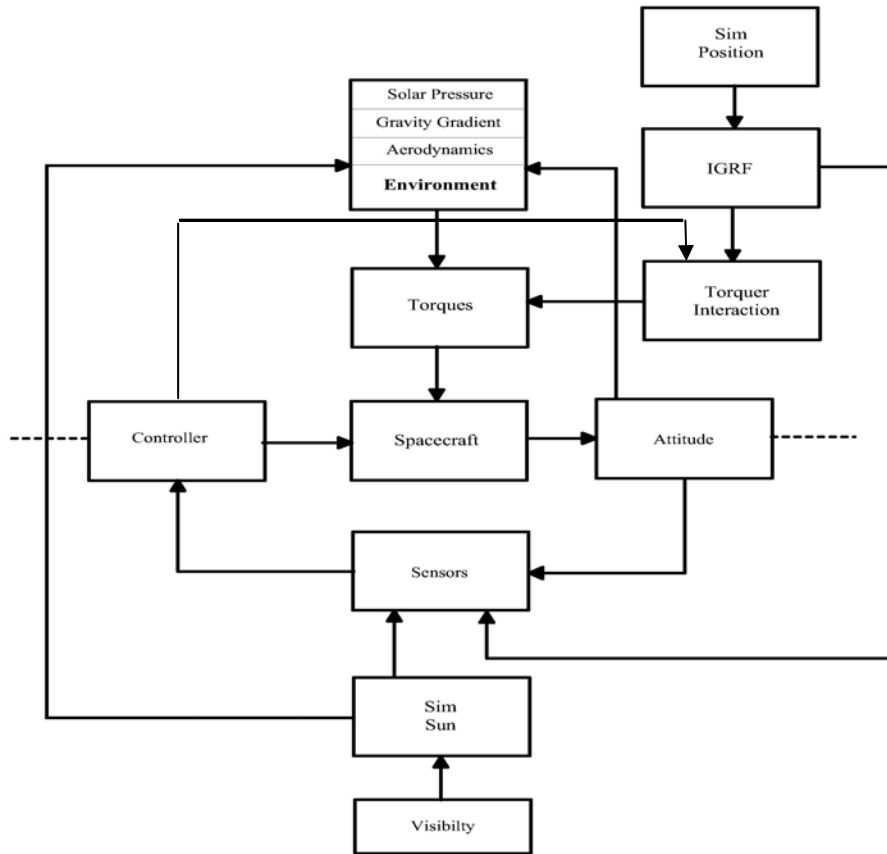


Figure 4: The functional Layout of the Simulation Tool

The Layout can be divided into two categories of blocks: external physical environment and internal states. The external environment part is comprised of the position and visibility of the sun ('SimSun'), the spacecraft position ('SimPosition'), the international geomagnetic reference field ('IGRF'), and the disturbance blocks ('Environment'). All these blocks model the external physical situation, the satellite will be subject to. In other words, these blocks span the 'virtual reality' of the satellite. The internal blocks are the 'Controller' with its control law implementation, the 'Spacecraft' containing the equations of motion, the 'Attitude', describing the state of the spacecraft, the 'Torquer Interaction', which constitutes the most important interface between internal and external states, and, besides the Controller the important block for translation into flight software, the 'Sensors'. This block is supposed to create a projection of the virtual reality spanned by the external blocks and 'tell' the virtual satellite its current state. However, the Sensors block is not subject of the software development in Phase B. For analysis purposes the exact process of attitude determination is not crucial. The program runs under the assumption that the measured attitude equals that of the current attitude. In reality this assumption is not completely valid, since the incorporated sensors measure their observables (position, local geomagnetic field and sun vector) within a certain range of uncertainty. However, it seems unlikely that this error has a catastrophic impact on the attitude stability which is the subject of this analysis section. For the advanced development of the system the code shall be extended by the exact attitude determination algorithms in order to enable the deviation from the initial analysis and, most of all, to serve as a guideline for the flight-software development since the procedures of the Sensor block will closely match the required features of the flight software.

During the development of the simulation tool special attention has been paid to the environmental block. The objective was to create a block with the highest feasible degree of

realism. All environmental influences that have an impact on the attitude have been carefully modeled, except for the magnetic disturbance torque, i.e. the torque generated by interaction of the residual electromagnetic dipole of the spacecraft and the geomagnetic field. This influence is difficult to model since the net magnetic dipole of the spacecraft under nominal conditions (while the ADCS is off-line) cannot be determined until integration and testing of the complete system is finished. Thus, every assumption made about the passive magnetic properties of the satellite may potentially negate the validity of the analysis. Ignoring the magnetic disturbance on the other hand will not have a great impact on stability since the magnetic disturbance level is expected to be extremely low. Note, that this statement is not valid for the control mode (while the ADCS is active), since the magnetic interaction is the dedicated control mechanism with magnetic dipole moments much greater than the residual moments.

Considerable effort was put into the modeling of the geomagnetic reference field. The selected geomagnetic reference data is the International Geomagnetic Reference Field (IGRF2000) in accordance with the ECSS standards [4]. The geomagnetic field has been computed for a reference orbit altitude of 600 km to a maximum obtainable accuracy (degree and order 10). More information about the simulation of the disturbance torques can be found in the section *Modeling the external environment*.

The ‘Spacecraft’ block contains a model of the dynamical behavior of Compass-1. The dynamics of a spacecraft can be described by the following differential equations of motion:

$$\begin{aligned}
 M_x &= I_x \dot{\omega}_x + \omega_y \omega_z (I_z - I_y) \\
 M_y &= I_y \dot{\omega}_y + \omega_x \omega_z (I_x - I_z) \\
 M_z &= I_z \dot{\omega}_z + \omega_x \omega_y (I_y - I_x)
 \end{aligned} \tag{19}$$

These equations are non-linear and coupled but they can be de-coupled under the assumption that the expected rotational rates $\omega_x, \omega_y, \omega_z \ll 1$, such that the decoupled EoMs can be written as

$${}^c \vec{T} = [I] \cdot \vec{\ddot{\theta}}, \tag{20}$$

with the torque vector expressed in the control frame, spanned by the orthogonal principal axes, and the vector of the three independent euler angles θ (pitch), ϕ (roll) and ψ (yaw).

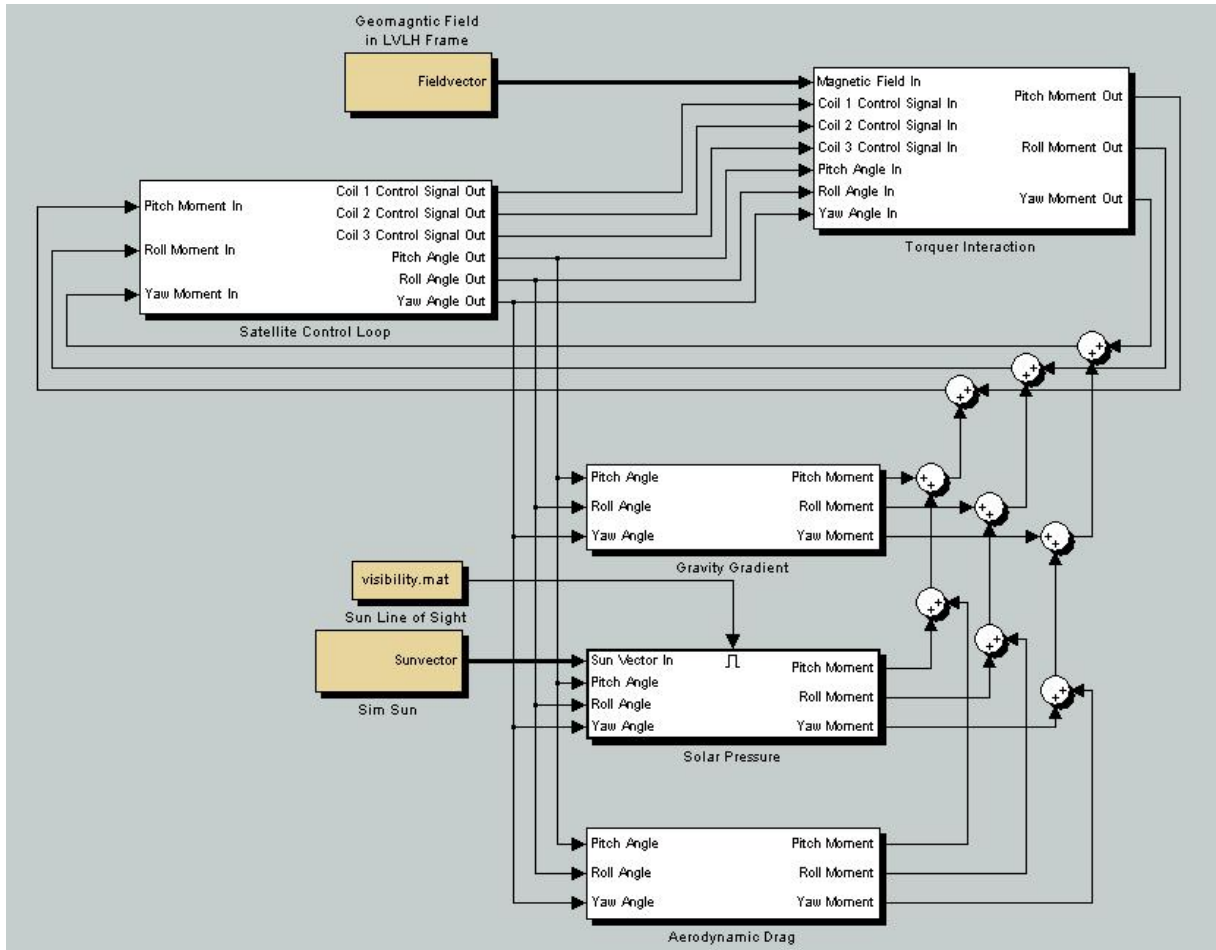


Figure 5: Top-Level Overview of the Simulink® simulation code

Modeling the external environment

For the preliminary study of phase A it was sufficient to estimate the torque levels the spacecraft will encounter in a worst-case scenario. For a numerical analysis, however, it is necessary to model the environment the satellite will be subjected to with the greatest feasible degree of realism.

The Geomagnetic Field

This equation (21) describes a coarse approximation of the absolute value of the geomagnetic field vector as a function of the magnetic latitude λ as it would be valid for an ideal dipole field.

$$B = MR^{-3} \sqrt{1 + 3 \sin^2 \lambda} \quad (21)$$

The simulation works with data that has been generated according to the following algorithm to account for the actual multi-pole field.

$$\vec{B} = -\nabla U \quad (22)$$

$$U = a \cdot \sum_{n=1}^k \left[\left(\frac{a}{R} \right)^{n+1} \sum_{m=0}^n [g_n^m \cos(m\phi) + h_n^m \sin(m\phi)] P_n^m(\cos\theta) \right] \quad (23)$$

This is the spherical harmonics expansion of the geomagnetic scalar potential field. The gradient of the field is closely related to the spatial magnetic field vector (the same theory holds for the gravitational potential field with respect to the force). In the equation, R, ϕ and θ describe the position in the spherical coordinate frame. ‘g’ and ‘h’ are the model coefficients and P are the schmidt normalized associated Legendre functions. The following figure 6 shows the solution of the absolute magnetic field strength for a constant altitude of 600 km.

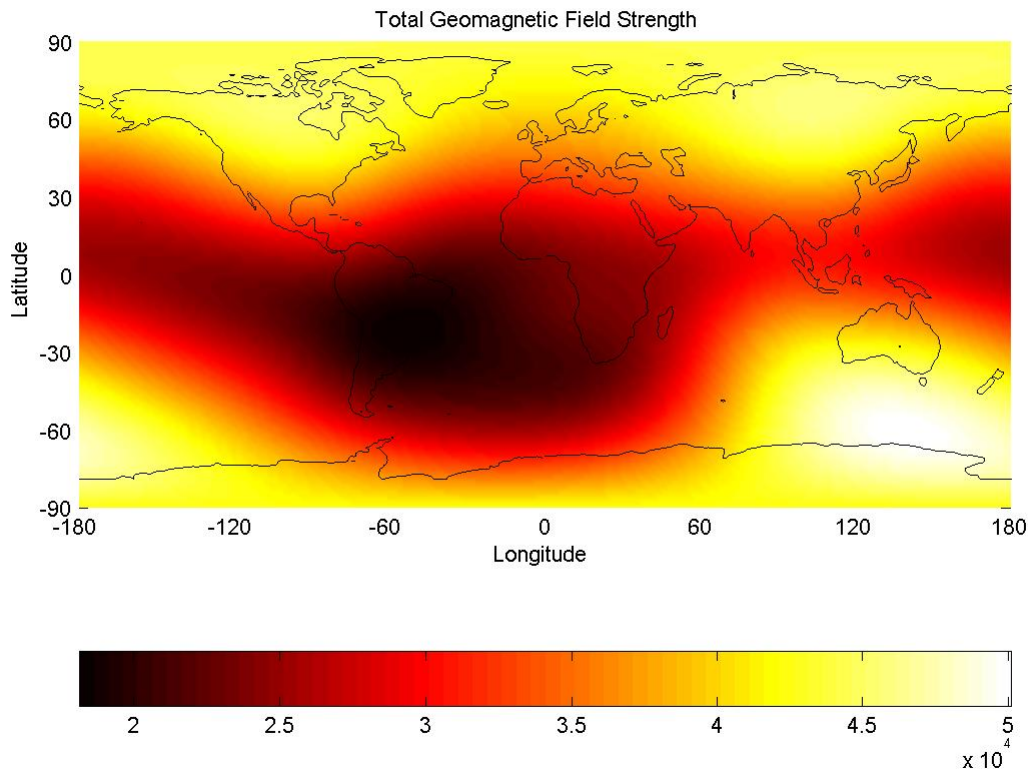


Figure 6: Total geomagnetic field strength in nT for a reference altitude of 600 km; computed using the complete IGRF2000 model consisting of 120 coefficients in total

As the satellite moves on its orbit (groundtrack shown in figure 7), it passes regions of different geomagnetic field intensity as well as different field gradients. The magnitude of the field vector ranges between 19000nT and 50000nT.



Figure 7: Ground track of Compass-1 for the reference orbit. Computed with STK's J4 propagator; (t=0 to 86400 s)

The described model of the geomagnetic field constitutes an interface between the simulation software and the flight software, since this model will also be implemented on the controller of the ADCS. In the development phase it has to be determined which effect the reduction of the number of coefficients will have on the model accuracy. A reduction of the coefficients is desirable in order to decrease the computational overhead of the algorithm. A different approach could be the pre-computation of the vector components as a function of longitude, latitude and altitude. However, while decreasing the computational demands, this would require significant memory space. Three 3D arrays would be required at least 300,000 float values to be stored in memory.

The Gravity Gradient

Equation 24 has been used for the estimation of disturbance torque resulting from the gravity gradient only. It does not contain any information about the direction of the torque. It is obvious that the gravity gradient torque is a function of the deviation angle θ . Since this angle could not be known in the preliminary analysis, a maximum (worst case) torque was assumed.

$$T_{GG} = \frac{3\mu}{2R^3} \cdot |I_{zz} - X| \cdot \sin(2\Theta) \begin{cases} I_{yy} \leq I_{xx}: X = I_{yy} \\ I_{yy} \geq I_{xx}: X = I_{xx} \end{cases} \quad (24)$$

The simulation tool solves the following set of equations for the gravity gradient torque

$$\begin{aligned} T_x &= \frac{3\mu}{2R^3} (I_{zz} - I_{yy}) \sin(2\phi) \cos^2(\theta) \\ T_y &= \frac{3\mu}{2R^3} (I_{zz} - I_{xx}) \sin(2\theta) \cos(\phi) \\ T_z &= \frac{3\mu}{2R^3} (I_{xx} - I_{yy}) \sin(2\theta) \sin(\phi) \end{aligned} \quad (25)$$

This description does allow for the calculation of the torque vector once the euler angles θ (pitch about principal y-axis), ϕ (roll about principal x-axis) and ψ (yaw about principal z-axis) are known. For the simulation to run properly, a set of input information, e.g. the principal moments of inertia are required. The preliminary values of the inertia tensor are yet to be determined by the STR group.

Solar Pressure Torque

The phase A studies described the torque due to the solar pressure with the following equation:

$$T_{sp} = \frac{S_0}{c} \cdot A \cdot (1 + q) \cdot \cos i \cdot (c_{ps} - c_g) \quad (26)$$

In this formulation the torque is dependent of the distance between the center of mass and the center of pressure only, i.e. the the result is a constant worst-case situation. The simulation accounts for the solar disturbance torque by means of the equation

$$T_{sp} = \frac{S_0}{c} c_a \cdot \sum_{k=1}^6 \vec{r}_{s,k} \times (\hat{n}_k^T \circ \hat{S}) \cdot \hat{S} \cdot A_k \quad (27)$$

This is the formulation of the solar pressure disturbance in its general discrete form, i.e. for a body with arbitrary geometric configuration. In practice, a general body shape will be divided into finite surfaces and the calculation will be performed by summing the torque contribution from each of the surfaces. Since the geometrical configuration of Compass-1 is fairly simple, a cube with six perpendicular faces of equal area will yield results with high accuracy. A simplifying assumption of coincidence of the geometric center with the center of mass cannot be allowed. Hence, the knowledge of the position of the CoM is essential. This information has to be extracted by the STR group.

Since 5 of the 6 panels of Compass-1 are covered with solar generators, all faces are assumed to have equal properties, which are governed by the properties of the solar cells.

The Aerodynamic Torque

The preliminary studies described the torque due to aerodynamic interaction according to the following equation:

$$T_a = \frac{1}{2} \cdot \rho \cdot c_D \cdot A \cdot v_c^2 \cdot (c_{pa} - c_g) \quad (28)$$

In this formulation the torque is dependent of the distance between the center of mass and the center of pressure only, i.e. the the result is a constant worst-case situation. The simulation accounts for the aerodynamic disturbance torque by means of the equation

$$T_a = \frac{1}{2} c_D \cdot \rho \cdot v^2 \cdot \sum_{k=1}^6 \vec{r}_{s,k} \times (\hat{n}_k^T \circ \hat{V}) \cdot \hat{V} \cdot A_k \quad (29)$$

The value of density can be obtained from the ECSS standard [4]. It should be noted that the density in LEO is not a constant property; variations are induced by short-term fluctuations of the solar activity. The values of density for the reference orbit (600km altitude) are:

Table 1: ECSS atmospheric density at 600 km altitude and for different levels of solar activity; the simulation assumes mean activity

Activity Level	Density	Unit
low activity	1.03e-14	kg/m ³
mean activity	1.56e-13	kg/m ³
high activity	6.20e-12	kg/m ³

Since the simulation cannot (and does not need to) account for the temporal fluctuations of the solar activity, a reasonable mean value has to be found and implemented into the code. Table 1 shows a value for mean solar activity. This value is assumed for the computation of the aerodynamic torque. It can, however, be changed to any other value by the user.

A coefficient of drag of 2.2 will be assumed for the cubic body ($c_D = 2$ for spherical shapes).

Simulation Objectives

The overall purpose of the simulation is to verify that the dynamics of the spacecraft are as desired. In particular the simulation needs to answer the following questions:

1. What is the desired value for C in the detumbling control law?
2. What is the most reasonable abort condition in terms of the geomagnetic rate of change?
3. How long does it take to detumble Compass-1 from a worst-case tumbling rate to the detumbling abort condition?
4. How long does it take to deviate Compass-1 to the maximum allowed attitude range of 8° naturally in a control safe-mode (no control action)?
5. How long does it take to recover the nominal attitude once the CDHS has flagged permission to switch to the normal control mode?
6. How is that affected by the maximum magnetic moment of the coils?
7. What is a reasonable target value for the magnetic moment of the coils as a trade-off between the spacecraft dynamic response and power consumption?
8. What are the most reasonable control gains in order to avoid a torquer overdrive?
9. How severe is the impact of sun obstruction (control mode intervals) on the spacecraft controllability?
10. Considering slew maneuvers, is there a slew direction of preference (with faster dynamic response)?
11. How long does it take to move to different slew positions?
12. Does it make sense to use different control gains for normal control and slew control?

The complete simulation will be conducted as a part of phase C.

Hardware Interfaces

Not all of the hardware components discussed in the following sections are mounted onto the ADCS Printed Circuit Board (PCB). Figure 8 summarizes the interfaces between the ADCS PCB and the adjacent components and subsystems and aids in obtaining an overall perspective on the ADCS hardware configuration.

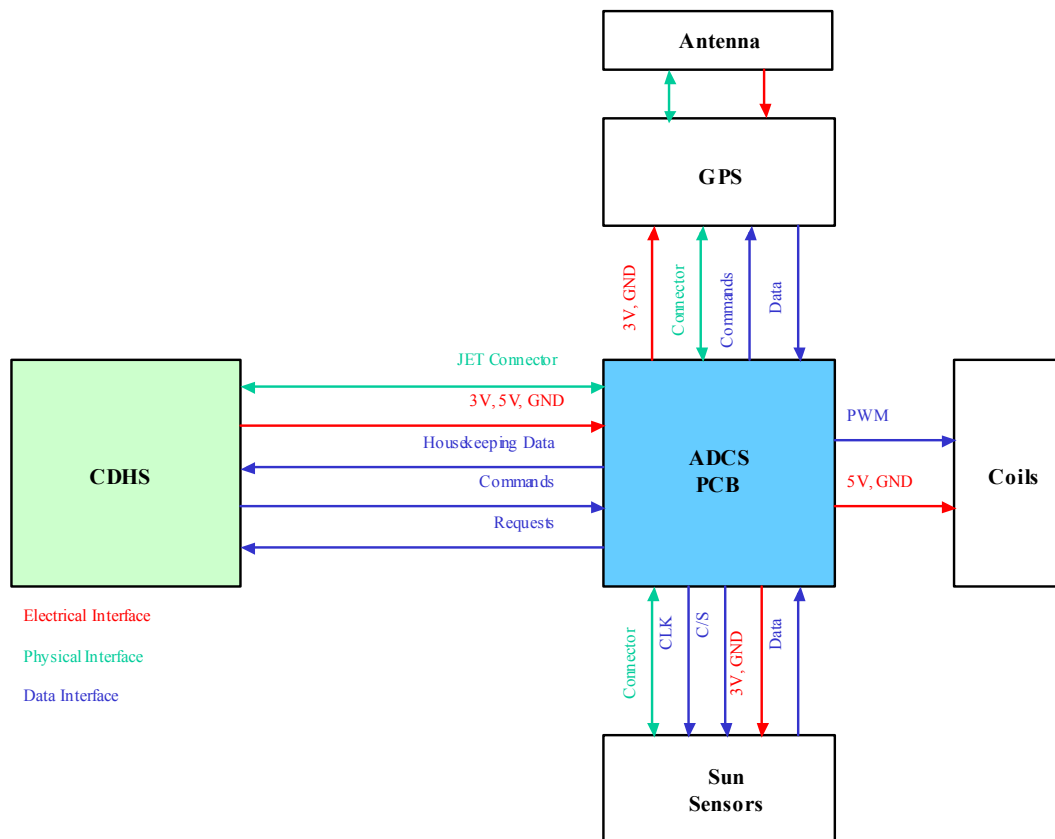


Figure 8: The interfaces between the ADCS PCB and adjacent components / subsystems

The Magnetic Torquers

Design Constraints

The electromagnetic coils of Compass-1 are the only actuators of the satellite's attitude control system. The analysis section already discussed the unique features of magnetic control and how a magnetic dipole moment can be produced as a function of electrical current supplied to the coils (eqn. 1).

An idea to implement 3 pairs of Helmholtz coils (2 per axis with total mass equal to the 3 coils) has been born in the preliminary design and will be discussed later.

Table 2 lists the physical design constraints as a basis for the hardware design. Table 3 shows the electrical constraints.

Table 2: Physical Design Constraints of the magnetic coils

Parameter	Symbol	Value	Unit
-----------	--------	-------	------

Maximum width	B	74	mm
Maximum height	H	74	mm
Maximum cross sectional width	D	2	mm
Maximum cross sectional height	s _h	5	mm
Cross sectional area	A _{c,max}	10	mm ²
Face area of coil	A	5184	mm ²
Circumference	C	296	mm
Total Mass	M _{ges}	60	g
Mass of coil(s) in each axis	M _c	20	g
Minimum temperature	T _{min}	-100	°C
Nominal temperature	T _{nominal}	20	°C
Maximum temperature	T _{max}	100	°C

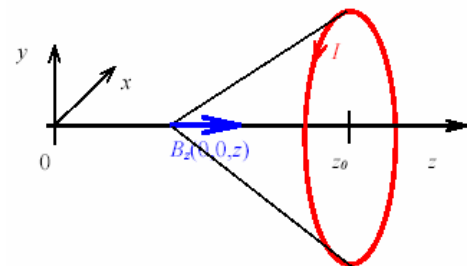
Table 3: Electrical Design Constraints of the magnetic coils

Parameter	Symbol	Value	Unit
Maximum Power per axis	P _{max}	0.25	W
Maximum Coil Voltage	U _C	4.8	V

Investigation of the Helmholtz coil configuration

A homogeneous magnetic field can be produced by parallelly placing two short circular coils with a radius R to each other. When a current is imposed on each of the coils in the same direction a homogeneous field is generated in a considerable volume between the coils. This configuration is named ‘Helmholtz coil pair’ after the German physicist. The magnetic field on the axis of a circular current loop is found by an application of the Biot-Savart law.

The Biot-Savart Law states that the intensity of the magnetic field set up by a current flowing through a wire varies inversely with the square distance from the wire. The magnetic intensity at the coordinates (x=0, y=0, z) generated by a single short coil with the radius R, the current I and the distance z can be described with the Biot-Savart law [5].

$$\vec{B} = \begin{pmatrix} 0 \\ 0 \\ B_z \end{pmatrix} \quad \text{with} \quad B_z = \frac{\mu_0 \cdot N \cdot I}{2} \cdot \frac{R^2}{(R^2 + (z - z_0)^2)^{\frac{3}{2}}}$$


The law allows for a description of the magnetic potential field of the individual short coil. Doing this for both coils and summing up the functions of the coordinate z gives an idea of the *ideal* magnetic field in the volume between the two coils. The objective of this investigation is to determine whether a homogeneous field can be established over a relatively wide distance of the coils with respect to the low individual magnetic density.

Defining the origin of the z-coordinate on the axis of symmetry results in a peak of the magnetic density for the right and left coil at z₀ and -z₀, respectively.

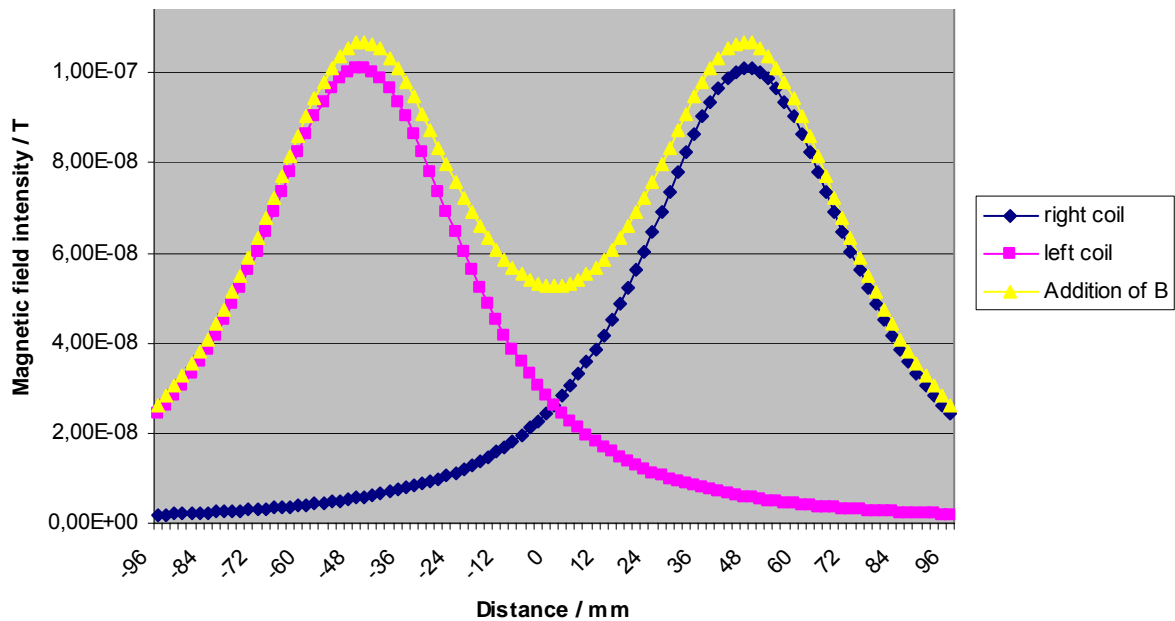


Figure 9: The magnetic intensity between two coils in Helmholtz configuration

Figure 9 shows the magnetic field intensity of the individual coils and the resulting magnetic field. It becomes obvious by this simple analytical investigation that for the given coil parameters, the magnetic field cannot be made homogeneous in the volume between the coils. It should be noted that the magnetic field would be distorted to some extent by the current carrying electronics components within the satellite, leading to an even less advantageous result.

In conclusion it can be stated that due to the results of the simple analytical investigation presented here, the design option of a Helmholtz coil configuration has been rejected for Compass-1. The satellite will carry one coil for each axis.

Design Preliminaries

The coils will require a significant fraction of the critical budgets (mass and power). Hence, sufficient analysis and optimization should be spent on the coil design in the development phase. During this current definition phase an efficient tool has been developed which enables a fast design output for a given set of input parameters. This tool will not be discussed in detail here, but it should be noted that the design is not only dependent of the required mechanical torque but also of commercially available wire properties, i.e. diameters and material, as well as the selected number of turns. It becomes obvious at this stage that the design process will be a trade-off between mass and power consumption. It is possible to reduce the weight, by reducing the number of turns but the power consumption will increase, and vice versa.

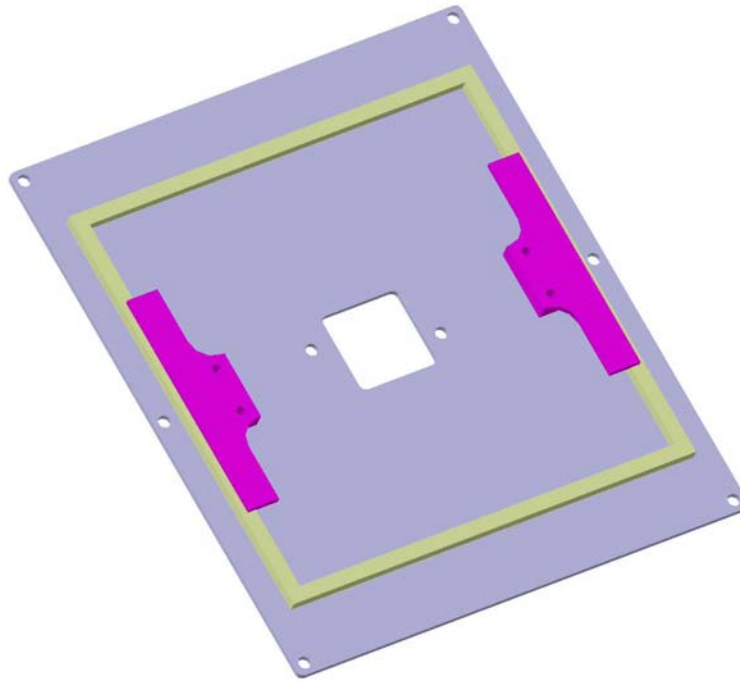


Figure 10: One magnetic coil and its integration onto a panel; the coil is shown sharp-edged now, manufacturing concerns will require a marginally different design later

A preliminary design run for a required mechanical design torque of $1\mu\text{Nm}$ yields the results listed in table 4.

Table 4: Preliminary design results for a coil made from copper

Parameter	Symbol	Value	Unit
Wire diameter	D	0,16	mm
Number of turns	N	250	-
Mass of one coil	M_C	13,70	g
Total Mass incl. insulation	M	41,20	g
Nominal Coil Current	I_{nom}	0,03925758	A
Magnetic dipole moment	M	5,09E-02	Am^2
Required cross sectional area	A_C	6,7824	mm^2

Note the difference between the actual and the design constraint mass (refer to table 5). A significant amount of mass could be saved when using the entire assigned power supply of 250mW per coil.

It is intended to conduct measurements of the magnetic field generated by the coils. During the entire discussion of the generation of a magnetic moment vector \mathbf{m} , simple vector arithmetics have been used, i.e. each coil produces one component of the vector \mathbf{m} . Possibly the case is more complex. The interaction between the individual fields must be experimentally investigated and the net magnetic moment determined by means of mapping the field generated by the designed coil configuration. This data must be compared with the design data to ensure better confidence in the design methods. Testing will be done in Phase C.

The Coil Driver

The Coil Driver is the device that translates a logic signal input from the microcontroller into an analog power output for the magnetic coils. Figure 11 shows a preliminary layout of the driver circuitry.

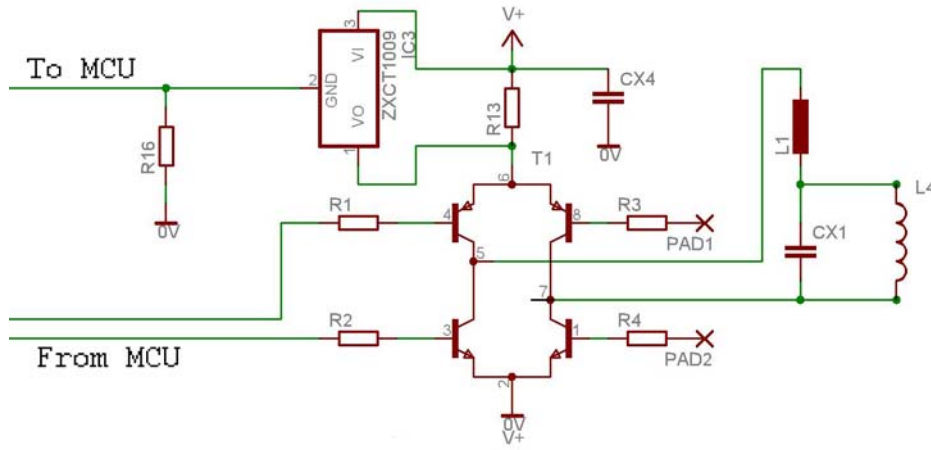


Figure 11: Coil Driver Circuitry Layout; PAD 1 and 2 are connected to the MCU

Each of the three magnetorquers has its own coil driver circuitry due to the fact that the coils must be operated separately. The three coil driver circuitries are identical to each other. Each driver consists of an H-Bridge amplifier, a low pass and a current monitor.

The H-Bridge (HB)

The H-Bridge (labeled T1 in figure 11) is the component that receives the logic signals from the ADCS MCU. It is a very straight forward standard electronics component. It basically consists of an array of transistors that enables signal amplification which can be influenced in such a manner to generate amplified output with a specific sign convention. This is important due to the fact, that the driver must generate output currents (on the order of several mAmps) with variable flow directions, such that the magnetic moment produced by the coils can be oriented either way. This would be difficult to achieve with regular Digital-to-Analog Converters. The input into the H-Bridge is comprised of two separate digital signals from the MCU:

- A pulse-width-modulated (PWM) digital signal
- A direction digital signal

The selected H-Bridge is the SM-8 bipolar transistor HB **ZHB6718** manufactured by Zetex.

The Low Pass (LP)

The HB is connected to a custom made simple low pass filter that translates the high frequency of the PWM signal into a linearly dependent voltage level applied to the coils. The design of the low pass with respect to the cut-off frequency will happen in the development phase. It is important to note that the design of the LP is tightly related to the design of the coils since the coil contributes a significant part of the inductance, which governs the characteristics of the filter. In figure 13, L4 is the magnetic control coil, whereas L1 is a inductance component which will have to be matched to the control coil.

The Current Sensor

The current sensor is a component which measures the current running through a control coil. The major purpose of the current sensor is to provide a means of health monitoring for the ADCS actuator system. If a coil happens to be damaged, no current will be measured, even if the MCU forces the coil driver to power the coil. The coils a relatively insensitive assembly. However, it should be noted that breaking a single one of the approximately 250 turns will cause the coil to cease function. This information must be refered to the controller. Possibly the current information will also be used to control the current to its desired level by means of a simple feedback loop. This might be necessary in order to account for the temperature dependent resistance of the coil lead material.

The selected current sensor is the **ZXCT1009** manufactured by Zetex. The ZXCT1009 is a high side current sense monitor, which eliminates the need to disrupt the ground plane when sensing a load current. It takes a high side voltage developed across a current shunt resistor and translates it into a proportianl output current. According to the data sheet, this simple component shows a quiescent current of 4 μ Amps and 1% typical accuracy. Each sensor requires two extra resistors (R13 and R16 in figure 11).

The GPS System

For the computation of the reference vectors for attitude determination, the information of the current position of the spacecraft is vital. In order to enable the autonomy of the system operation, a GPS will be incorporated. For Compass-1 the GPS system can be sub-divided into two separate system components:

- The **antenna** receives the GPS signal and transmits it to the GPS receiver.
- The GPS **receiver** is the device that receives a signal from the antenna, conditions and processes the signal into a location information, and sends the data, with a time stamp, to the ADCS unit.

The Phoenix Receiver

No critical selection is necessary for the GPS receiver system since the choice of the receiver hardware was determined in the very early stages of the definition phase already. In-orbit position determination is part of the mission goals for technology demonstration. As such, the GPS system can be considered a part of the payload of Compass-1.

The GPS receiver (in this documentation referred to as Phoenix) on Compass-1 is a follow-on of the DLR's flight proven GPS Orion receiver for space applications. The functionality of Phoenix, unlike Orion, has never been verified in space.

The receiver is built around the GP4020 chip of Zarlink, which combines a 12 channel correlator for L1 code and carrier tracking, a microcontroller core with a 32-bit ARM7TDMI microprocessor and several peripheral functions in a single package.



Figure 12: Phoenix (MG5001) receiver board

Two manufacturers (Sigtec and CMC/Nov Atel) have employed the GP4020 chip in commercial receiver boards (MG5001) for terrestrial mass market applications, i.e. the receiver is not a designated hardware for space applications.

The MG 5001 board provides a 512 kByte Flash ROM for storing the receiver software and a 256 kByte RAM memory for run time code and data (side note: according to the manufacturer only 128 KB Flash and 128 KB SRAM are required for normal operation, indicating the significant increase in software performance requirements of the DLR high dynamics application development.). The backup battery drives a 32.768kHz clock crystal and a real time clock inside the GP4020 to maintain the current time during separation from the main

power supply. By default, the MG5001 receiver is operated at a +5V supply voltage, which is internally down-converted to +3.3V required by the correlator and microprocessor.

Mechanical Specification

The overall dimensions of the receiver board are shown in figure 13. The profile depth is 12 mm.

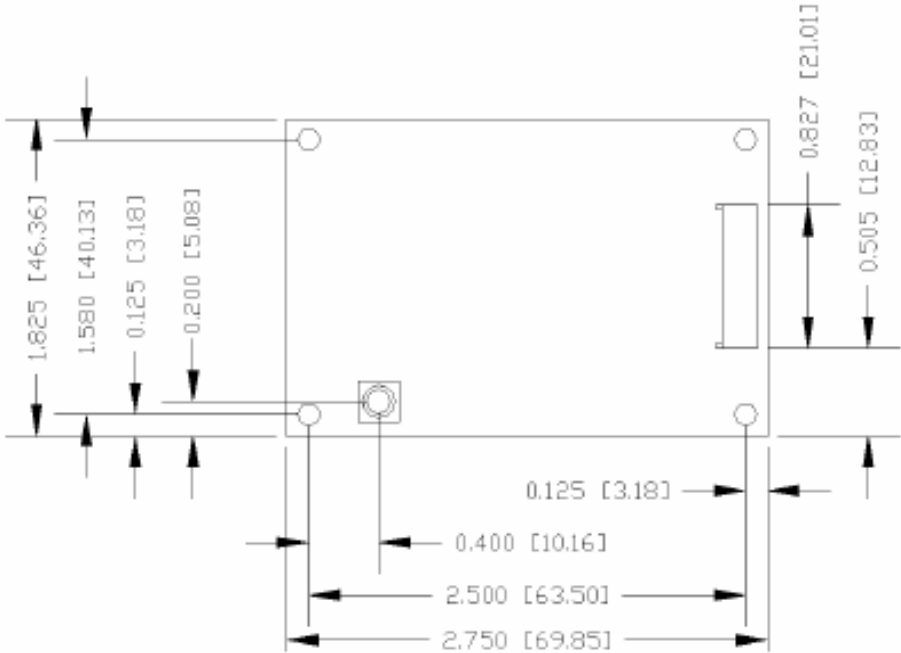


Figure 13: Receiver dimensions in inches [mm]

The overall dimensions of about 70x50x12mm allow for mounting the GPS receiver board directly onto the ADCS PCB, thus complying with the modular approach of the system design.

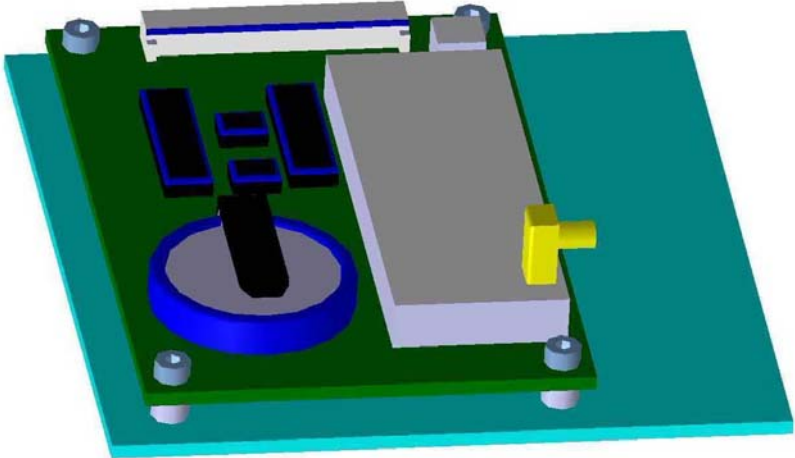


Figure 14: intended integration of the Phoenix receiver on the ADCS PCB

The MG5001 GPS board features a single row, right angle, 12-pin male connector.

Housing	ZHR-12
Crimp Contact	SZH-002T-P0.5 (26 to 28 AWG wire) SZH-003T-P0.5 (28 to 32 AWG wire)

Electrical Specification

The nominal power consumption of the receiver board is approximately 800mW when taking position data. Perhaps a way can be found to reduce the operating supply voltage. According to the manufacturer (Sigtec) the board may be operational at a supply voltage as low as +2.7VDC. A +3VDC supply may reduce the power consumption and overrides the need for a step-down converter. The receiver has a ‘stand-by’ mode in which the MCU does not execute any more instructions. In this mode, the power dissipation is about 600mW. This is still an unacceptable power drain for continuous operation. Consequently, power will only be provided to the GPS, when position data is to be taken. In between the GPS measurements, the power supply will be switched off.

Antenna Interface

The Phoenix receiver supports and recommends the use of an active GPS antenna. However, power consumption considerations should be taken into account, when making the decision. The interface incorporates provisions for an antenna power supply at a voltage level of 5VDC. With some minor modifications, external voltage levels can be routed to the antenna, such that the antenna selection would not be restrained by the operation voltage. The antenna will be connected to the receiver with an MCX connector, which is a standard RF connector.

Interface Data Protocol

The MG5001 contains two full duplex serial ports that operate at CMOS (high = +3.3V) voltage levels. The data transmission protocol of the MG5001 is a RS232 type protocol (asynchronous serial communication). This protocol is straight forward: in default mode the baud rate is 9600 bits per second, 8 bits data, no parity and one stop bit. Deviations from the default settings are possible via software initialization.

Environmental Characteristics

Table 6: The MG5001 receiver environmental characteristics; discard the specs concerning altitude and velocity

	Minimum	Typical	Maximum	Units
Operating Temperature	-20		+70	°C
Storage Temperature	-50		+80	°C
Velocity			1000	nm/h
Altitude			60,000	ft
Acceleration			8	g
Jerk			8	g/s
Shock	All levels specified for ground environments in [3]			
Vibration	MIL-STD-810E Test 514 Category 8			

The specifications shown in table 6 are deviating from the characteristics of the Phoenix Receiver Board with respect to maximum velocity and altitude. Legal regulations prohibit the allowance of receiver hardware for high altitudes and velocities. Hence, a regular terrestrial receiver cannot be used on a high dynamics satellite at high altitudes. The Phoenix receiver, however, incorporates the necessary software required for such extreme applications by using a dedicated software under legal protection. As mentioned before, the Phoenix hardware is completely identical to the MG5001 receiver, hence the specifications with respect to the physical environment shown in table 6 hold valid. Note that the hardware has been vibration tested under specific military standard conditions. Also, the DLR conducted tests to quantify the radiation hardness of the device. The test results indicate a maximum survivable radiation energy of 15krad.

GPS Antenna

Product Comparison

The general form of antennas for use in GPS applications is the patch antenna design. Typically made from a ceramic material the antenna is a robust device of little complexity. According to the design approach of incorporating COTS products a product research has been performed on the basis of low cost, commercially and widely available antenna devices. Phase A already suggested the consideration of the TOKO DAX1575MS63T as a result of an early product research. This device and two active alternatives are listed in table 7 to enable a simple way of performance comparison and subsequently a selection of a best-fit device.

Table 7: Antenna options in comparison

	Synergy Systems	TOKO	San Jose Nav. Inc
	SMK-4	DAX1575MS63T	F-15
Mode	active	passive	active
Dimensions [mm]	<34x25.3x10.9	18x18x4.5	15x15x8.6
Mass [g]	30	18	30
Gain [dB]	24	0	15
Supply Current [mA]	6 to 11	---	4.5 to 8
Supply Voltage [+VDC]	3 to 5	---	2.5 to 3.3
Power Consumption [mW]	36	---	18
Operating Temperature	-30°C - +85°C	-40°C - +105°C	-30° to +85°C

All antennas found are flat patch devices incorporating a rectangular micro-strip design for right-hand circular polarized wave reception. Two distinct types of antennas are commercially available: active and passive. Active antenna solutions incorporate a low noise amplifier (LNA) as in the case of the integrated Synergy Systems SMK-4 model. It is obvious that these active devices possess higher output gains than the simpler passive solutions on the cost of power consumption (6 to 11 mA @ 3 to 5 V for SMK-4) and weight. However, a moderate output gain is advisable since the strong output signal might overdrive the receiver. For the connection of the antenna LNA with the receiver input a certain minimum shielded signal cable length is recommended. It should also be noted that all of the above solutions were originally developed for terrestrial / airborne applications.

The SMK-4 antenna comes with a polycarbonate radome housing on a metal base. For the integration into the structure of Compass-1, removal of the casing would be necessary, saving some weight but also shifting up the center frequency by approximately 5MHz (L1 GPS signal frequency: 1575.42MHz). An approach to separate the LNA from the antenna body likely causes signal degradation and must be avoided. The need to mechanically modify the device is a significant disadvantage.



Figure 15: Synergy Systems SMK-4 GPS Antenna

The F-15 claims to be the most compact GPS antenna module currently available on the market without compromising performance. According to the manufacturer, the device is immune to electromagnetic interference to some extent. A larger version, F-19, is also available. With dimensions of 19x19x8.6 this patch is expected to show better reception characteristics. All other properties (weight, center frequency, gain, power consumption) are equivalent to the F-15 model. The F-19 model has explicit provisions for screw mounting,

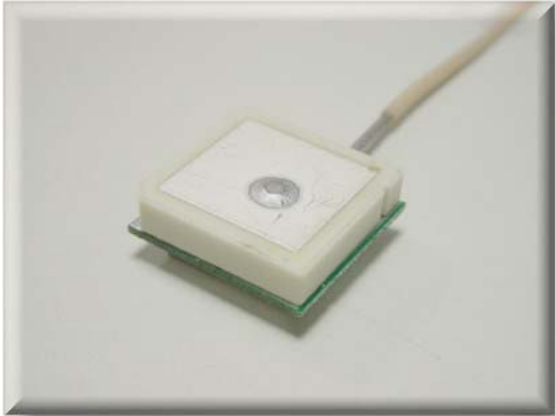


Figure 16: The San Jose F-19 active patch antenna

such that the integration is expected to be unproblematic. Adhesive mounting will be considered for structural integration as well. Permissible antenna output gains in conjunction with the Phoenix receiver range from 0dB (passive) to 26dB, with a recommended gain of 12dB. Compass-1 will most likely use the F-19 antenna due to its larger reception area compared to the complementary F-15. Both devices will be ordered and a final product selection will be conducted on the basis of hardware tests.

Table 8: Comprehensive data overview of San Jose Navigation, Inc F-19 active GPS antenna

PHYSICAL CONSTRUCTION	
Dimension:	19mm (L) x 19mm (W) x 8.6mm (H)
Weight:	30 grams (excluding cable & connector)
Standard Mounting:	Screw Mounting
ANTENNA ELEMENT	
Center Frequency:	1575.42 MHz +/- 1.023 MHz
Polarization:	R.H.C.P. (Right Hand Circular Polarization)
Absolute Gain at Zenith:	+3 dBi typically
Axial Ratio:	3.0 dB typically
Output VSWR:	1.5 dB typically
Output Impedance:	50 ohm
LOW NOISE AMPLIFIER	
Center Frequency:	1575.42 MHz +/- 1.1 MHz
Gain:	17 dB
Band Width:	2 MHz
Noise Figure:	1.3 dB typically
Supply Voltage:	2.5 ~ 3.3 V DC
Current Consumption:	4.5 ~ 8.0 mA
Output Impedance:	50 ohm
BPF OR SAW FILTER	
Out-of-band Attenuation:	30 dB typically
CABLE & CONNECTOR	
RF Cable:	RG174/U (standard), with RG-178/U and RG-316/U as customized options
Pulling Strength:	6 Kg/5 sec. with molded plastics on connector end for strain relief (w/o cable loss)
Connector Available:	BNC, TNC, FME (to be adapted), GT5, MCX (OSX), SMA, SMB or SMC in straight or right angle type
Optional Adapters:	FME~MCX, FME~BNC, FME~SMA, FME~SMB, FME~TNC
OVERALL PERFORMANCE (Antenna Element, LNA & Cable)	
Center Frequency:	1575.42 MHz
Gain:	15 dB
Noise Figure:	1.3 dB
Band Width:	2 MHz
Axial Ratio:	3 dB max.
VSWR:	1.5 dB
Output Impedance:	50 ohm
ENVIRONMENTAL CONDITIONS	
Operating Temperature:	-30°C~+80°C
Storage Temperature:	-40°C~+90°C
Relative Humidity:	95% non-condensing

The Magnetometer

The measurement of the local magnetic field vector for attitude determination requires the implementation of magnetometers on the subsystem. The selected hardware is the HMC6352 digital compass developed and distributed by Honeywell.

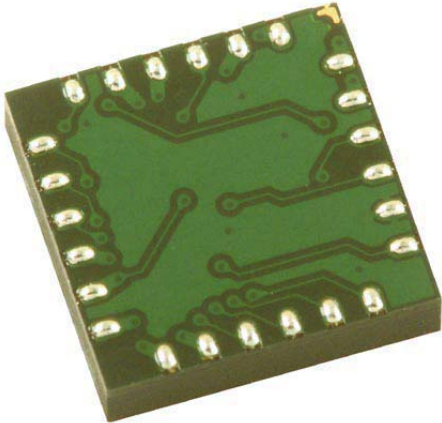


Figure 17: The HMC6352 digital magnetometer

The HMC6352 communicates via a two-wire I²C bus system as a slave device. The HMC6352 uses a layered protocol with the interface protocol defined by the I²C bus specification, and the lower command protocol defined by Honeywell. The data rate is the standard-mode 100kbps defined in the I²C bus specification. The bus bit format is an 8-bit data/address and 1 acknowledge bit. The format of the data bytes shall be case sensitive ASCII characters or binary data to the HMC6352 slave, and binary data returned. Negative binary values will be in two's complement form. The default HMC6352 slave address is 0x42 for commands, or 0x43 for response data bytes, and is a 7-bit address with the 0 bit (LSB) being the Read/Write section.

The HMC6352 is a two-axis magnetometer. The preliminary design suggested a 4-axis (3 active axes, 1 back-up axis) magnetometer. The ADCS needs 3 axes to support the determination of the attitude. Each additional axis adds redundancy / failure tolerance. The orthogonal two-axis nature of the HMC6352 makes a 4-axis design mechanically impossible. It is envisaged to implement 3 identical HMC's on the PCB, to span a set of fully redundant axes in addition to the 3 orthogonal active measurement axes. This solution is made possible by the very small physical dimensions and power consumption of the component as shown in table 9. However, the need for such a configuration is a disadvantage of the device. A great advantage on the other side is the highly integrated solution including amplifiers and the digital I²C interface. No other component-based Honeywell solution has a digital interface.

Table 9: typical specifications of the HMC6352

Supply Voltage	3V
----------------	----

Supply Current	1mA
Field Range	0.1 to 0.75 Gauss ¹
Heading Accuracy	3degRMS
Heading Resolution	0.3deg
Operating Temperature	-20 to 70°C
Storage Temperature	-40 to 125°C
Output	I ² C digital
Size	6.5 x 6.5 x 1.4 mm

It should be noted that there are two different versions of the HMC6352 available. An enhanced version carries the identification number HMC6352E and is distinguished by a better accuracy. The value listed in table 9 shows the performance specification of HMC6352E, since it is envisaged to invest into higher performance components for better measurement accuracy. For comparison, the heading accuracy for the HMC6352 is 9degRMS. The simplicity of the magnetometer interface is illustrated in table 11. Out of 24 pins in total only 13 are connected, many of them are predetermined or not intended for user connection.

Table 10: HMC6352 Interface Pin-Out

Pin	Name	Description
1	OF-	No User Connection (offset Strap Negative)
2	SR+	No User Connection (Set/Reset Strap Positive)
5	GND	Supply / System Ground
7	SDI	I ² C Data Output
9	PGM	Program Enable
10	SCL	I ² C Clock
11	SS	No User Connection (Slave Select)
14	VDD	Supply Voltage Positive Input (+2.7 to +5 VDC)
19	CB2	Amplifier B Filter Capacitor Connection
20	CB1	Amplifier B Filter Capacitor Connection
22	CA2	Amplifier A Filter Capacitor Connection
23	CA1	Amplifier A Filter Capacitor Connection
24	OF+	No User Connection (Offset Strap Positive)

The HMC6352 magnetometer chip requires few additional standard electrical components (resistors and capacitors). The HMC6352 Serial Clock and Serial Data lines do not have internal pull-up resistors and require resistive pull-ups (R_p) between the master device and the HMC6352. Pull-up resistance values of about 10k are recommended with a nominal +3VDC supply voltage. The design of the complete circuitry will be conducted in the hardware development phase.

¹ 1 Gauss = 10⁻⁴ T

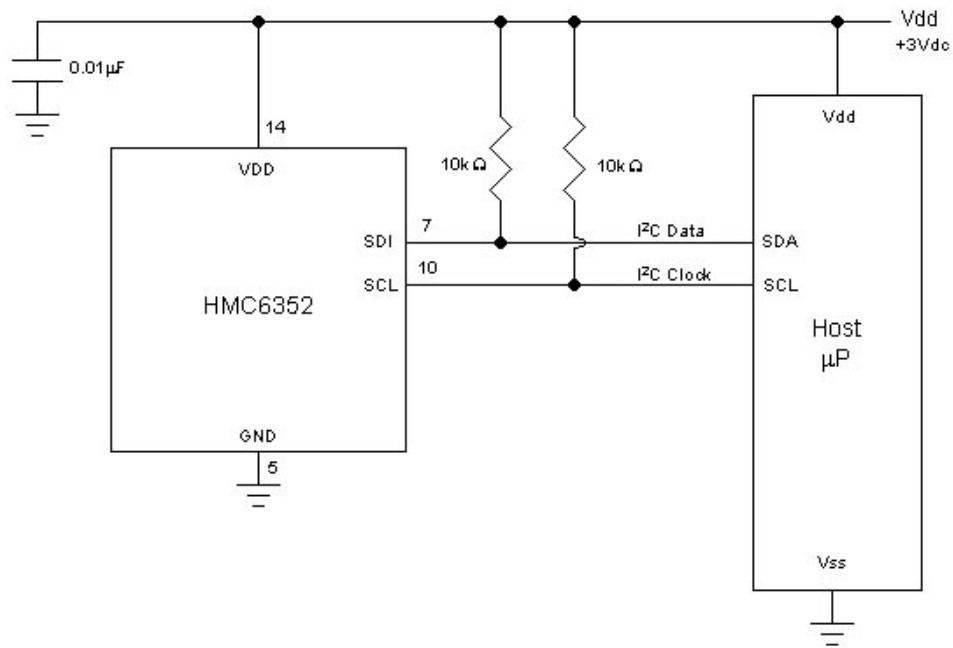


Figure 18: Connection diagram for the HMC6352E

The Sun Sensors

The objective of the sun sensors is to measure the relative position of the sun in order to aid the attitude determination procedure. The sun sensors used on Compass-1 have been developed by the Micro Electronics Institute (MIC) of the Denmark Technical University (DTU) in MOEMS² technology. They are extremely lightweight, small and power saving. Refer to [7] for further details on the sensor principle.

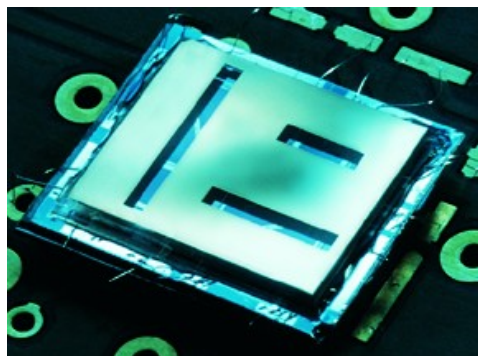


Figure 19: The MIC sun sensor chip mounted on a PCB

In total five sensors will be implemented on the satellite; one on each cube face, except the payload panel. This guarantees an unobstructed, redundant view onto the sun in almost every attitude situation. The layout of the sensor is divided into the sensor chip and the carrier PCB. The chip shown in figure 19 is the active sensing surface. The PCB carries the chip as well as

² Micro-Opto-Electro-Mechanical System

additional electrical components which condition the signal and convert it from an analog to a digital nature. The components that define the interface with the ADCS PBC are the analog-to-digital converter AD7450, the operation amplifier AD8552 and the digital thermometer DS18S20.

Table 11: Sun Sensor Interface Pin-Out

Pin	Name	Description
2	C/S2	Chip Select 2
3	C/S1	Chip Select 1
4	CLK	Clock
5	Data	ADC Output
6	TEMP	digital thermometer I/O
7	Vadc	ADC Supply Voltage 3VDC
8	GND	System Ground
9 to 12	Vamp	Amplifier Supply Voltage 3VDC

A problem that has to be addressed in the attitude dynamics simulation is the fact, that the satellite will be in umbra conditions for approximately 30% of the orbit / mission time. As described earlier, during umbra no attitude determination is possible. Penumbra and umbra entry can be detected by the sun sensors to toggle the ADCS.

Table 12: Power and Temperature requirements of the sun sensors; values are in accordance with the respective data sheets

Qty	Component	Function	Active Power per Unit [mW]	Operational Temperature Range	Recommended Supply Voltage
2	AD7450	ADC	3,75	-40° to 85°	+3 OR +5VDC
2	AD8582	OPAMP	2,7	-40° to 125°	+2,7 to +5VDC
2	74HC1G00	NAND	3	-40° to 125°	+2 to +6VDC
1	74HC1G66	bil. switch	2,5	-40° to 125°	+2 to +9VDC
1	DS18S20	therm.	4,5	-55° to 125°	+3 to +5,5VDC
Total			25,9	-55° to 85°	+3VDC

An important prerequisite for the management of the sun sensor data acquisition and also for evaluating the controllability of the spacecraft is the analysis of the Field of View (FOV) of the individual sensors and any possibly resulting ‘dead zones’ for sun vector acquisition. Figure 20 shows a simplified 2-D geometry of the FOVs.

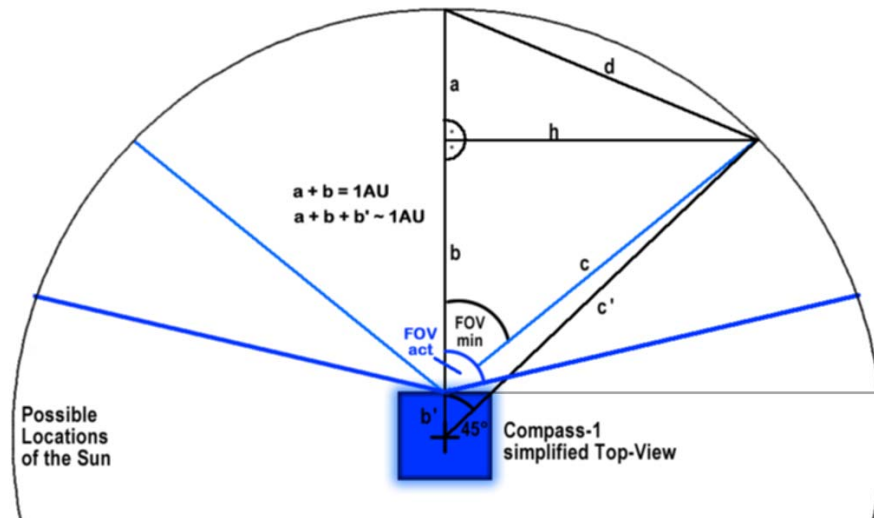


Figure 20: Sun Sensor 2D-Field of View geometry; minimum and actual FOV

Consider the orthogonal triangles in figure 20 in order to determine the minimum FOV requirement such that complete coverage is achieved, assuming that a single sun sensor is mounted on the center of each CubeSat panels. Pythagoras yields

$$c = \sqrt{b^2 + h^2} \quad \text{as well as} \quad c' = \sqrt{(b + b')^2 + h^2}$$

But b is very large compared to b' . Recall that $a + b$ is approximately 1 astronomical unit, whereas b' is 5 centimeters, such that

$$c \approx c'$$

Let us call the minimum required Field of View half-angle $\text{FOV}_{\min} \rightarrow \alpha$.

$$h = c \cdot \sin \alpha \quad \text{and also} \quad h = c' \cdot \sin 45^\circ$$

It is obvious now, that the minimum FOV half-angle must be 45° in order to achieve complete coverage of the sphere of possible locations of the sun without overlap. Figure 20 also shows the actual FOV half-angle of 70° determined by measurements, resulting in a welcome overlap of coverage areas. This effect is illustrated in the following figures.

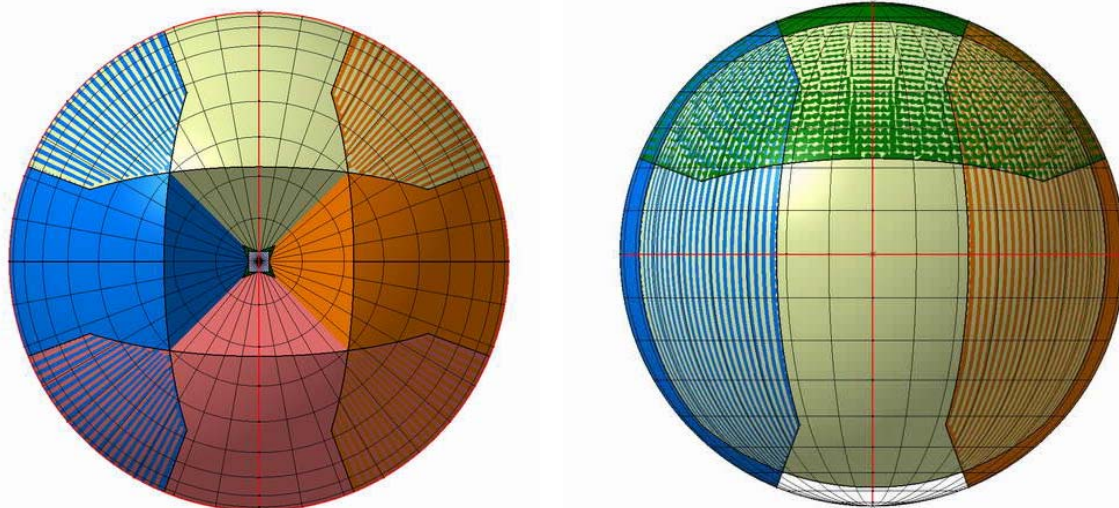


Figure 21: 3D Fields of View for all 5 sun sensors projected onto a sphere which is large compared to the spacecraft dimensions

In 3D the fields of view can be represented as square-based pyramids which originate from the center of all CubaSat faces except the payload panel. A reasonably realistic result can only be obtained if the projection sphere is large compared to the satellite's dimensions. As can be seen from the figures, there are areas in which the sun is seen from either one, two or three sensors at a time. More importantly there is a 'dead area' at the payload side of the CubeSat where no sensor coverage is provided. If the sun is located in this area, no attitude determination is possible. This area has the approximate shape of a square-based pyramid with a total opening angle of 40° in both directions. It should be noted however, that during normal operations of Compass-1 attitudes with this sun-pointing characteristics are to be avoided such that the camera module will not be blinded by the sun. Hence, these attitudes have no practical value.

The reduction of power consumption is made possible by selectively supplying only those sensors which are currently viewing the sun. If the sun is seen by more than one sensor at a time all of those sensors will be active to enhance accuracy. The exact terms of power consumption reduction will be examined in phase C. The following development phase will also feature a comprehensive test campaign to verify the space worthiness of the hardware under special investigation of signal stability and noise when subjected to space environment conditions.

The Digital PCB Thermometer

This LM75 digital thermometer is the only device described in this documentation which is not truly a part of the ADCS. Although physically mounted on the ADCS PCB, the thermometer is part of the TCS. Connected to the I²C bus, which the LM75 is interfaced for, the EPS controller can read the temperature at the location of the ADCS PCB and use this information for supporting the thermal management. The ADCS controller will not read the temperature from this device, unless a temperature information is found necessary during the development phase. For further details on this component, refer to the TCS/EPS documentation.

The Controller Core of the ADCS

The controller core is the ‘brain’ of the subsystem. It has the objective to coordinate the subsystem’s component interaction, to perform all computations necessary for determining and controlling the attitude of the spacecraft and to monitor the status/health of the subsystem. Additionally, it manages the communication with the adjacent CDHS. Due to the high computational demand of the subsystem and the approach to perform all computations on the subsystem board (as opposed to on a main OBC), the controller hardware must possess the highest performance characteristics of all MCU’s on Compass-1.

The selection of the controller core is governed by three major requirements:

1. high computational demands
2. high demands in terms of I/O capability
3. low power consumption

This is the reason why it has been decided in the early stages that a 32-bit RISC controller will be implemented on the ADCS of Compass-1. However, while a high bit size has significant advantages in terms of accuracy, it does not necessarily mean higher computational performance. In common microcontroller designs a DSP (Digital Signal Processor) is used, whenever the computational demands are high. DSPs allow for faster arithmetic operations and better compatibility with high level languages, such as C. Sometimes the DSP comes on-chip in an embedded controller system, but these embedded systems usually do not offer the same degree of I/O flexibility. Hence, a different solution has been found to benefit both from the I/O flexibility of a microcontroller and the computational power of a DSP. The controller core of the ADCS system will consist of one host microcontroller with various I/O options and an external DSP. This way the hardware architecture is close to the modular software concept: all external I/O operations are performed by the microcontroller, i.e. gathering sensor data, generating PWM actuator output. The internal algorithms which make up the vast majority of computational demand are being processed by the DSP, using the sensor data from the μ C. The results of the algorithms, i.e. necessary actuator load are being returned to the μ C for output operations to the actuator. This way the DSP can be regarded as a ‘black box’ similar to a software function which requires input and returns a processed output.

Microcontroller Unit (MCU)

The most important factor in selecting a COTS MCU component is the satisfaction of the interface requirements. Secondly an adequate bit size and memory size should be present on the selected MCU. The chip must run at a +3VDC or +5VDC supply and should have a standard industrial operational temperature range. To accurately handle the I/O actions, the bit size should be 16-bit. The RAM and ROM space should be sufficient to store program machine code equivalent to a few thousand lines of C-Code and respective runtime data. At this stage it is difficult to specify more accurate requirements for memory space. Whether or not the memory of the chosen MCU is sufficient can only be determined during or after the flight software coding. When selecting the MCU it has been kept in mind that spare capacity is no problem, while under-capacity is a significant problem. Non-volatile Flash memory is preferred over EEPROM.

With the technical solution in mind it is now possible to outline the requirements for I/O operations and other peripheral subsystems. The MCU needs

- serial synchronous communication subsystem for the sun sensors (SCI)
- serial asynchronous communication subsystem for the GPS (SPI)
- I²C subsystem for magnetometers and CDHS interface
- appropriate interface for DSP
- PWM channels for magnetorquer operation
- Analog-to-Digital converters for the current sensors
- sufficient number of general purpose I/O
- real-time interrupt system
- watch-dog-timer / computer-operating-properly system
- timer monitoring
- power management options

The choice of the semiconductor manufacturer is a personal matter: since the author has experience with the MotorolaTM 68HC11 and 12 family instruction set and terminology this manufacturer is preferred in order to minimize the development time for assembly code sections.

Unfortunately the 68HC11 or 12 family does not offer any hardware I²C compatibility. This may also be achieved by means of interface software. However, developing the software is considered too efforty and will most importantly increase performance demands. Also, the HC11 is a pure 8-bit controller. The same limitation in terms of I²C compatibility is true for the HC12 family. The only controller family which appears to satisfy all the requirements stated above is the HCS12 family.

Table 13: HCS12 options in comparison

Product	Internal RAM (byte)	EEPROM (byte)	Flash (byte)	Serial Interface Types	Bus Frequency (max) (MHz)	Supply Voltage (typ) (V)	A/D Converter		Pulse Width Modulators		I/O Pins
							Channels	bit	Channels	bit	
MC9S12A64	4096	1024	65536	IIC, SCI, SPI	25	5	8	10	4,7,8	8,16	59,91
MC9S12A128	8192	2048	131072	IIC, SCI, SPI	25	5	8	10	4,8	8,16	59
MC9S12A128B	8192	2048	131072	IIC, SCI, SPI	25	5	8	10	4,8	8,16	59,95
MC9S12A256B	12288	4096	262144	IIC, SCI, SPI	25	5	2,3,8	10	4,8	8,16	59,95

The four product options shown in table 13 are the options which satisfy all interface requirements. All options have the same serial interfaces (IIC = I²C, SCI, SPI), the same bus frequency (25MHz) and the same supply voltage (5V). Differences are the available memory space, memory expandability and minor differences in ADC and PWM ports. The controller of choice is the MC9S12A128 because of its larger memory space and optional memory expandability. Running the controller in an extended mode may be necessary for operation in conjunction with the digital signal processor.

Motorola's short description of the controller reads:

“The MC9S12A128 microcontroller unit is a 16-bit device composed of standard on-chip peripherals including a 16-bit central processing unit (HCS12 CPU), 128K bytes of Flash EEPROM, 8K bytes of RAM, 2K bytes of EEPROM, two asynchronous serial communications interfaces (SCI), two serial peripheral interfaces (SPI), an 8-channel IC/OC enhanced capture timer, two 8-channel, 10-bit analog-to-digital converters (ADC), an 8-channel pulse-width modulator (PWM), 29 discrete digital I/O channels (Port A, Port B, Port K and Port E), 20 discrete digital I/O lines with interrupt and wakeup capability and an Inter-IC (I²C) Bus. System resource mapping, clock generation, interrupt control and bus interfacing are managed by the System Integration Module (SIM). The MC9S12A128 has full 16-bit data paths throughout. However, the external bus can operate in an 8-bit narrow mode so single 8-bit wide memory can be interfaced for lower cost systems. The inclusion of a PLL circuit allows power consumption and performance to be adjusted to suit operational requirements.”

Features:

- HCS12 Core
- 16-bit HCS12 CPU
 - Upward compatible with M68HC11 instruction set
 - Interrupt stacking and programmer's model identical to M68HC11
 - Instruction queue
 - Enhanced indexed addressing
- MEBI (Multiplexed External Bus Interface)
- MMC (Module Mapping Control)
- INT (Interrupt control)
- BKP (Breakpoints)
- BDM (Background Debug Mode)
- CRG (low current oscillator, PLL, reset, clocks, COP watchdog, real time interrupt, clock monitor)
- 80-pin QFP or 112-pin LQFP package
- operating temperature range: -40°C to 85°C.

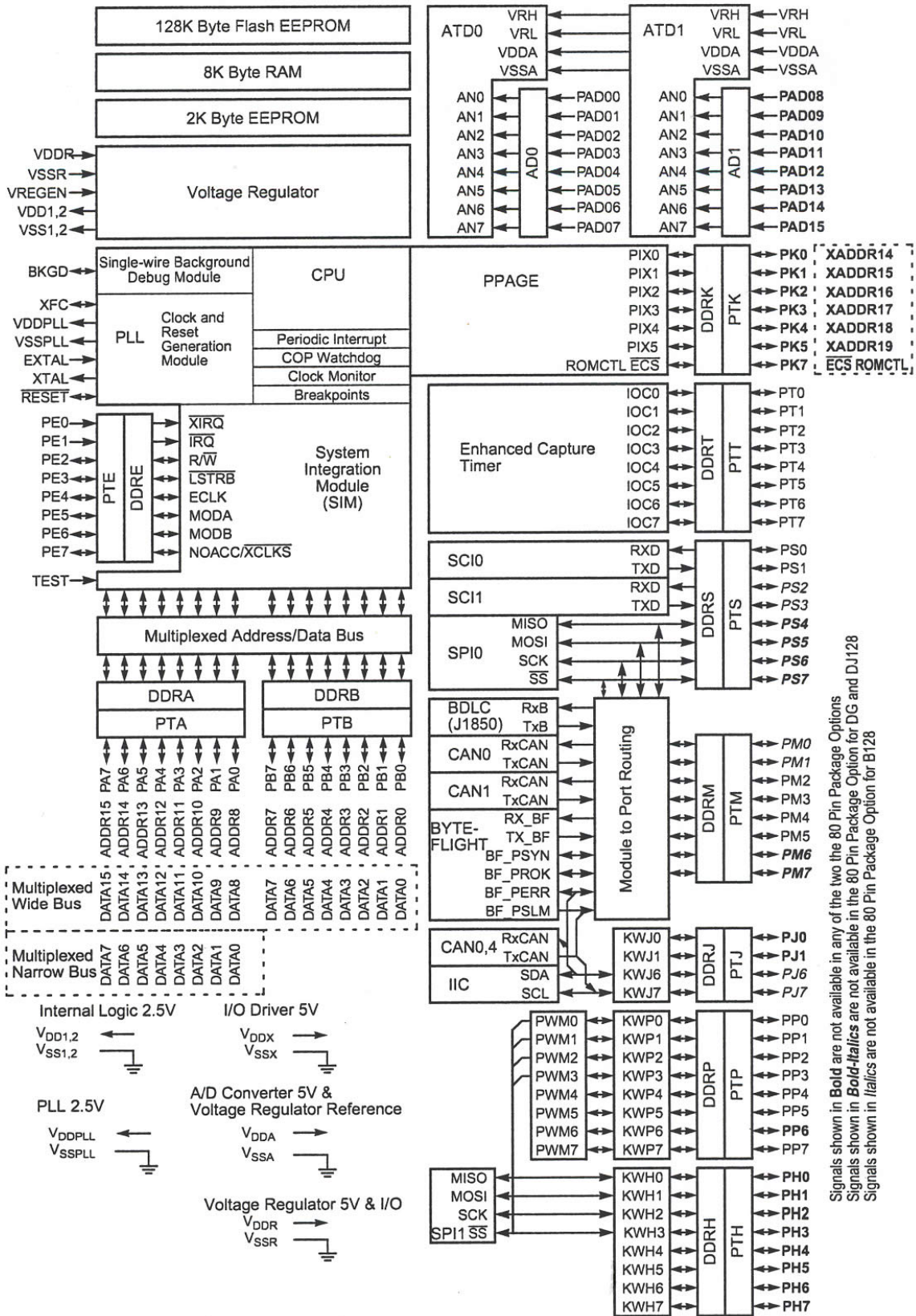


Figure 22: HCS12 Microcontroller Block Diagram; note, that block diagrams are family, not version specific. Some of the depicted subsystems are not implemented on the A128 version.

Digital Signal Processor

Introduction

Reference [11] gives a good introduction into the new field of digital signal processing and should be included to give a brief overview at this point.

“In the strict sense of the term, digital signal processing refers to the electronic processing of signals such as sound, radio, and microwaves. In practice, the same characteristics that make Digital Signal Processors (DSPs) so good at handling signals make them suitable for many other purposes, such as high-quality graphics processing and engineering simulations. DSPs are essentially super fast number-crunchers and just about any application that involves rapid numeric processing is a candidate for digital signal processing.

[...] At its heart, digital signal processing is highly numerical and very repetitive. As each new piece of signal data arrives, it must be multiplied, summed, and otherwise transformed according to complex formulas. What makes this such a keen technological challenge is the speed requirement. DSP systems must work in real time, capturing and processing information as it happens. Like a worker on a fast-moving assembly line, Analog-to-Digital converters and DSPs must keep up with the work flow. If they fall behind, information is lost and the signal gets distorted. The Analog-to-Digital converter, for instance, must take its signal samples often enough to catch all the relevant fluctuations. [...] The DSP, too, must keep pace, churning out calculations as fast as the signal data is received from the ADC. The pace gets progressively more demanding as the signal gets faster. [...]

DSPs differ from microprocessors in a number of ways. Microprocessors are typically built for a range of general purpose functions, and normally run large blocks of software, such as operating systems like UNIX. Microprocessors aren't often called upon for real-time computation. Usually, they are at liberty to shuffle their workloads around and choose their own course of action, waiting to finish a printing job, for instance, before responding to a user command. And though microprocessors have some numeric capabilities, they're nowhere near fleet enough for most DSP applications. Where a microprocessor is well-rounded and versatile, the DSP is a single-minded specialist, racing through a smaller range of functions at lightning speed. DSPs are often used as a type of "embedded controller," a processor that, accompanied by all necessary software, is built into a piece of equipment and is dedicated to a single group of tasks. In computer systems, DSPs may be employed as attached processors, assisting a general purpose host microprocessor.

One way to classify DSP devices and applications is by their dynamic range. The dynamic range is the spread of numbers, from small to large, that must be processed in the course of an application. It takes a certain range of values, for instance, to describe the entire waveform of a particular signal, from deepest valley to highest peak. The range may get even wider as calculations are performed, generating larger and smaller numbers through multiplication and division. The DSP device must have the capacity to handle the numbers so generated. If it doesn't, the numbers may "overflow," skewing the results of the computation. The processor's capacity is a function of its data width (i.e. the number of bits it manipulates) and the type of arithmetic it performs (i.e., fixed or floating point). A 32-bit processor has a wider dynamic range than a 24-bit processor, which has a wider range than 16-bit processor. And floating-point chips have wider ranges than fixed-point devices. Each type of processor is ideal for a particular range of applications. [...]

Just a decade and a half ago, digital signal processing was more theory than practice. The only systems capable of doing signal processing were massive mainframes and supercomputers and even then, much of the processing was done not in real time, but off-line in batches. [...] The first practical real-time DSP systems emerged in the late 1970s and used bipolar "bit-slice" components. Large quantities of these building-block chips were needed to design a

system, at considerable effort and expense. Uses were limited to esoteric high-end technology, such as military and space systems. The economics began to change in the early 80s with the advent of single-chip MOS (Metal-Oxide Semiconductor) DSPs. Cheaper and easier to design-in than building blocks, these "monolithic" processors meant that digital signal processing could be cost-effectively integrated into an array of ordinary products. The early single-chip processors were relatively simple 16-bit devices, which, teamed with 8- or 10-bit ADCs, were suitable for low-speed applications, neural-coders such as talking toys, simple controllers, and vocoders; (voice encoding devices used in telecommunications). [...] The company [Motorola] introduced the first 24-bit DSP56000 in 1987 and the first 16-bit single-chip ADC in 1989. These chips have since been joined by the 16-bit DSP56100 and DSP56800, 24-bit DSP56300 and DSP56600, 32-bit 96002, and together make up the first and only architecturally compatible line of 16-, 24- and 32-bit DSPs."

Component Selection

Motorola offers a variety of different DSP solutions. Some DSPs come as an integral on-chip part of a microcontroller. An example of such a DSP embedded controller is the 65800/E family. A major drawback is the limited I/O capacity. This is the reason why the ADCS core uses a host controller and an external DSP. No version of the 65800/E family has an I²C interface.

Another solution incorporating an external chip is the MSC7100 family which is a high-performance, cost-effective family of DSPs based on the StarCore™ SC1400. Devices in the MSC7100 family target high-bandwidth, highly computational DSP applications. Although suited for the application on the ADCS, all members of the MSC7100 family are packaged in a BGA (Ball Grid array). The same is true for the members of the MSC8100 family. The use of BGA on Compass-1 is prohibitive due to complex manufacturing techniques involved. The desired package type is one of the standard SMD (surface mounted device) packages. Ruling out all of the above DSP types the only one left is the DSP56300 family.

The DSP56300 Family

"The broad DSP56300 family is based on the DSP56300 core, a design integrating advanced features that dramatically boost performance, simplify system design, and drive system costs down. These devices are code-compatible with the DSP56000 Family of Processors.

The DSP56300 core family uses a high performance, single clock cycle per instruction engine providing a twofold performance increase over Motorola's popular DSP56000 core family, while retaining code compatibility. Significant architectural enhancements to the DSP56300 core family include a barrel shifter, 24-bit addressing, instruction cache, and DMA. The DSP56303 offers 100 MIPS using an internal 100 MHz clock at 3.0 to 3.6 volts. The DSP56300 core family offers a new level of performance in speed and power provided by its rich instruction set and low power dissipation, enabling a new generation of wireless, telecommunications, and multimedia products."

The selection of the DSP that will be used on the ADCS has to be made between the DSP56301 and the DSP56303 since the other members are highly specialized DSP not suited for the ADCS or incorporate the BGA packaging.

- The **DSP56301** is intended for general-purpose digital signal processing, particularly in multimedia and telecommunication applications, such as videoconferencing and cellular telephony.
- The **DSP56303** is intended for use in telecommunication applications, such as multi-line voice/data/fax processing, videoconferencing, audio applications, control, and general digital signal processing. It is also intended as a RAM-based emulation part for low-cost ROM-based solutions.

The major difference between the two components is the amount of external memory space and the bit size of the host device interface (HDI). 56301 supports a 32-bit PCI compatible interface whereas the 56303 has a 8-bit ISA compatible interface. Both components include a ESSI (enhanced serial synchronous interface) peripheral. It is intended to use this serial interface for communication with the host μ C. The 56301 has 9600kB data memory and 4800kB program memory access. The 56303 only 1536kB and 768kB, respectively. The latter one should more than satisfy the requirements with respect to the host μ C parametrics. The DSP56303 has been chosen for the ADCS of Compass-1.

High performance DSP56300 core

- 100 Million Instructions Per Second (MIPS) with a 100 MHz clock
- Object code compatible with the DSP56000 core
- Highly parallel instruction set
- Fully pipelined 24 x 24-bit parallel Multiplier-Accumulator (MAC)
- 56-bit parallel barrel shifter
- 24-bit or 16-bit arithmetic support under software control
- Position independent code support
- Addressing modes optimized for DSP applications
- On-chip instruction cache controller
- On-chip memory-expandable hardware stack
- Nested hardware DO loops
- Fast auto-return interrupts
- On-chip concurrent six-channel DMA controller
- On-chip Phase Lock Loop (PLL) and clock generator
- On-Chip Emulation (OnCE™) module
- JTAG Test Access Port (TAP)
- Address Tracing mode reflects internal accesses at the external port

On-chip memories

Program RAM, Instruction Cache, X data RAM, and Y data RAM size is programmable:

Program RAM Size	Instruction Cache Size	X Data RAM Size	Y Data Ram Size
4096 x 24-bit	0	2048 x 24-bit	2048 x 24-bit
3072 x 24-bit	1024 x 24-bit	2048 x 24-bit	2048 x 24-bit
2048 x 24-bit	0	3072 x 24-bit	3072 x 24-bit
1024 x 24-bit	1024 x 24-bit	3072 x 24-bit	3072 x 24-bit

192 x 24-bit bootstrap ROM

Off-chip memory expansion

- Data memory expansion to two 256 K x 24-bit word memory spaces
- Program memory expansion to one 256 K x 24-bit word memory space
- External memory expansion port
- Chip select logic requires no additional circuitry to interface to SRAMs and SSRAMs
- On-chip DRAM controller requires no additional circuitry to interface to DRAMs

On-chip peripherals

- 8-bit parallel Host Interface (HI08), ISA-compatible bus interface, providing a cost-effective solution for applications not requiring the PCI bus
- Two Enhanced Synchronous Serial Interfaces (ESSI)
- Serial Communications Interface (SCI) with baud rate generator
- Triple timer module
- Up to thirty-four programmable General Purpose I/O pins (GPIO), depending on which peripherals are enabled

Reduced power dissipation

- Very low power CMOS design
- Wait and Stop low power standby modes
- Fully-static logic, operation frequency down to DC
- Optimized power management circuitry

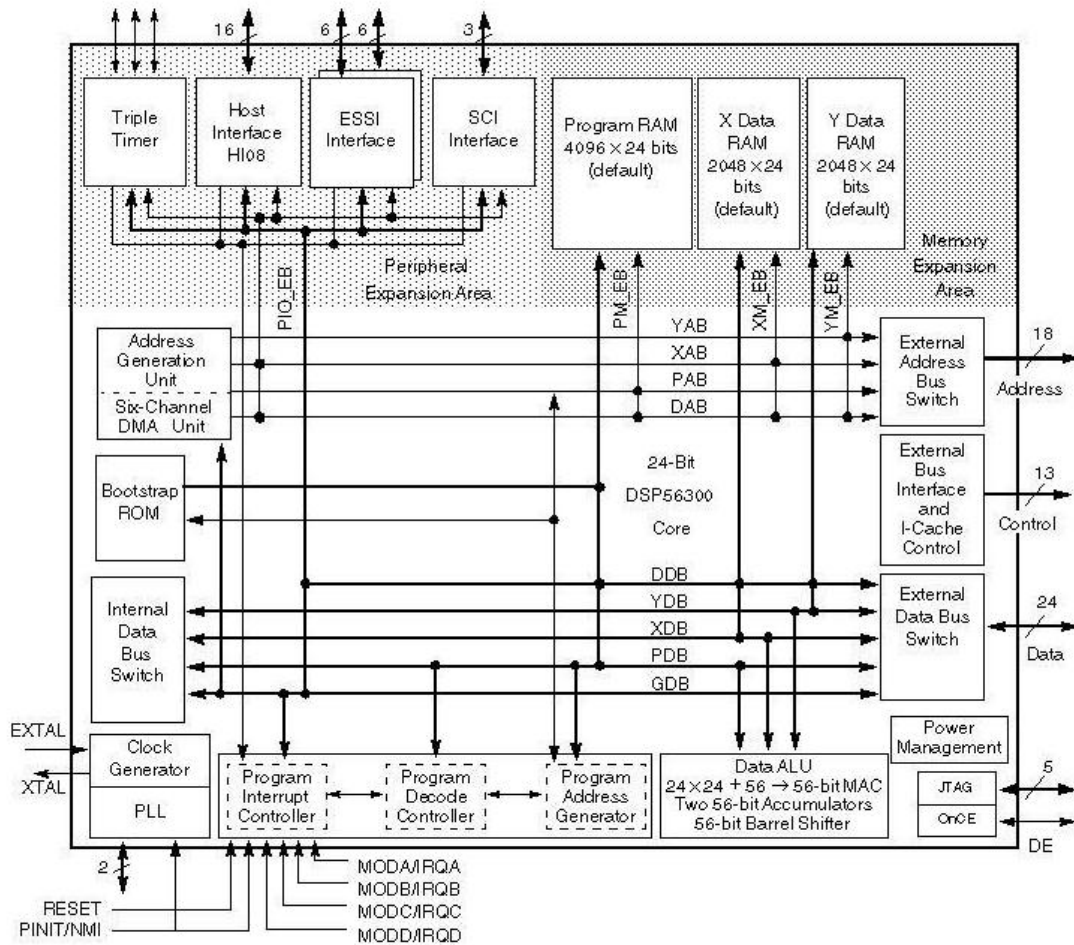


Figure 23: DSP56303 Block Diagram

System Budget Estimation

The budgets were established in the preliminary design study to share the restricted resources among the subsystems. Concluding the hardware section and with the chosen technical solution in mind, it is now possible to draft the estimated amount of mass and power consumption of the ADCS.

Mass Budget

The exceedence of the mass budget by 15% presented in table 14 states a minor problem. Some of the figures in table 14 are estimates. Weight reduction is a possibility to counteract the issue as well redistribution of mass budgets. The first solution tends to be complicated. Many components have a fixed mass, that cannot be altered. The magnetic coils have an optimized mass. Weight reductions might be possible in the harness design, the PCB shape and the redesign of the sun sensor PBC layout including its interface. If the over-weight causes immediate problems from the system engineering point of view these solutions will have to be investigated during development.

Table 14: Estimated ADCS Mass Budget; ‘others’ mainly means standard electrical components like resistors and capacitors

Item	Unit Mass (g)	Quantity	Mass (g)
Magnetic Coil	14	3	42
Coil Driver	4	3	12
GPS Receiver Board	22	1	22
GPS active Antenna	20	1	30
Connectors, Wires	10	1	10
MCU	3	1	3
DSP	3	1	3
Magnetometer	0,15	3	0,45
Sun Sensors	7,10	5	35,5
PCB	10	1	10
others	7	1	7
TOTAL			174,95
Assigned Budget			150
Margin			% -16,63

Power Budget

Table 15: Estimated ADCS Power Budget

Qty	Item	Voltage [V]	Current [mA]	Peak Power [mW]	Total Power [mW]
3	Magnetic Coil	5	39,25	196,25	588,75
1	GPS Receiver Board	3	210	630	630
1	GPS active Antenna	3	8	24	24
1	MCU	5	55	275	275
1	DSP	3	125	375	375
3	Magnetometer	3	1	3	9
5	SunSensor	3	9	27	135
TOTAL					2036,75
Assigned Budget					240

The summation of power dissipation is not a representative information, since not all of the listed components will be active at all times or to full extend. For instance, the coils will only be active during detumbling, slew and control modes. Not all of the coils will be saturated simultaneously. The GPS (including antenna) will only consume power during the safe mode and only for short periods of time. Also, there are numerous ways to reduce the system’s power consumption. The investigated approaches to reduce the overall power consumptions will be

- use of power-management features of electronic devices
- development of minimal duty cycles
- putting sensor components (sun sensors, magnetometers) off-line whenever possible

The ADCS Flight-Software

The flight software module of the ADCS subsystem must coordinate the component interaction, the communication with the CDHS, monitor the status of the subsystem and, last but not least, perform all calculations necessary to determine and control the spacecraft's attitude. The software development will be divided into two different major parts, the hardware related and the algorithm related. Hardware related means the interaction between the MCU and hardware components, e.g. reading sensor output. In total 12 (or 15) sensors making up 4 different sensor types (or 5, depending on whether the sun sensor PCB will be redesigned or not) with different software routines have to be handled. The PWM signal for the actuators are a separate module. 'Algorithm related' refers to all computations that remain within the core of the MCU/DSP, e.g. the control law and reference vector computation for attitude determination. The software will be written in a combination of assembly and C-Code. Assembly sections will mainly deal with low-level I/O routines, whereas the lengthy algorithms implemented on the system will be written in a high level language for shorter development time. The following sections will look at the software schemes that will run during the different modes of operation. Additionally, the data interface between the ADCS and the CDHS has been defined as a framework for further expansion in phase C.

Modes of Operation

Boot procedure/Detumbling

Once the ADCS MCU receives power from the EPS the boot procedure will be enabled. In microcontroller terminology this equals a 'Power-On-Reset'. As soon as the controller is booted and loaded with the operating system, the detumbling action can be performed. Detumbling means to compensate any rotational rates induced by the separation and deployment of the COM antennas. The P-POD specifications imply a worst-case initial tumbling rate of 0.1 rad/sec (that is 5.73 deg/sec) about at least one body axis. The accurate simulation of the tumbling scenario is yet to be performed but it is reasonable to assume that this phase of operation requires a maximum torque output related to a maximum power requirement. Consequently, the detumbling procedure has been tailored to minimize power demands of sensors and controller and maximum power supply to the actuators.

The detumbling procedure is initialized once the MCU sees 'first light', i.e. it is powered up for the first time. After a certain abort condition is achieved / detumbling is finished, the MCU will set itself into the normal control mode, where a more accurate control algorithm can compensate for minor rotations and point the satellite into a nadir pointing initial attitude. Before the controller starts the detumbling activities, an initial memory check will determine if the memory hardware and/or the software stored therein have been corrupted during launch. The test of ROM and RAM could be conducted using standard fault detection routines. The ROM test will incorporate a checksum procedure. If a checksum mismatch occurs, this error will be handled by informing the CDHS. To resolve the problem, three alternative countermeasures can be initiated:

1. the operating system (which is the complete flight software) can be reloaded via communication link from the ground station,
2. the operating system can be reloaded into FlashROM from an allocated ADCS FlashROM partition directly,
3. the operating system can be reloaded into FlashROM from a CDHS non-volatile ROM section indirectly.

All of the above options have advantages and draw-backs. The need to reload the entire operating system (or sections thereof) in a critical phase of the mission like the detumbling is very unpleasant. During severe, uncontrolled tumbling motion after separation, a working communication link cannot be guaranteed. This is less problematic for the second and third option, however, the memory demands will increase for the sake of software redundancy.

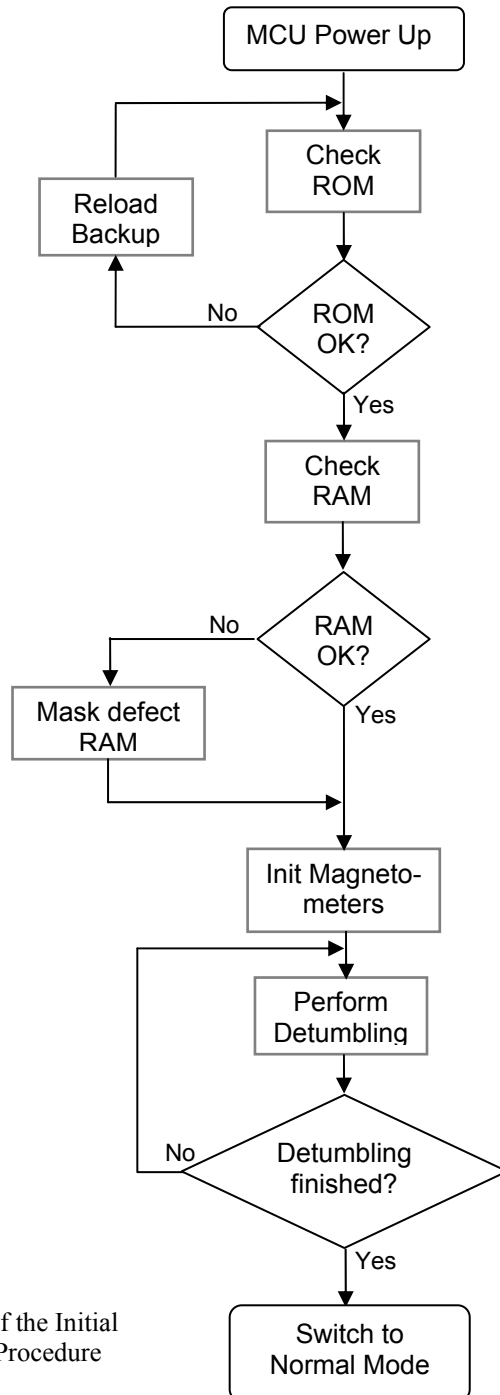


Figure 24: Flow Chart of the Initial Detumbling Procedure

An option is to store the operating system in a CDHS flash memory section which is intended for use during payload data storage. After the ROM is checked and possible error situations removed, this back-up software may be completely removed from the CDHS Flash memory. It would be even simpler to store a back-up copy of the flight software in a logically separated section of the ADCS Flash. Since the volume of the flight software machine code can not be

easily estimated at this point it remains unclear if sufficient ROM space is available for this option.

The ROM checksum routine must be performed every time the controller experiences a power-on-reset, that is during initial boot-up or in the event of an ADCS secondary boot-sequence (induced by a power-on-reset) after being forced into the Safe-Mode.

In case of a checksum-mismatch during a secondary boot-up at a later (non-tumbling) stage of the mission, the operating system must be reloaded into RAM.

The GPS system will not be active at any time during the boot-up and detumbling sequence. The detumbler does not require information of the orbital position and operating a power demanding system like the GPS during this critical phase is considered too efforty. The GPS will take its first readings once the detumbling is finished and the ADCS switched automatically into the normal mode for orbit propagator initialization and fine attitude adjustments.

Control Mode

The control mode utilizes the full-blown accurate control algorithm to keep the spacecraft within a certain range of a specified attitude. The normal control mode is only enabled as long as the CDHS permits the ADCS to operate. The attitude simulation has to make sure that a specific attitude can be reached in a steady-state fashion in the shortest possible time, such that the ADCS operation does not cover a major fraction of the overall mission time. A previous discussion described the process of requesting permission for a activation. This section deals with the logic flow of the flight software under normal control conditions. It is not intended to use the GPS in this mode. The position information necessary for attitude determination should evolve from computational medium-fidelity orbit propagation based on the most recent GPS reading taken during the safe mode.

Safe Mode

Under optimum conditions the safe mode will cover the major fraction of the mission time. During this mode, the ADCS operations will be reduced to a minimum in order to decrease the subsystem's power consumption. The attitude will be acquired in (larger) regular intervals for monitoring purposes only, i.e. no control action will be performed. The GPS will be active in this mode only. Position data will be taken in each interval and stored in ROM. Between the determination phases the sensors shall be powered down and the microcontroller power management features should be applied. Some of the digital sensors incorporate power-down modes. These will have to be carefully investigated and applied whenever possible.

As mentioned, regular attitude determination procedures will be performed for the purpose of monitoring the actual attitude. If the attitude angles exceed a certain range, which is yet to be identified as a result of the analysis, a request for activation is flagged to the CDHS. The decision whether or not the ADCS will be activated upon this request is under the authority of the CDHS.

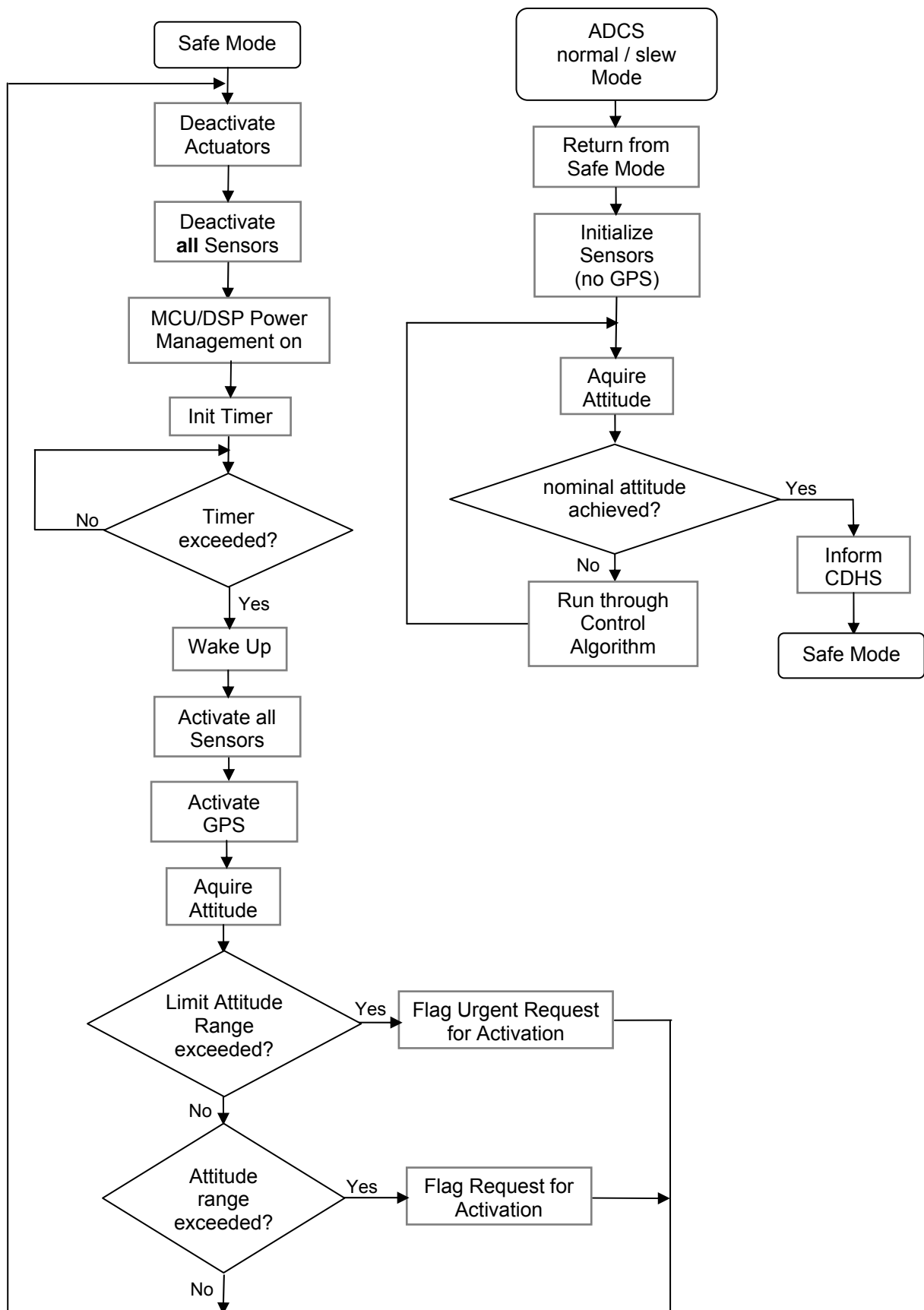
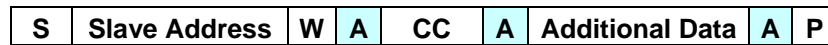


Figure 25: Flow Chart of ADCS Safe and Normal Mode operations

Communication between ADCS and CDHS

The I²C Data bus

Figure 26 shows the general protocol of data transmission on the I²C bus. Whenever the ADCS communicates with the CDHS, data will be transmitted using this standard format. Details on this format are explained in the CDHS section of the documentation and, in greatest detail, in reference [8].



S = Start
P = Stop
A = Acknowledge
W = Write
CC = Command Code

Figure 26: Data transmission protocol of the I²C bus

The Command Codes (CC)

The internal communications protocol on Compass-1 makes use of so called ‘command codes’ (CC). Each command is determined by its own 1-byte (8 bits) code. Upon reception of the code, the operating system of the respective subsystem must decode the command to initiate the appropriate reaction. The ADCS has data interfaces with the CDHS only. Refer to the CDHS section for a valid list of command codes.

Some commands / requests do not require additional data to be attached to the command code, like the ‘ADCS activate’ command. Others do require more or less long attachments of data, like the housekeeping data transmission and updated attitude parametrics.

As far as the operational concept is concerned, the ADCS will gather subsystem specific housekeeping data in regular intervals of two hours. This housekeeping data will be comprised of

- 5 sun sensor temperatures 5 bytes
- most recent attitude determination 4 bytes
- most recent position determination 3 bytes
- Timestamp 2 bytes
- ADCS status 1 byte

Total: 15 bytes

Assuming that each information is coded in a 8-bit byte this amounts to a total package size of 15 bytes. Packages will not be sent automatically but upon request from the CDHS. Further commands relevant to the ADCS are activation allowance, deactivation and slew parameters.

The ADCS can send data to the CDHS, request for activation and request for urgent activation. This is a security feature that will be implemented to omit repeated CDHS refusal to activate the ADCS. Not being able to control the attitude of the satellite can have a severe effect on the communication and image taking objectives, thus undermining the mission success. The ADCS determines the attitude in regular intervals. If the attitude is exceeding limit parameters (which have to be specified yet, but a reasonable value would be 15° on one

or more axes), the ADCS can issue an urgent request, represented by a different command code, which has a higher priority in the decision making procedure of the CDHS (refer to the priority list / ‘task manager’ in the CDHS section).

The Status Codes

The housekeeping data contains sensor readings as well as a status / health information. This information is important to keep track of the health of the subsystem. In the unpleasant case of subsystem failure, the status information contains a minimum amount of information to aid the evaluation of which problem caused the failure, in order to support a post-mission analysis.

The status of the ADCS is expressed by a code similar to the CC, called the status code (SC). Contrary to the CC, the SC cannot appear in the CC section of the data transmission protocol, obviously, but in the ‘additional data’ section. Furthermore, the SC will only be appended to the data string during a housekeeping request response. Similar to the CC, the SC contains a coded information. This information can be decoded on the ground station (and possibly the CDHS) in order to provide the operator with specific information about the current health status of the ADCS.

The status code summary in table 16 shows a preliminary set of codes referring to hardware problems only. This table will most likely be refined and expanded during the actual software development.

Table 16: ADCS Hardware Status Codes (SC)

Status Code	Description	Status Code	Description
0x00	ADCS nominal	0x10	Magmeter 1 damage
0x01	Coil 1 Damage	0x11	Magmeter 2 damage
0x02	Coil 2 Damage	0x12	Magmeter 3 damage
0x03	Coil 3 Damage	0x13	GPS damage
0x04	Controller Problem	0x14	open
0x05	Memory Corrupt	0x15	open
0x06	Sun 1 damage	0x16	open
0x07	Sun 2 damage	0x17	open
0x08	Sun 3 damage	0x18	open
0x09	Sun 4 damage	0x19	open
0x0A	Sun 5 damage	0x1A	open
0x0B	no T1 reading	0x1B	open
0x0C	no T2 reading	0x1C	open
0x0D	no T3 reading	0x1D	open
0x0E	no T4 reading	0x1E	open
0x0F	no T5 reading	0x1F	open

The status code is 1 byte (2 hex digits) in length, such that a total number of $16^2 = 256$ status codes must not be exceeded. This number will be sufficient to code all possible hardware and software malfunctions. SC’s ranging from 0x00 through 0x1F are reserved for hardware errors only, all other codes contain software status / error information. These will have to be added while the software is being written. The succeeding development phase documentation will contain a detailed description of the status codes and its exact implications for the subsystem’s operational status.

Conclusions

The definition phase results of the Attitude Determination and Control System design for the pico-satellite Compass-1 have been presented. The problems that must be faced when dealing with an entirely magnetic control of the spacecraft and their solutions have been presented in a comprehensive manner. The analysis tool for accurate and flexible attitude dynamics simulation has been described. Final analysis results are yet to be produced and implemented into the design of the actuator hardware, but design strategies are available already, such that the transition step from the analysis results to physical specifications will not be a major time issue in case of the magnetorquers. Other hardware components which are not primarily influenced by the attitude dynamics have been selected and presented with special attention paid to their interfaces. Also, a brief conceptual overview of the operating software design has been given. The results of the definition phase presented in this documentation are to be regarded as the precursor to the development phase. Hardware decision have been made and will not be altered unless technical obstacles can be avoided when incorporating a different hardware solution.

Outlook on future development challenges

More analytical work has to be done. The simulation tool described in the beginning of this documentation has to be extended to account for a wide range of mission scenarios and to aid the flight software design. In particular the determination branch of the simulation will have to be added. At the same time, the ADCS PCB will have to be designed using the information given in the hardware section of this document as a basis. This task will require additional research for appropriate connector solutions for the various internal and external interfaces of the system, with special consideration of reliability and weight. Also part of the electronics design task will be the design of the various fundamental electric components (like resistors, capacitors and inductances), e.g. for the coil driver low pass. However, it is expected that the major share of the electronics development phase will be spent on the hardware interfacing of MCU and the DSP of the ADCS. Important boundary conditions (design rules) received from the university electronics manufacturing unit will have to be obeyed for prompt and inexpensive manufacture of the PCB.

Once the hardware has been designed, development hardware has to be obtained and flight software modules designed and coded. It is crucial to carefully plan the software development in order to achieve a well-structured and comprehensible software lay-out. The better the software development is prepared, the more straight-forward will be the actual coding. Structuring the development will require the design of flow-charts for every coded subroutine, with the charts shown previously as a basis for development. It is intended to begin the software development with hardware level subroutines and, from there, to work up into the pure algorithm sections. Each routine will be coded at a time; software modules will be integrated at a later stage of the development and carefully tested for functionality and performance. In parallel, test will have to be conducted on a component level and, later on a subsystem level. At the end of the development an integration plan has to be established.

References

- [1] CubeSat Team Aachen, Phase A Study of Compass-1, Aachen, Germany, 2003
www.raumfahrt.fh-aachen.de
- [2] Sidi, M. J., Spacecraft Dynamics and Control, Cambridge Aerospace Series, 1997
- [3] Giesselmann, J., Software Documentation for the Attitude Determination and Control Simulation Tool – Verion 1.0, for the Compass-1 project, 2003
- [4] ECSS-E-10-04A, Space Environment, ESA-ESTEC, Noordwijk, The Netherlands
- [5] Weißgerber W, Elektrotechnik für Ingenieure, 5. Auflage, Vieweg & Sohn Verlagsgesellschaft mbH, Braunschweig/Wiesbaden,2000
- [6] Montenbruck,O. et al., A Miniature GPS Receiver for precise Orbit Determination of the Sunsat 2004 Micro-Satellite, DLR, Germany, 2004
- [7] Pederson, M. et al., Linear Two-Axis MOEMS Sun Sensor and the need for MEMS in space, International Astronautical Congress, Bremen, Germany, 2003
- [8] Philips Semiconductors, The I²C-Bus Specification, Version 2.1, January 2000
- [9] C.C.Bissel, Control Engineering, Second Edition, Chapman&Hall, London, 1994
- [10] R.C.Dorf, R.H.Bishop, Modern Control Systems, 7th Edition, Addison-Wesley, USA, 1995
- [11] Internet resource: Motorola semiconductor homepage
<http://e-www.motorola.com/webapp/sps/site/overview.jsp?nodeId=03M0ylgz6wYM0ym2yWDp>



2004-06-08

WBS430: COM

Communications System

Phase B: Detailed Definition

Author

Oscar Moreno

FH Aachen, Germany



Contents.....	70
Acronyms & Abbreviations.....	71
1. Introduction	72
2. Amateur Frequencies	73
3. Link Budget	74
3.1 Introduction.....	74
3.2 Basic Principle	74
3.3 Calculation of the Link Budget.....	75
3.3.1 Calculation of the Pass Loss.....	75
3.3.1 Calculation of Link Budget for Uplink	75
3.3.2 Calculation of Link Budget for Downlink	76
3.4 Summary	77
4. Telemetry, Tracking and Command (TT&C).....	77
4.1 Telemetry Subsystem.....	78
4.2 Command Subsystem.....	79
4.3 Tracking Satellite Position	80
5. Hardware	81
5.1 Antenna	81
5.1.1 Uplink Antenna	82
5.1.2 Downlink Antennas.....	82
5.1.3 Antenna Switcher	84
5.2 Transceiver.....	85
5.3 DTMF Chip.....	87
5.4 Terminal Node Controller (TNC)	88
5.5 Morse Code Transmitter	90
5.6 Modem	91
6. Software.....	93
6.1 AX25 Protocol	93
6.2 TNCs Programming	94

6.4 DTMF Configuration	95
------------------------------	----

References	96
-------------------------	-----------

Acronyms & Abbreviations

ADCS	Attitude Determination and Control
Bps	Bits per seconds
BPSK	Binary Phase-Shift-Keying
CDHS	Command and Data Handling System
CMOS	Complementary Metal Oxide Semiconductor
COM	Communication System
COTS	Commercial-Off-The-Shelf
CW	Continuous Waves
DARC	Deutscher Amateur Radio Club
DCE	Data Circuit Equipment
DTE	Data Terminating Equipment
DTMF	Dual-Tone Multi-Frequency
EPS	Electrical Power System
ESOC	European Space Operation Center
FHACC	Fachhochschule Aachen Control Center
FM	Frequency Modulated
FSK	Frequency-shift-keying
GSOC	German Space Operation Center
HF	High frequency system
HPA	High Power Amplifier
Hz	Hertz
I2C	Interface Bus
Kb	Kilobytes
LNA	Low Noise Amplifier
MCU	Micro Control Unit
MHz	Megahertz
mW	milliwatts
PIC	Programmable Interface Controller
PM	Post Meridian
PSK	Phase-Shift-Keying
RF	Radio Frequency
RX	Receivers

T/R	Transmitting /Receiving
TNC	Terminal Node Controller
TRX	Transceivers
TT&C	Telemetry, Tracking and Command
TX	Transmitters
V	Volts
W	Watts

1. Introduction

This communication subsystem is the gateway for the user/operator to the functionality of the satellite. Communication with the spacecraft takes place over two types of links:

The *uplink* carries commands from a ground station to the spacecraft. These commands are formed by uploads and redirected to the CDHS and then either processed immediately or stored and executed at a specified time.

The *downlink* carries data, which consists of two different types of information. One is image data generated by the payload. The other data is information about the spacecrafts vital characteristics, so-called housekeeping data. This is the total of all information for a specific time gathered by various sensors, e.g. temperature, voltage etc. Downloads usually have a much higher data rate than uploads. [1]

Users can send commands to the Compass-1 Pico satellite and get images and housekeeping data during its mission. It needs to be ensured that an image can be down-linked during a single access frame, which is at least around 10 minutes. Commands and Payload Data (images) are communications services that Compass-1 must be able to produce through its hardware and software facilities. Downloads and uploads are data bits of information; they have to be coded, digitalized, modulated, demodulated and transmitted. These bits need to be carried by components like modems, transceivers, antennas etc.

The following definition phase focuses on the onboard components and not so much on the ground segment. This subsystem is called COM and satellite communication literature and previous CubeSat projects will be the main resources to help choosing the most suited components to accomplish a sophisticated communication system for the Compass-1 Pico satellite.

Table 1: COM Constraints

Constraints
- Small size (no dimension larger than 10 x 10 cm ²)
- Power consumption for transmission < 2W

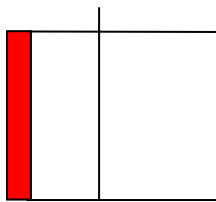
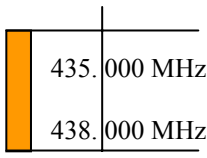
- Power consumption in standby < 160mW
- Mass below 130g
- Possible data: >1200/ 9600 bps
- Images: from 85 kB to 300 kB
- 3.0-5.0V Supply
- Industrial temperature range [-40..+85°C]
- I²C Interface desirable

Note: An integrated system solution (receiver and transmitter together: transceiver to save weight) as well as a separate system will be considered.

2. Amateur Frequencies

For this CubeSat project it is proposed to use amateur radio frequencies for the communication between the satellite and the ground station. The Compass-1 Project Team at the Aachen University of Applied Sciences plans to use 145MHz band for uplink and 435MHz band for downlink. According to the information from satellite radio amateurs, 435MHz has inherent advantages for the control of elevation and azimuth for data reception and tracking.

Table 2: German Amateur Frequency Regulation

Amateur Frequency Authorities	
Band plan 2m, 144 - 146 MHz	Band plan 70cm, 430 - 440 MHz
<p style="text-align: center;">145.800 V64 (6)</p>  <p>145.800-146.000 Amateur Satellites</p>	 <p>435.000 MHz 438.000 MHz</p> <p>435.000-438.000 Amateur Satellites</p>
by DARC VHF/UHF/SHF , 06/2000	

It is recognized that the amateur radio frequency band is open to the public for the following objectives:

The term “amateur radio service” means a radio communication service for the purpose of self-training, intercommunication and technical investigations carried out by duly authorized persons interested in radio technique solely with a personal aim and without pecuniary interest

(Article 3 of the Ordinance for Executing the Radio Law), as defined in the Radio Regulations of the International Telecommunication Union. [2]

On the Compass-1 Picosatellite, amateur frequency bands shall be used for the following objectives:

Anyone, who holds amateur radio equipments and the appropriate license, can send commands to the Compass-1 Picosatellite and get images and housekeeping data during its 11 minutes frame flight. Thus, data can be shared, discussed and analyzed with hams around the world.

It will be difficult to identify the orbital parameters of the Compass-1 Picosatellite immediately after launch. Thus, in order to track the on-orbit satellite, it is important and valuable to ask the ham network for assist in tracking the satellite as well as using it.

Communication and educational demonstrations will be conducted between the Compass-1 Picosatellite and the ground station using the well-known communication protocol (AX.25) and DTMF tones.

Giving the opportunity to students to be involved in amateur satellite tracking will motivate them to go forward into TT&C applications in order to increase interest in European and German Space Centers (ESOC, GSOC, etc.)

3. Link Budget

3.1 Introduction

In this Phase B documentation the planned equipment of the FH Aachen Ground Station as well as by Compass-1 are determined whether the planned components are sufficiently dimensioned for a safe data exchange. For this calculation a Link Budget has to be established.

3.2 Basic Principle

For the calculation of the link budget (simplified) the following components must be considered:

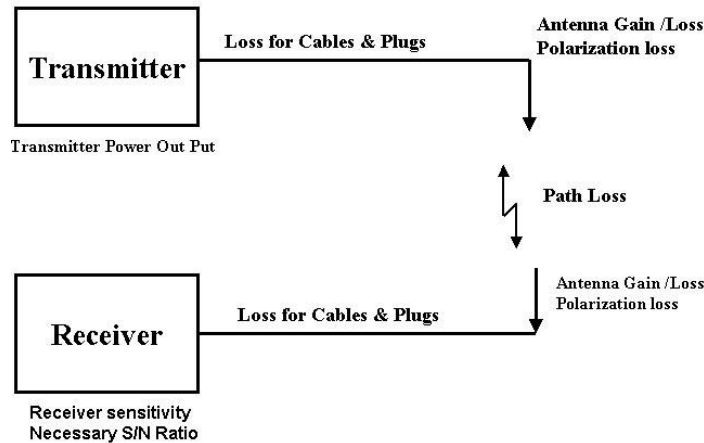


Fig.1: Link Budget

The calculation of link budgets for commercial satellite systems, which usually operate in the GHz range, is substantially more complex, since further factors have to be added. For the intended frequency ranges (145MHz and 435MHz) these values are sufficiently dimensioned.

The link budget substantially depends on the hardware components such as transmitters, receivers, cables and antennas. The path loss essentially depends on the distance between Compass-1 and the FH Aachen ground station, as well as of the used frequencies, according to the following equation: [3]

$$L (db) = 32.45 + 20 \log f (MHz) + 20 \log d (km)$$

3.3 Calculation of the Link Budget

3.3.1 Calculation of the Pass Loss

for $f = 145$ MHz, $d = 800$ km (closest point, 90 degrees zenith):

$$L = 32,45 + 20 \log 145 + 20 \log 800 = 32,5 + 43,2 + 58,1 = \mathbf{133,8 \text{ dB}}$$

for $f = 145$ MHz, $d = 3000$ km (farthest point, close to horizon):

$$L = 32,45 + 20 \log 145 + 20 \log 3000 = 32,5 + 43,2 + 69,5 = \mathbf{145,2 \text{ dB}}$$

for $f = 435$ MHz, $d = 800$ km (closest point, 90 degrees zenith):

$$L = 32,45 + 20 \log 435 + 20 \log 800 = 32,5 + 52,8 + 58,1 = \mathbf{143,7 \text{ dB}}$$

for $f = 435$ MHz, $d = 3000$ km (farthest point, close to horizon):

$$L = 32,45 + 20 \log 435 + 20 \log 3000 = 32,5 + 52,8 + 69,5 = \mathbf{154,8 \text{ dB}}$$

3.3.1 Calculation of Link Budget for Uplink

The calculations are based on the design presented in figure 1. The losses for cables and plugs are roughly estimated and rounded up. [4]

Table 3: Uplink Budgets

Item	Value
Output Power transmitter 100 Watt	+ 20 dB _W
Loss of 35m RG-214 Cable for 145 MHz	- 1.5 dB

plugs and wattmeter Loss	- 1 dB
Antenna gain on Dipole	+ 10.4 dBd
parallel connection Cross Yagi Loss	- 3 dB
Polarizations error circular/linear Loss	- 3 dB
Path loss	-133.8 dB (800), -145.2 dB (3000 km)
Antenna gain on Dipole	0 (Dipole), -3 dB (Monopole)
Cable & plug loss	-1 dB
Expecting power at the receiver	-112.9 dB_W / -127.3 dB_W

dB_W in Volts corresponds to:

- 20 μV for 800 km, Dipole
- 3 μV for 3000 km, Monopole

The sensitivity of the 2m-Receiver of approx. 0.5 μV 10dB S/N is deemed good enough for the expected Uplink.

3.3.2 Calculation of Link Budget for Downlink

The calculations are based on the design presented in figure 1. The losses for cables and plugs are roughly estimated and rounded up.

Table 4: Downlink Budgets

Item	Value
Output Power transmitter	+ 0 dBW (1W) , -10 dBW (100 mW)
Cable & Plugs Loss	- 1.0 dB
Antenna gain on Dipole	0 dB (+2 dB to lamda/4 distance)
Polarizations error circular/linear Loss	0 dB
Path loss	-143.7 dB (800), -154.8 dB (3000 km)
Antenna gain on Dipole	+ 16.5 dBd
Loss of 35m RG-214 Cable & Plugs until Preamplifier	- 1 dB
Preamplifier Gain	0*
Loss of AIRCOM 35 Cable for 435 MHz	0*
Cable & plug loss	0*
Expecting power at the receiver	-129.2 / -140.3 / -139.2 /-150.3 dbW

The gain and loss of the preamplifier and the cable are not included here; the preamplifier brings about 10.20 dB and thus bridges the cable absorption of the 35m-AIRCOM-Cable and plug, but does not improve the S/N ratio substantially. However, the latter is selected for the quality of reception.

dB_W in Volts corresponds to:

- 2.5 μV for 800 km 1W-Receiver, or
- 0.7 μV for 3000 km 1W-Receiver, or
- 0.8 μV for 800 km, 100 mW-Receiver, or
- 0.2 μV for 3000 km, 100 mW-Receiver

3.4 Summary

The following planned components for the ground station and COMPASS-1 should ensure a safe data transfer for 1200 bps on AX.25 with 1W transmitting power and optimized antennas. 300mW out power will be used for the data DJ-C5 transmitter. The probabilities of reception have not been computed in detail yet; these values have been compared with link budgets of other amateur radio satellites and will be updated and improved continuously regarding eventual modifications and new specifications of the parts.

4. Telemetry, Tracking and Command (TT&C)

The Telemetry, Tracking and Command (TT&C) systems support the function of spacecraft management. These functions are vital for successful operation of Compass-1 and treated separately by the communication management. The main functions of a TT&C system are to: [5]

- monitor the performance of all Compass-1 subsystems and transmit the monitored data to the FH Aachen Control Center (FHACC) and ham stations
- support the determination of orbital parameters
- provide a source to earth stations for tracking
- receive commands from FH Aachen Control Center for performing various functions of the satellite.

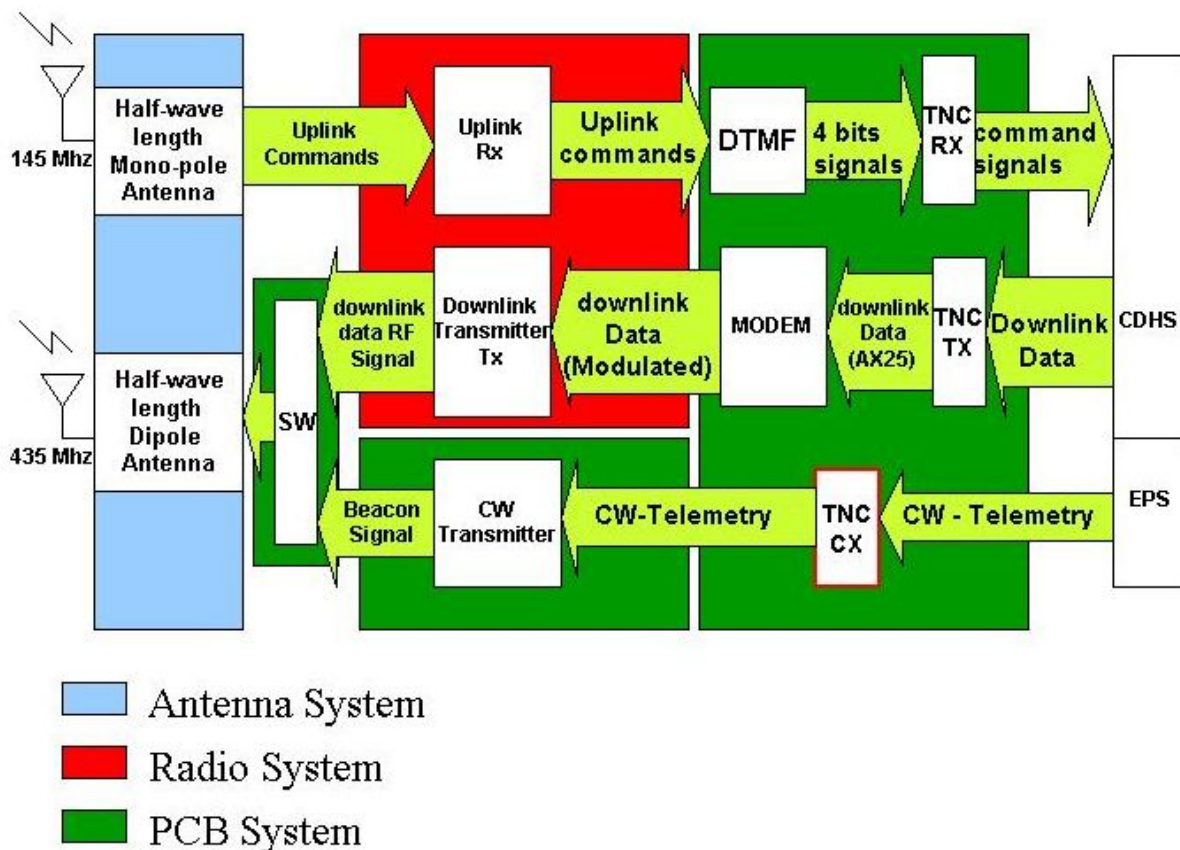


Fig. 2: Block Diagram

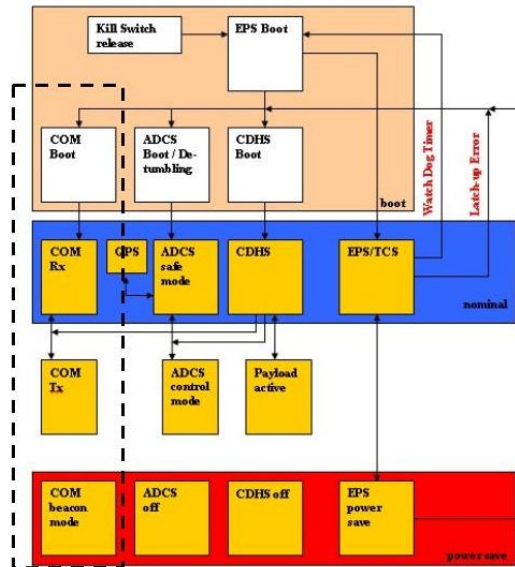


Fig.3: COM modes

4.1 Telemetry Subsystem

The function of the Telemetry subsystem is to monitor various spacecraft parameters such as voltage, temperature and equipment status, and to transmit the measured values to the FHACC and ham stations. The telemetry data will be analyzed at the FHACC and used for routine operational and failure diagnostic purposes. Initially the following parameters will be monitored: [5]

- a. battery voltage, battery current, battery temperature, bus voltage, solar cell voltage, uplink command, FM transmitter power, protocol and maybe more
- b. outputs from attitude sensors

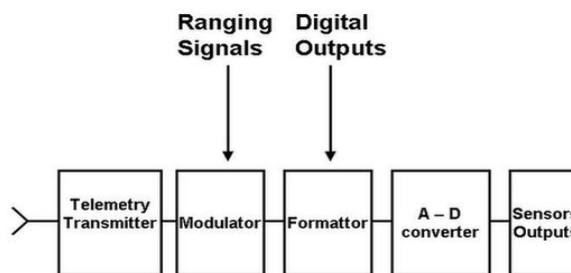


Fig. 4: The main elements of a telemetry subsystem

Figure 4 shows the main elements of a telemetry subsystem. The monitored signals are all multiplexed and transmitted as a continuous digital stream. Several sensors provide analog signals whereas others give digital signals. Analog signals are digitally encoded and multiplexed with other digital signals, typical telemetry streams are in the range of 150-100 bps. For low-bit rate telemetry a sub-carrier modulated with frequency-shift-keying (FSK) or phase-shift-keying (PSK) is used before RF modulation. It is vital that telemetry information is available at the FHACC; therefore a redundant chain among more ham ground stations is can improve reliability. Distributed telemetry systems are being favored. Digital encoders will be located in each subsystem of COMPASS-1-1 and data from each encoder are sent to a central encoder via a common I²C bus. This scheme reduces the number of wire connections

considerably. This type of modular design also permits easy expansion of the initial design and facilitates testing during assembly of the Compass-1.

Table 5: Preliminary Housekeeping for Compass-1 [6]

#	Parameter	Value
1	Data Acquisition Time:	2005/05/19 17:36 CET (GMT+2) (example)
2	COMPASS-1 Internal Time:	
3	Battery Voltage:	V
4	Percentage of Battery Remaining Quantity:	
5	Charging Current:	mA
6	Current Consumption of Communication System:	mA
7	Solar Array Voltage:	V
8	Solar Array Current:	
9	Side 1 (No solar array here)	0
10	Side 2	mA
11	Side 3	mA
12	Side 4	mA
13	Side 5	mA
14	Side 6	mA
15	Temperature	
16	Side 1 (No solar array here)	0
17	Side 2	deg
18	Side 3	deg
19	Side 4	deg
20	Side 5	deg
21	Side 6	deg
22	Battery:	deg
23	Transmitter:	deg
24	Uplink Counter:	?
25	Camera Counter:	?
26	SEL Counter:	?
27	CW Duty Ratio:	?

4.2 Command Subsystem

The Command system receives commands transmitted from FHACC, verifies reception and executes these commands. A preliminary command list is:

Table 6: Command & Data Agenda

From	To	CC	Additional Data	Description
COM	CDHS	0x56	-	Request housekeeping data
COM	CDHS	0x55	3 Byte	Send slew command to ADCS
COM	CDHS	0x54	1Byte	Request for image number X
COM	CDHS	0x53	-	Request for image capturing

Typically, over 300 different commands could be used on a communication satellite but it is not the case for Compass-1. Commands have to be decoded and executed correctly.

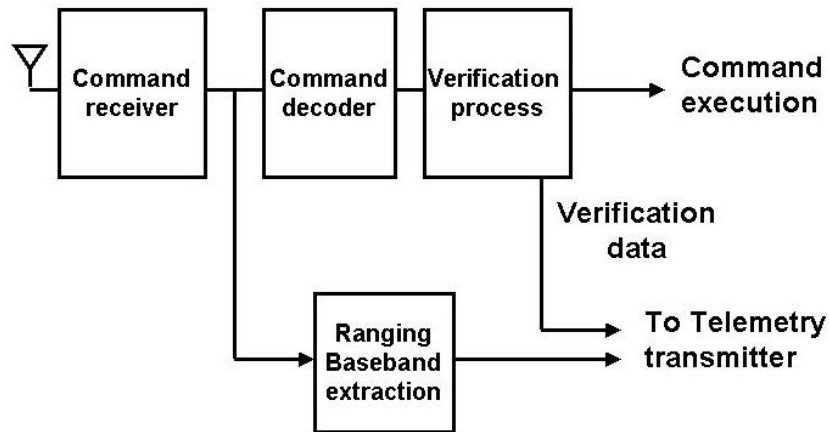


Fig. 5: The main blocks of a command system

A fail-safe operation has to be achieved under low carrier to noise conditions (typically 7..8 dB). A commonly used safety feature will demand verification of each command by FHACC before execution. To reduce the impact of high-bit error rate, coding and repetition of data will be employed. Typical bit rates are around 100 bps. A command decoder the commands this is followed by a verification process. This is known as a Digipeater, which usually involves the transmission of the decoded commands back to the FHACC via telemetry carrier. The command is stored in a memory and is executed after verification. The command system hardware is duplicated to improve reliability. The tele-command receiver also provides the baseband which is modulated on the telemetry beacon and transmitted back to FHACC.

4.3 Tracking Satellite Position

To monitor Compass-1 in its assigned orbital slot and provide view angle information to ham earth stations it is necessary to estimate the orbital parameters regularly. The orbital parameters can be obtained by tracking the satellite from the ground and measuring the angular position and range of the satellite. A monopulse technique will be used for angular tracking. Angular positions measured through FHACC are adequate for the determination of orbital parameters. The round-trip time delay of a signal will be measured. This is achieved by transmitting a signal modulated with a tone. This signal is received by the spacecraft and demodulated in the command receiver; the tone is then remodulated and transmitted back to the ground on the telemetry carrier. The time delay is obtained by measuring the phase difference between the transmitted and received tones; this can be more than 360°, leading to errors in multiples of tone period. Additionally Compass-1 will carry a GPS receiver from German Aerospace Center (DLR).

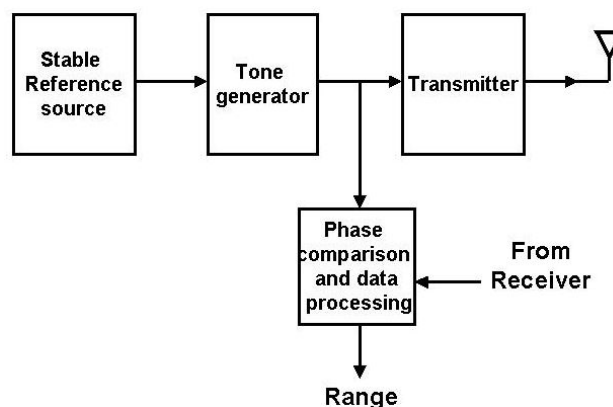


Fig.6: The main blocks of a multitone ranging system

5. Hardware

5.1 Antenna

Antennas are essential components on a satellite. They are the interface between free-space and electronic devices. Their purpose is to provide a transition from a guided wave on a transmission line to a free-space wave and vice versa in the receiving case. If the antennas fail to work the satellite can be considered dead. To establish a communication link between satellite and ground station even in conditions where the position and attitude of the spacecraft is not exactly known, an antenna with a broad beamwidth must be designed. Furthermore, no pointing mechanism on board the satellite can be provided for the antenna. Thus, parabolic dishes and other narrow-beam devices are not applicable. Antennas that theoretically radiate equally in all directions are called omni-directional. The disadvantage is that those antennas require much more power than directional antennas. A reasonable compromise between large beamwidth and available power is a monopole antenna.

A radio transmitter emits a power P_t equally in all directions (isotropic). At distance d from the transmitter the transmitted power is distributed equally on the surface of a sphere with radius d and area $4\pi d^2$. The flux density in W/m^2 of an isotropic radiating antenna at distance d is therefore: [5]

$$S = \frac{P_t}{4 \cdot \pi \cdot d^2}$$

Any physical antenna will have some directivity, i.e. ability to concentrate the emitted power in a certain direction. Thus, less than the full surface area of the sphere is “illuminated”, i. e. less than 4π steradian of solid angle. The ratio between the full 4π steradian spherical coverage and the actually illuminated solid angle Ω is called the directivity and assumes that power is evenly distributed over Ω and zero outside. The “antenna gain” G_t is the ratio of flux density in a specific direction at distance d and the flux density from the same transmitter using a hypothetical isotropic antenna.

The receiving antenna is assumed to have an “effective area” which “collects” the radio waves by intercepting the flux of electromagnetic energy. This means that the receiving antenna collects the total power $P_r = S \cdot A_r$.

A receiving antenna has an antenna gain in the same way as the transmitting antenna. The relationship between the antenna gain and the effective area is given by:

$$A_r = \frac{\lambda^2}{4\pi} \cdot G_r$$

$\lambda = c/f$ is the wavelength of the transmitted signal also known as the carrier
 c is the velocity of light (and radio waves) in vacuum, $c = 2.99792458 \cdot 10^8$ m/s.
 f is the frequency of the carrier.

It can be shown theoretically that the transmitting and receiving antenna gain is the same for the same antenna at the same frequency.

For Compass-1, a reliable and simple solution for the antenna design must be found. Dipole and monopole antennas for downlink and uplink respectively are the most common and successful antenna option and comply best with the design philosophy. The difficulties that have to be mastered are to find an optimum antenna configuration. The antennas will have to be stored in a launch configuration during the launch and deployed after separation from the launch vehicle. [1]

5.1.1 Uplink Antenna

A monopole is a dipole that is divided in half at the center feed point and fed against the ground plane. The currents and charges are the same as the half of the dipole, but the terminal voltage is only half of the dipole. This antenna is one of the simplest and most common antennas. This antenna will be mounted on Compass-1 and its function will be to receive uploads from ground.

Table 7: Uplink Antenna

	Freq. (MHz)	Antenna length (mm)	Antenna width
Uplink Commands	144MHz Band	¼ wavelength (500)	~ 4mm

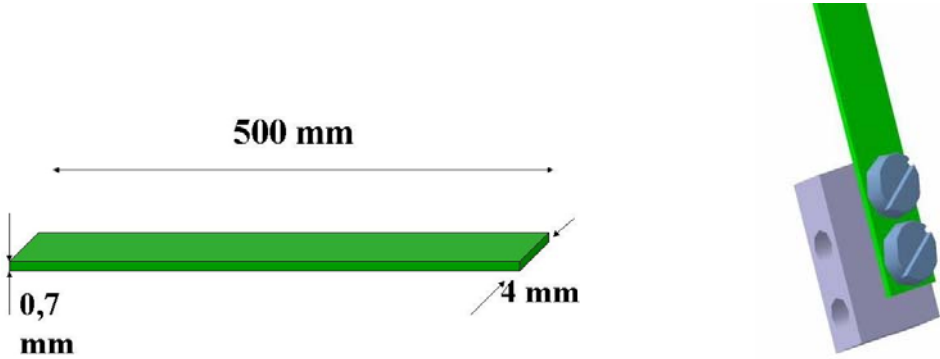


Fig.7: Uplink Monopole Antenna

5.1.2 Downlink Antennas

A half-wave dipole antenna is a straight electrical conductor of steel connected at the center to a radio-frequency (RF) feed line. The dipole is inherently a balanced antenna, because it is bilaterally symmetrical. It is also omni-directional. The length of the dipole antennas is a quarter of the wavelength; it will be built from two metal tapes of 175 mm each, one for the 435Mhz band for downlink data and beacon data. The dipole antenna has its best RF link when the transmitting and the receiving antennas are parallel to each other. In any other cases the performance decreases. In addition, along the axis of the dipole there is no signal radiation. In this case the received signal is zero.

Table 8: Downlink Antenna

	Freq.	Antenna length	Antenna
--	--------------	-----------------------	----------------

	(MHz)	(mm)	width
Downlink Data and Housekeeping, Morse Code Data	435MHz Band	$\frac{1}{4}$ wavelength (175)	~ 4 mm

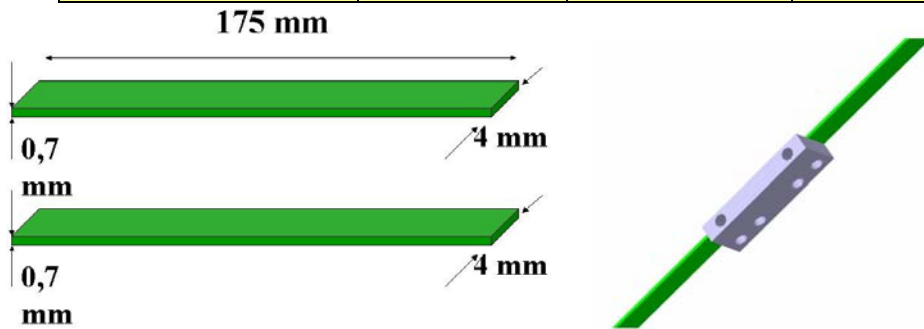


Fig. 8: Dipole Antenna for Downlink and Morse Code Data

A preliminary antenna pointing test was conducted in February 2004 at the Communication Laboratory at FH Aachen in order to gain a basic idea of possible antenna configuration. This test brought enlightening results and helped to visualize general antenna capabilities and placement options. Similar testing will be done in phase C/D.



Fig. 9: Dipole and Monopole Antennas Test at FH Aachen

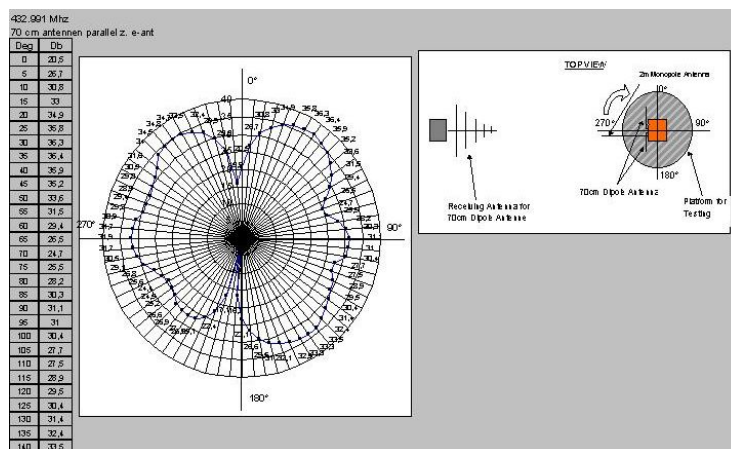


Fig. 10: Antennas Test Results at the FH Aachen

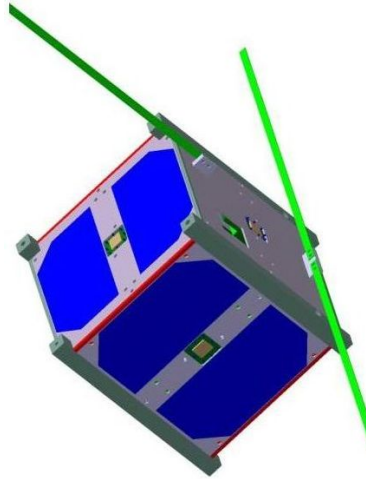


Fig. 11: Preliminary Antenna Configuration

5.1.3 Antenna Switcher

An antenna switcher is required to switch between payload data and Morse code data. M/A-COM's SW-425 has been selected. This is a GaAs monolithic switch in a low cost SOT-26 surface mount plastic package. The SW-425 is ideally suited for applications where very low power consumption ($<10\mu\text{A}@5\text{V}$), low intermodulation products and very small size are required. Typical applications include Internal/External antenna select switch for portable telephones and data radios using dipole antennas. In addition, because of its low loss, good isolation and inherent speed, the SW-425 can be used as a conventional T/R switch or as an antenna diversity switch. The SW-425 can be used in power applications up to 3 watts and is suited for analog/digital wireless communications. [7]

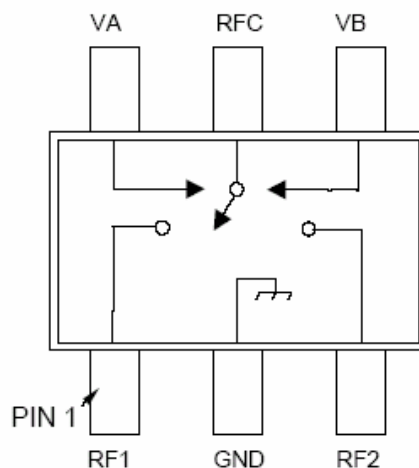
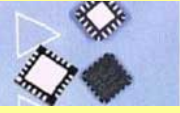




Fig. 12: Antenna SW-425 Switcher

Table 9: Antennas Dealer

Hardware	Quantity	Manufacturer/ Dealer	Weight (g)	Part Number	Description	Picture
Switcher	2	www.macom.com/ Tyco Electronics AMP GmbH		SW-425 PIN	Low Cost Plastic SOT-26 Package, Low Insertion Loss <0.6dB @ 1900 MHz, Low Power Consumption <20µA @ +3V, Very High Intercept Point: 53 dBm IP3, Both Positive and Negative 2.5 to 8 V Control	
Antennas	1(2m) 500 mm	www.conrad.de	4	Nr.: 540706 - 14	-80 to +540 °C Material: SteelTyp 316	
	1(70cm) 175 mm	www.conrad.de	3	Nr.: 540706 - 15	L681 x 3,6W x 0,3H (mm)	

5.2 Transceiver

Amateur radio mark offers an abundance of transmitters (TX), receivers (RX) and transceivers (TRX) with high operator comfort. For the ground control station these components can be taken easily, since they are available for a low price. For the employment in the Compass-1 these COTS components are not less suitable; however, these COTS should resist the following requirements:

- Mechanical maximum stress (vibrations during rocket launch)
- Mechanical dimensions (Compass-1 10x10x10 cms)
- Electronic reliability (cosmic radiation)
- Maximal energy consumption

It is intended to build very simple home-made transmitters and receivers which do not possess redundant comfort. Experienced amateur radio operators or companies like Alinco, Icom, Kenwood and Yaesu, who are specialized in the development and the production of such amateur radio components have proved to be supportive. These COTS products can be stripped from unnecessary equipment like speakers, antenna, display and cover. The remaining device (PCB) will have a sufficiently small size for integration into the CubeSat structure.

The high-frequency system (HF) for Compass-1 is conformed by:

- Receiver 145 MHz (2-Meter-Amateur radio- range), for the reception of control Commands of Dual-Tone Multi-Frequency DTMF
- Transmitter 435 MHz, for the transmission of data by means of AX.25-Protocol being the most critical device for the Compass-1 mission due to its high power-out
- Transmitter 435 MHz, 100mW of power-out for telemetry data in Morse code

The transceiver is a combination of a transmitter and a receiver as the name indicates. The transmitter part is needed because the signal from the carrier phase modulator is too weak for transmission. Therefore, power amplification is required. Basically there are two types of amplifiers: solid-state and traveling wave tube. Although the output of the latter one is higher, solid-state amplifiers succeed in size and weight. They are called HPA (high power amplifier). The output from the power amplifier is filtered and passed to the antenna for transmission. The receiver works vice-versa. The signal from the antenna is amplified and filtered to provide a stronger input signal to the demodulation process. The abbreviation for this component is LNA (low noise amplifier).

An important objective is that amateurs with satellite ground stations will be able to simply and inexpensively decode telemetry data from Compass-1 and forward that data to FHACC. Consequently, only a single transceiver and antenna are required. Specifically, two modified Alinco DJ-C5T identical transceivers, [8] shown in figure 13 and 14, are used to provide redundancy and the command computer alternates between these transceivers on each communications cycle. These radios are inexpensive, low power (300mW RF Output), and extremely small.



Fig.13: Alinco DJ-C5T Transceiver



Fig.14: Alinco DJ-C5T Transceiver Comparison

Initially, a bandwidth of 9600bps was considered due to expected high data rate requirements, resulting from a large quantity of data to be transmitted (300kb images). Furthermore, it was desirable to reduce transmission times by increasing data rates.

Unfortunately an adequate 70cm COTS transceiver for 3V-5V supply has not yet been found. A 1200bps bandwidth has been chosen due to the availability of COTS devices on the market. A 9600 bps 70cm transceiver could be investigated later if time and more resources are provided. At the same way a new modem for 9600 bps must be selected.

Table 10: Transceiver Dealer

Hardware	Quantity	Manufacturer/Dealer	Weight (g)	Part Number	Description
Transceiver	2(Engineering Models)	ALINCO/ www.boger.de	35	DJ.-C5T	VHF TX:144~147.995 MHz RX:118~173.995 MHz UHF TX:420~449.995 MHz RX:449.995 Mhz

5.3 DTMF Chip

DTMF stands for *Dual-Tone Multi-Frequency*. That is, a DTMF signal is one that consists of the sum of two pure sinusoids at valid frequencies. Compass-1 can be commanded to provide a bulk data dump while within range of an authorized ground station.

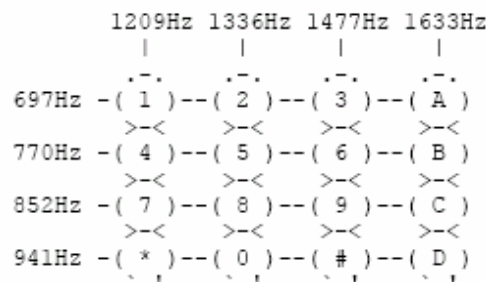


Fig.15: Frequencies that compose the tones

In DTMF, the tone '8' is represented by the sum of 852 Hz and 1477 Hz sinusoids. A significant reduction in volume, mass, and power consumption is achieved by generating DTMF tones in software. This innovative approach eliminates the need for a hardware terminal node controller or modem. The used microcontroller has built-in functions for providing DTMF and single-tone signals from any digital output. Only a simple RC filter and attenuator circuit are required to deliver the audio signal to the microphone input of the transceiver. DTMF is used to transmit command data. Compared to modern digital modes, DTMF is extremely slow, clocking at an equivalent data rate of 60 bits per second. [9]

The California microdecoder CM8870 DTMF for command control provides full DTMF receiver capability by integrating both the band-split filter and digital decoder functions into a single 18-pin DIP, SOIC, or 20-pin PLCC package. The CM8870 is manufactured using state-of-the-art CMOS process technology for low power consumption (35mW, max) and precise data handling. The filter section uses a switched capacitor technique for both high and low group filters and dial tone rejection. The CM8870 decoder uses digital counting techniques for the detection and decoding of all 16 DTMF tone pairs into a 4-bit code. This DTMF receiver

minimizes external component count by providing an on-chip differential input amplifier, clock generator, and a latched three-state interface bus. The on-chip clock generator requires only a low cost TV crystal or ceramic resonator as an external component. [10]

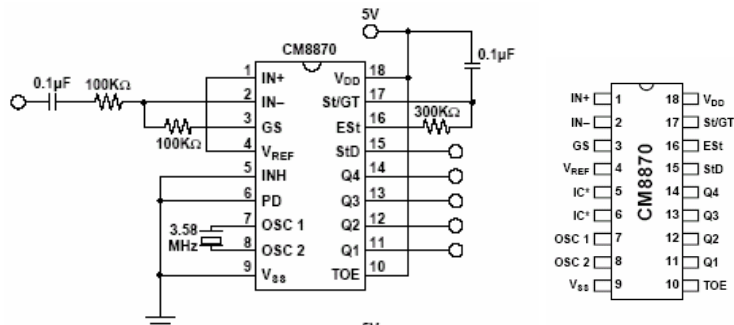


Fig. 16: DTMF M8870 Decoder

Table 11: DTMF Dealer

Hardware	Quantity	Manufacturer/Dealer	Weight (g)	Part Number	Description	Picture
DTMF Chip	2	California Micro Devises/ www.dema.net		CM8870PI	All voltages referenced to VSS, VDD = 5.0V ±5%, TA = -40°C to +85°C, fCLK = 3.579545 MHz	

5.4 Terminal Node Controller (TNC)

Most amateur satellites require a specialized Terminal Node Controller (TNC) to correctly modulate the digital signal. A TNC is a microcontroller, previously also introduced as micro control unit (MCU). Two TNCs will be used. TX-TNC takes Telemetry data from CDHS and packetizes it into an AX25 format and The RX-TNC decodes DTMF 4 bits signal to command signals and sends these signals to CDHS. CW-Generator send Morse coded beacon data by controlling the KEY of the CW Transmitter. It CW-TNC will be installed as an extra device but CW-data will be delivered from Electrical Power System (EPS).

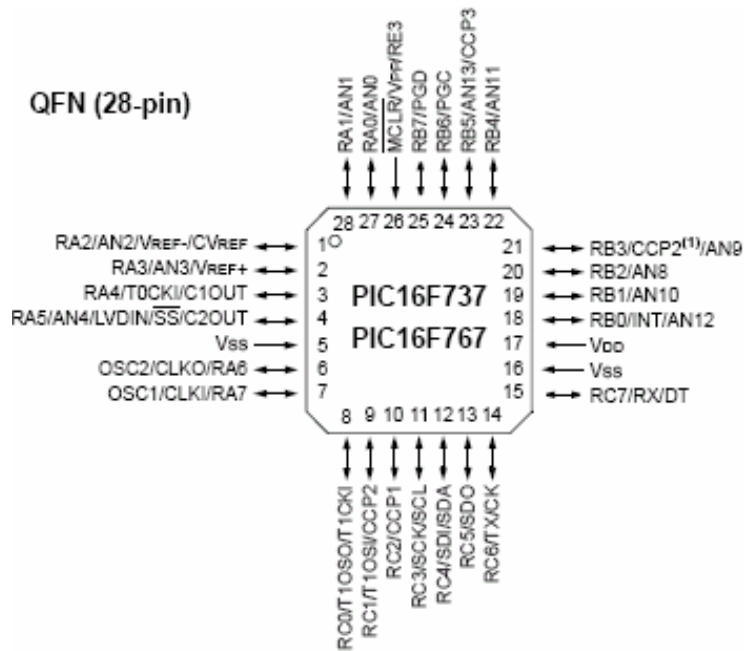


Fig. 17: PIC 16F737 TNC

Table 12: TX-TNC & RX-TNC Dealer [11]

Hardware	Quantity	Manufacturer/ Dealer	Weight (g)	Part Number	Description	Picture
TNC-TX TNC-RX	2	Microchip/ www.atlantikelektronik.com		TNC 16F737	<ul style="list-style-type: none"> Power Managed modes: <ul style="list-style-type: none"> - Primary Run (XT, RC oscillator, 76 μA, 1 MHz, 2V) - RC_RUN (7 μA, 31.25 kHz, 2V) - SEC_RUN (9 μA, 32 kHz, 2V) - Sleep (0.1 μA, 2V) Timer1 Oscillator (1.8 μA, 32 kHz, 2V) Watchdog Timer (0.7 μA, 2V) <ul style="list-style-type: none"> • Two-Speed Oscillator Start-up 	

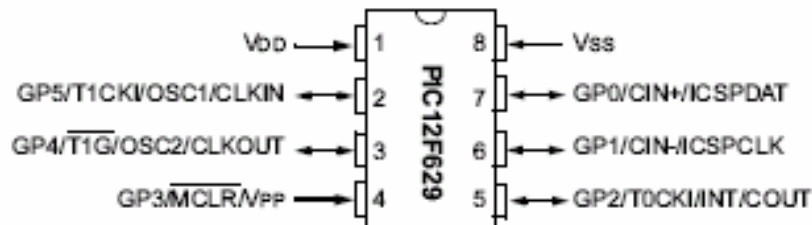
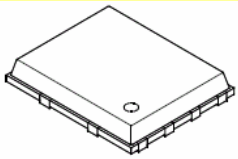


Fig. 18: PIC12F629/675 TNC

Table 13: CW-TNC Dealer

Hardware	Quantity	Manufacturer/	Weight	Part	Description	Picture
----------	----------	---------------	--------	------	-------------	---------

		Dealer	(g)	Number		
CW-TNC	1	Microchip/ www.atlantikelektronik.com		PIC12F629/675 TNC	<ul style="list-style-type: none"> • Standby Current: <ul style="list-style-type: none"> - 1 nA @ 2.0V, typical • Operating Current: <ul style="list-style-type: none"> - 8.5µA @ 32 kHz, 2.0V, typical - 100µA @ 1 MHz, 2.0V, typical • Watchdog Timer Current <ul style="list-style-type: none"> - 300 nA @ 2.0V, typical • Timer1 oscillator current: <ul style="list-style-type: none"> - 4 µA @ 32 kHz, 2.0V, typical 	

5.5 Morse Code Transmitter

The construction and design of a 70cm transmitter for downlink Morse code for Compass-1 is a good challenge to be realized, this transmitter will be built at Aachen University of Applied Sciences by me and with support of Georg Kinzy (EPS supervisor) and Hams developers.

Figure 19 shows a basic flow diagram of a low power FM transmitter as an example.

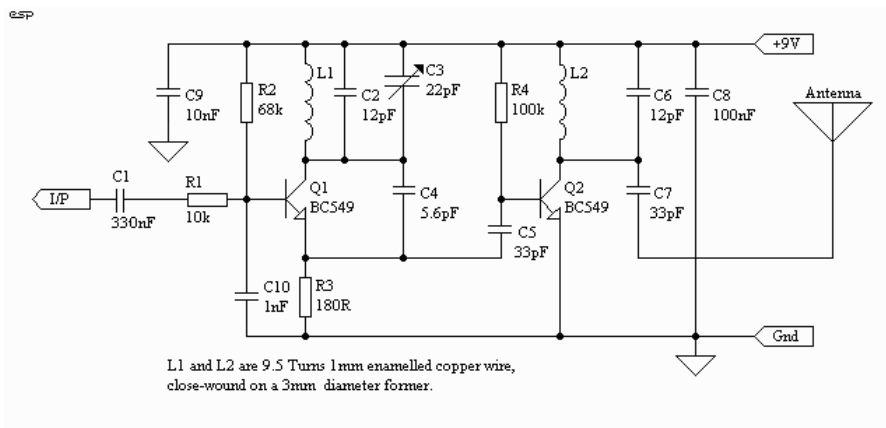


Fig. 19: Low Power FM Transmitter

5.6 Modem

Communication is accomplished using a series of translations. Modems use modulation to translate digital information utilized by the computer to analog waves carried by radio lines, when information is sent out, and reverse the process for incoming data (demodulation). This conversion prevents distortion of the information during transfer. Because computers use binary codes (a series of 1s and 0s) for information, two different signals must be conveyed and recognized in order for satellite communication to occur. One common method for accomplishing this is using *phase modulation*. This requires that the receiving and transmitting phases are synchronized, because the technology operates by comparing two sinusoidal waveforms. There are four possible phase shifts: 0, 90, 180, and 270 degrees. For example, a phase shift of 0 degrees might represent a 1, while a phase shift of 90 degrees might represent a 0. It is the modem's job to create and interpret these signals.

The data transfer speed is affected by several factors. First of all, the speed of CDHS will affect the rate at which information is processed. The noise on the radio line may also affect speed, along with the bandwidth (the range of information that can be transmitted at any given time). Information may be slowed down as it is altered to match the bus speed of the slot. The last important speed-affecting factor is the speed of the serving modem and the Compass-1 modem. The two must "handshake", in order to communicate correctly. This means that they 'agree' on a speed to communicate, so that a successful transfer can occur. Essentially, the connection is limited by the slowest factor in the system.

Modem speed (transmission and reception) is measured in bps (bits per second). Generally, the higher the speed, the better the modem. Some radio lines, however, are unable to handle these high transfer rates, in which case a high-speed modem will not provide significant benefits to the ham user. According to the stated mission objective, a 1200bps modem speed satisfies the requirements. This modem has to support the data transfer (images 50kB-300kB). Modems that support data compression allow higher transfer rates. In order to use this feature, however, the receiving modem must be able to decompress the information using the same method. The most expensive modems have some advantages, but generally a mid-range modem will perform equally well for general needs.

Modulation

A radio signal, a modulated carrier is a sinusoidal alternating voltage, normally expressed using cosine:

$$S(t) = A \cdot \cos(\omega t + \varphi) = A \cdot \cos(2\pi \cdot f \cdot t + \varphi)$$

Where **t** is the time, **A** the signal amplitude, ω the angular frequency of the carrier, φ is the phase and **f** the carrier frequency

The process of transferring information to a carrier is denoted modulation and involves varying one of the three parameters

A amplitude modulation – AM
 ω frequency modulation – FM

ϕ phase modulation - PM.

The most common format for space communications is phase modulation – PM.

Digital Modulation

Consider digital information as a bit stream of speed B bits per second, the duration of each bit is

$$\tau = 1/ B \text{ [seconds]}$$

Phase Modulation - PM

Let the phase 0° represent binary 0 or phase 180° represent binary 1.

Hold the phase of the carrier for τ seconds, after which the next bit period occurs.

This format is denoted “Phase Shift Keying – PSK” or BPSK, where B means Binary. Using simple arguments it is obvious that PSK using phases 0° and 180° is identical to amplitude modulation using the amplitudes +1 and -1. [12]

The MX614 is a low voltage, low power CMOS integrated circuit designed for the reception or transmission of asynchronous 1200bps data. This device is compatible with Bell 202 type systems and is ideal to accomplish the spacecraft’s modulation task. The MX614 supports 5bps and 150bps 'back channel' operation. Asynchronous data rates up to 1818bps are also supported. The MX614 provides an optional Tx and Rx data retiming function which can eliminate, based on user preference, the need for a UART in the associated μC when operating at 1200bps. An optional line equalizer has been incorporated into the receive path and is controlled by an external logic level. On Compass-1, the MX614 will be used for modulation of TX with a very low current “Zero Power Mode ($1\mu\text{A}$ typ.) and an operating current of 1mA typ. @ $V_{\text{DD}} = 3.3\text{V}$. A standard 3.58MHz Xtal/Clock is required and the device operates with a supply range of 3.0V to 5.5VDC. [13]

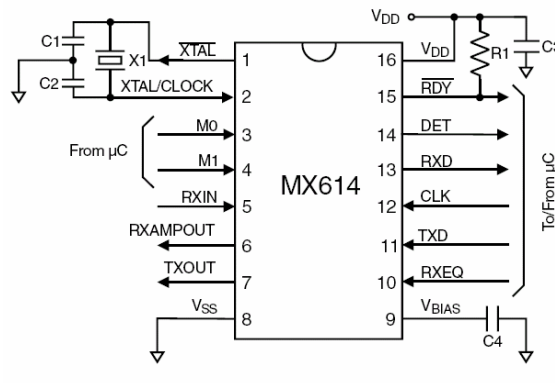
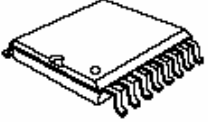


Fig. 20: MX614 Modem

Table 14: Modem Dealer

Hardware	Quantity	Manufacturer/ Dealer	Weight (g)	Part Number	Description	Picture

MODEM	1	Microchip/ www.atlantikelektronik.com		MX 614	<ul style="list-style-type: none"> • 1200bps - 1800bps half duplex Bell 202 Compatible Modem • Optional 1200bps Data Retiming Facility can eliminate external UART • Optional 5bps and 150bps Back Channel • Optional Line Equalization 	
-------	---	--	--	--------	---	---

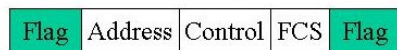
6. Software

6.1 AX25 Protocol

In order to provide a mechanism for the reliable transport of data between two signaling terminals, in our case FHACC and Compass-1 , it is necessary to define a protocol that can accept and deliver data over a variety of types of communications links. The AX.25 Link-Layer Protocol is designed to provide this service, independent of any other level that may or may not exist.

This protocol has been designed to work equally well for direct connections between two individual amateur packet-radio stations or an individual station and a multiport controller. This protocol allows for the establishment of more than one link-layer connection per device, if the device is so capable. This protocol does not prohibit self-connections. A self-connection is considered to be when a device establishes a link to itself using its own address for both the source and destination of the frame. Most link-layer protocols assume that one primary (or master) device (generally called a DCE, or data circuit- terminating equipment) is connected to one or more secondary (or slave) device(s) (usually called a DTE, or data terminating equipment). This type of unbalanced operation is not practical in a shared-RF Amateur Radio environment. Instead, AX.25 assumes that both ends of the link are of the same class, thereby eliminating the two different classes of devices. Link layer packet radio transmissions are sent in small blocks of data, called frames. Each frame is made up of several smaller groups, called fields. Fig.21 shows the two basic types of frames. [14]

- Unnumbered/Supervisory Frame



$$8 + 112 + 8 + 16 + 8 = 152 \text{ bits (19 bytes)}$$

- Information Frame



$$8 + 112 + 8 + 8 + N*8 + 16 + 8 = 2368 \text{ bits (296 bytes)}$$

$$N=256 \text{ (max)}$$

Fig. 21: AX.25 Frames

The available AX 25 version 2.0 has the following properties:

- a. Simple and Secure
- b. Standard for Amateur Packet Radio
- c. TNC support
- d. Connection Oriented, packets arrive in order
- e. Some control fields to be hard coded

This protocol has to be implemented on the Compass-1 COM system. More details will be elaborated in phase C/D.

6.2 TNCs Programming

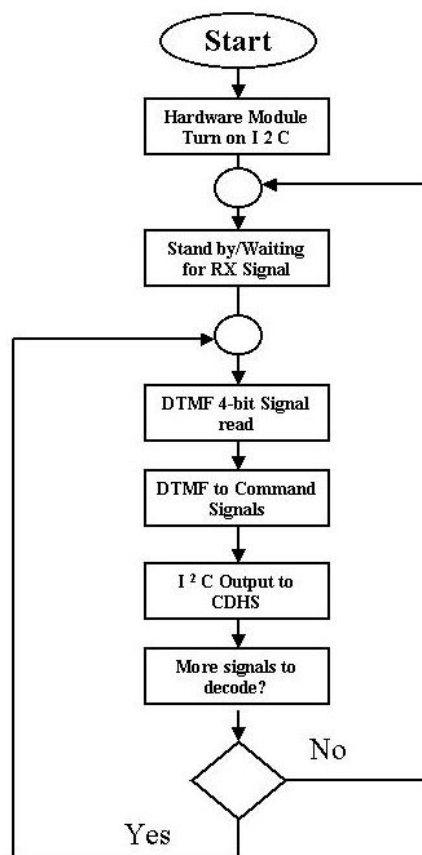


Fig. 22: RX -TNC Flow Chart

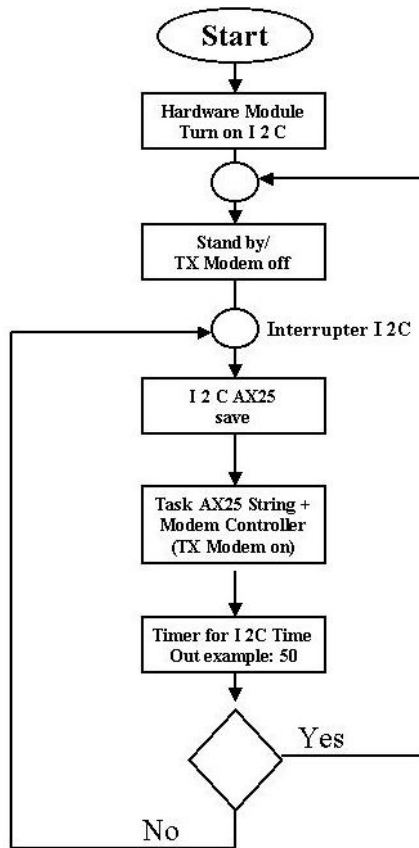


Fig. 23: TX-TNC Flow Chart

6.4 DTMF Configuration

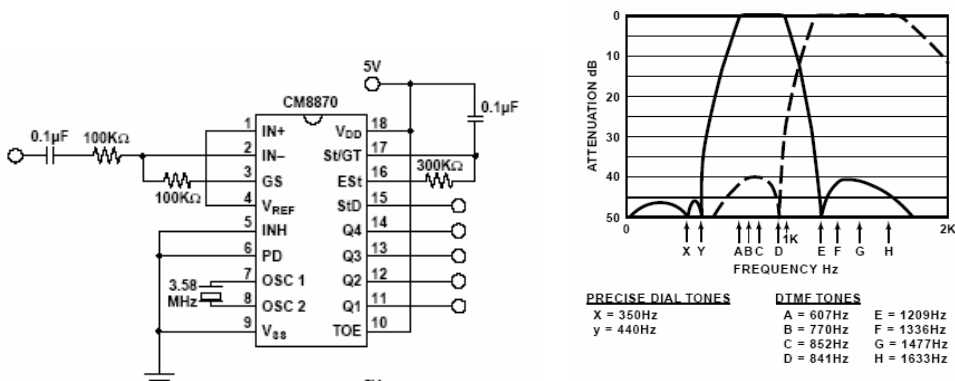


Fig. 24: DTMF Diagram

References

- [1] CubeSat Team Aachen. (2003) *Phase A Study of COMPASS-1*. www.raumfahrt.fh-aachen.de
- [2] International Telecommunication Union(ITU), www.itu.org
- [3] Link budget calculations, Kiwisat,
http://homepages.ihug.co.nz/~jpsl/Kiwisat_discussion2.htm
- [4] DARC G25, www.amsat.de
- [5] Satellite Communications System, Second Edition, *M. Richharia*
- [6] XI-IV Cubesat, University of Tokyo, <http://dat15.t.u-tokyo.ac.jp/cubesat/index-e.html>
- [7] www.tycoelectronics.com
- [8] www.alinco.com
- [9] <http://www.ece.utexas.edu/~mason/codesign/dtmf.html>
- [10] http://www.calmicro.com/swf_index.html
- [11] www.microchip.com
- [12] Elements of Spacecraft Design, communication chapter, *Charles Green*
- [13] www.microchip.com
- [14] AX.25 Link Access Protocol for Amateur Packet Radio, Version 2.2 Revision:11
November 1977



2004-05-17

WBS440: CDHS

Command and Data Handling System

Phase B: Detailed Definition

Author

Artur Scholz

FH Aachen, Germany



Scope

This paper documents the detailed definition of the on-board computer system for the COMPASS-1 spacecraft, i.e. the Command and Data Handling System (CDHS). Its definition is based upon the preceding results gained in the phase A study 0 and goes in accordance with the cubesat specifications [5] wherever applicable.

Contents

1. Hardware Definition	100
1.1 Component Selection	100
1.1.1 Microcontroller Unit	101
1.1.2 Memory Unit	103
1.1.3 System Bus	104
1.1.4 Payload Interface Unit.....	107
1.1.5 Main Board.....	108
1.2 Integration	110
2. Software Definition	111
2.1 Boot Procedure.....	112
2.2 Main Loop.....	113
2.3 Agenda	113
2.4 List of Commands.....	114
3. Budgets	115
3.1 Mass	115
3.2 Power	115
3.3 Volume.....	115
4. Conclusion.....	116
5. References	116

1. Hardware Definition

This simplified picture depicts the architectural concept of the main components of the CDHS, which are the MCU, the memory, the system bus and the external camera module.

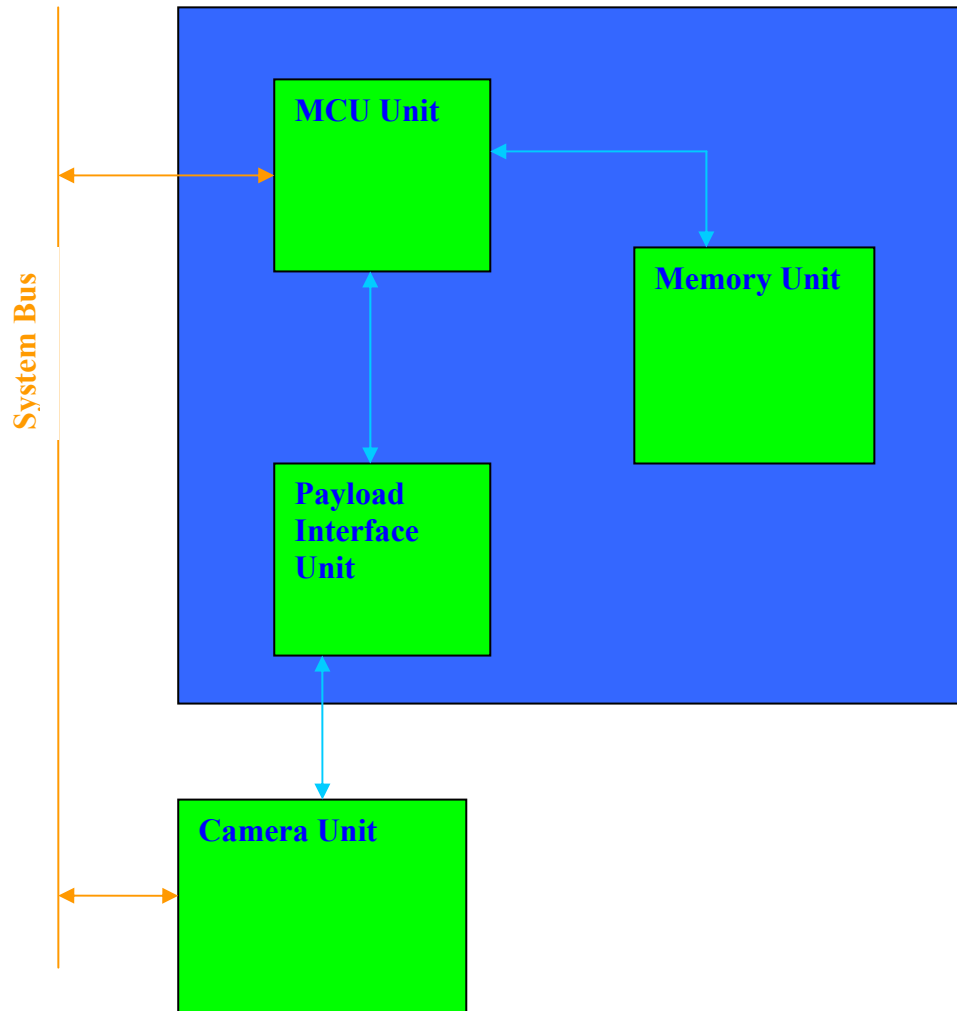


Fig. 1.1: CDHS architecture

1.1 Component Selection

Since decades now all kinds of satellites have utilized electronic components, with some of them being proven most reliable. Especially in terms of resistance to radiation there are some available that have very good space heritage. Specially developed radiation hardened microcontrollers can be purchased from a range of manufactures. The prices for those however are far beyond our tight projects budget. Furthermore from the very beginning we decided not to make use of dedicated space products but to employ COTS products preferably and apply engineering solutions to ensure functionality. As for the CDHS and other subsystems this will increase the risks of component malfunctions by magnitudes. Concrete countermeasures are not intended because they would most definitively result in violations to the subsystems budgets and definitively would increase complexity, hence introducing more sources of error. An optimization for this will be implemented in follow-on missions. Though, graceful degradation is utilized, by ways of having the chance to receive information from the satellite even in case of heavy damages. Again, if electrical components of the CDHS suffer

from radiation, the results can be bit errors (which would be found by data check on ground) or a total failure of the subsystem.

1.1.1 Microcontroller Unit

Contrary to the ADCS controller the CHDS MCU program code does not consist of complex algorithms but is rather straight forward. During its duty cycle it is mainly concerned with payload control and data transfer. In addition in terms of power saving a well matured 8-bit controller seems to be the best solution for that. The selection process of the microcontroller is in fact arbitrary to some extent. In comparison with other CubeSat groups it was verified that a lot of products would fulfill the requirements we have set up before. Finally a MCU with an 8051 processor was targeted as this is a well matured and versatile architecture. Software development tools are commonly available for those processors at low prices.

Table 1.1: Comparison of suitable microcontrollers

Manufacturer	Product	Program Memory (Byte)	RAM (Byte)	I/O Pins	A/D	Speed (MHz)	Power consumption (max.)	Features
Microchip	PIC16F877	256	368	33	8 (10Bit)	20	20mW	I ² C, PWM, USART
Infineon	C515C-8E	64K	2304	57	8 (10Bit)	10	100mW	USART
Atmel	AT89C2051x2	2K	-	20	-	16		UART
Silicon Laboratories	80C51F12X	128K	8K		8 (10Bit)	24 MHz	75mW	I ² C, ISP

The final choice is a C8051F123 from Silicon Laboratories [6]. The device is a fully integrated mixed-signal System-on-a-Chip MCU with 32 digital I/O pins as shown in fig. III.1.2. Highlighted features are listed below.

- High-Speed pipelined 8051-compatible CIP-51 microcontroller core (up to 100 MIPS)
- In-system, full-speed, non-intrusive debug interface (on-chip)
- 128k bytes of in-system programmable FLASH memory
- 8448 (8k + 256) bytes of on-chip RAM
- External Data Memory Interface with 64k byte address space
- SPI, SMBus/I²C, and (2) UART serial interfaces implemented in hardware
- Five general purpose 16-bit Timers
- Programmable Counter/Timer Array with 6 capture/compare modules
- On-chip Watchdog Timer, VDD Monitor

With this device a fully integrated solution is found. The program code can be stored in the sufficient available FLASH memory whilst the variables etc. occupy the on-chip RAM. The FLASH memory can be reprogrammed even in-circuit, providing non-volatile data storage. In addition the chip offers plenty of I/O pins to connect the other electrical components on the CDHS board.

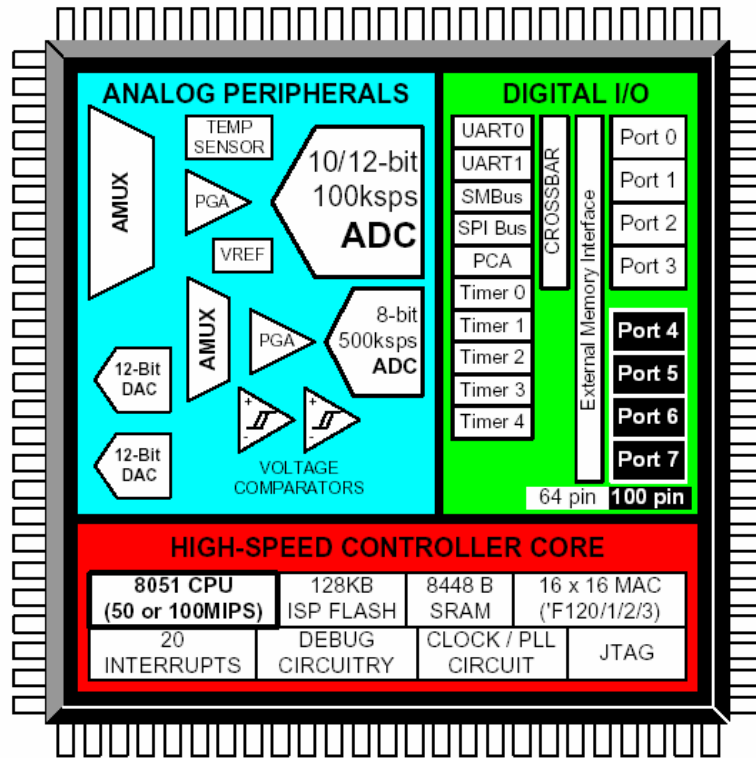


Fig. 1.2: C8051F123 features

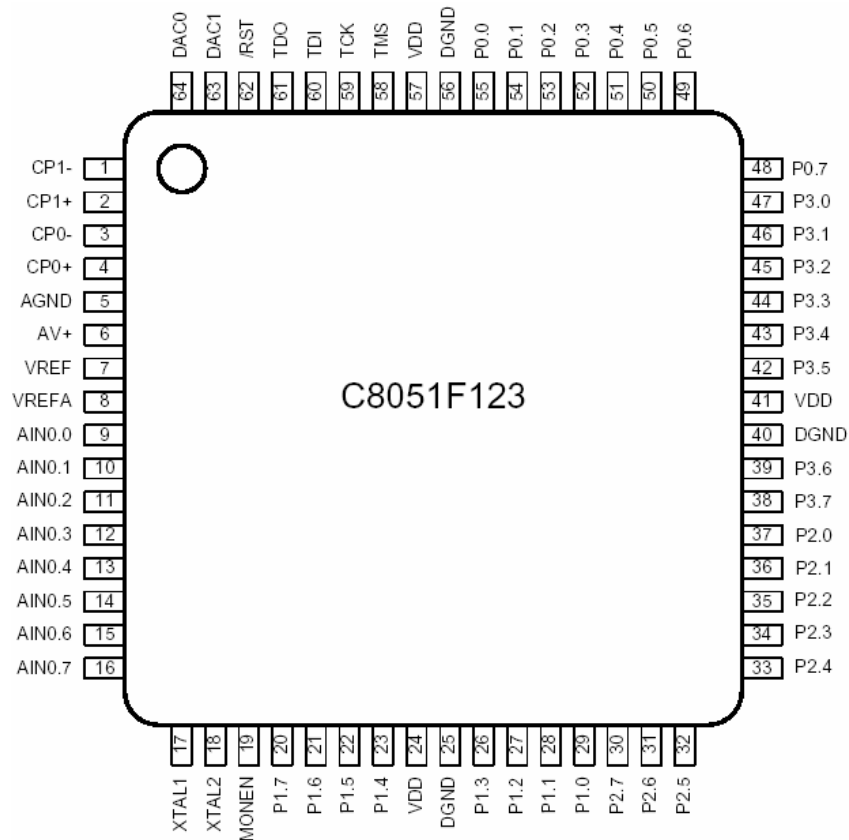


Fig. 1.3: Pinout diagram of C8051F123

With the on-chip VDD monitor, Watchdog Timer, and clock oscillator, the device is truly a stand-alone System-on-a-Chip solution. All analog and digital peripherals are enabled or

disabled and configured by software. Those features and pins that are not going to be used for the mission will be disabled or switched off to decrease the chip’s power consumption.

The JTAG debug circuitry allows non-intrusive (uses no on-chip resources), full speed, in-circuit debugging during the development phase using the production MCU installed in the final application. This debug system supports inspection and modification of memory and registers, setting breakpoints, watchpoints, single stepping, run and halt commands. All analog and digital peripherals are fully functional while debugging using JTAG.

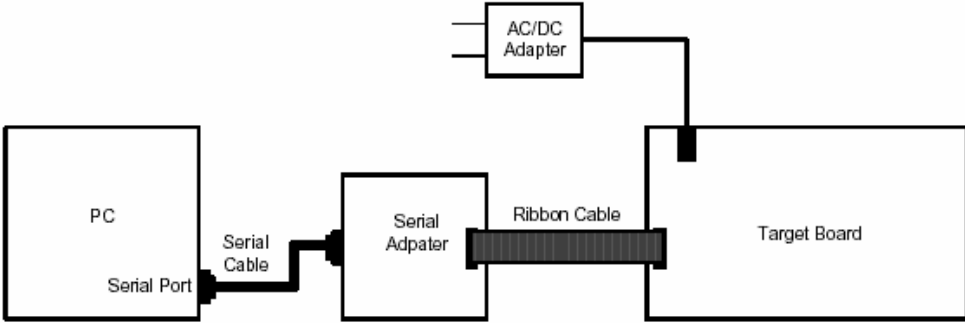


Fig. III.1.4: 80C51F123 Development Kit Hardware Setup

The MCU is specified for operation over the industrial temperature range (-45° C to +85° C). The Port I/Os, /RST, and JTAG pins are tolerant for input signals up to 5V. The C8051F123 comes in a 64-pin TQFP package.

1.1.2 Memory Unit

Being a kind of mixture between EEPROM and RAM, Flash memory technology was chosen to be used for data storage exclusively. Flash devices can be programmed and keep their information until re-programmed. Both can be done by software in-system. While powered off, no data is lost, which will be an excellent way for the CDHS to reduce its power consumption. Flash is a relatively new technology and technical improvements take place at fast pace. Some suitable up-to-date products are listed below. All devices supply 8-bit parallel bus.

Table 1.2: Comparison of suitable Flash devices

Manufacturer	Product	Memory (Mbit)	Pins		Read time (byte)	Power consumption (max.)
Atmel	AT29LV040A	4	48		100 ns	45 mW
Samsung	K9F6408U0B-TCB0	64	44		50ns	66 mW
AMD	Am29PDL129H	128	BGA		53ns	

The first choice was the K9F6408U0B-TCB0 from Samsung as it incorporates enough memory in a single module with reasonable power consumption and at the same time fulfill to the required industrial temperature range. A request at Samsung about its availability revealed that this device is not in production anymore. Fortunately the next generation of its family, the K9F2808U0C-YIB0000 [7] is available and has the same features plus a more of 100% memory capacity. Main features are:

- Memory Cell Array : (16M + 512K)bit x 8bit
- Automatic Program and Erase
- Page Program : (512 + 16)Byte
- Block Erase : (16K + 512)Byte
- 528-Byte Page Read Operation
- Random Access : 10ms(Max.)
- Serial Page Access: 50ns
- Fast Write Cycle Time
- Program Time: 200ms (typ.)
- Block Erase Time : 2ms (typ.)
- Command/Address/Data Multiplexed I/O Port
- Hardware Data Protection
- Program/Erase Lockout During Power Transitions
- Reliable CMOS Floating-Gate Technology
- Endurance : 100K Program/Erase Cycles
- Data Retention : 10 Years
- Package: 48 - Pin TSOP I (12 x 20 / 0.5 mm pitch)

The data storage is organized by rows (pages) and columns. 1 column by 32 pages makes up a block. Invalid blocks are defined as blocks that contain one or more invalid bits.

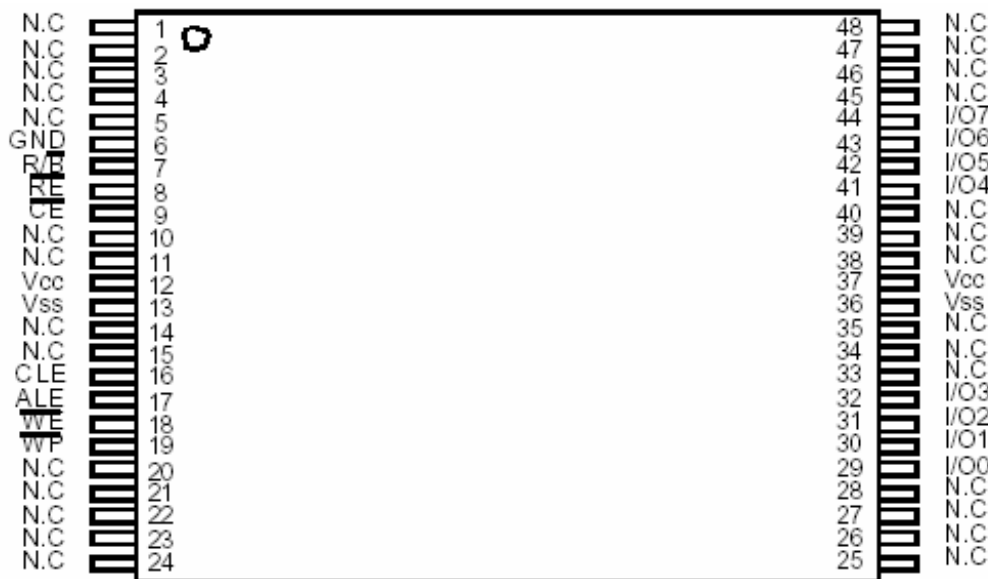


Fig. 1.5: Pinout of K9F2808U0C-Y1B0 Flash

1.1.3 System Bus

The I²C-Bus (Inter Integrated Circuit Bus) from Philips [8] will be used as the internal data and command bus. This bus was developed by Philips in 1992 and has become a de facto world standard that is implemented in over 1000 different ICs, hence much versatile to modified system architectures. It is a ring topology.

The relevant features of the I²C bus are:

- Only two bus lines are required; a serial data line (SDA) and a serial clock line (SCL);

- each device connected to the bus is software addressable by a unique address and simple;
- Master/slave relationships exist at all times; masters can operate as master-transmitters or as master-receivers;
- It's a true multi-master bus including collision detection and arbitration to prevent data corruption if two or more masters simultaneously initiate data transfer;
- serial, 8-bit oriented, bi-directional data transfers can be made at up to 100 KBit/s in the Standard-mode;
- I²C-Bus interface is integrated on-chip on many ICs;
- Extremely low current consumption;
- High noise immunity;
- Wide supply voltage range;
- Wide operating temperature range.

Each device that is connected to the bus is recognized by a unique address and can operate as either a transmitter or receiver, depending on the function of the device. In addition to that, devices can also be considered as masters or slaves when performing data transfers. A master is the device which initiates a data transfer on the bus and generates the clock signals to permit that transfer. At that time, any device addressed is considered a slave.

The I²C-bus is a multi-master bus. This means that more than one device capable of controlling the bus can be connected to it.

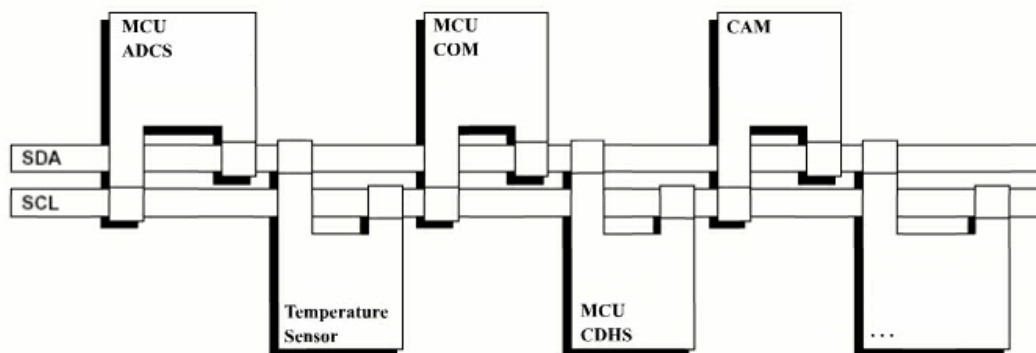


Fig. 1.6: I²C-bus architecture

Possible data transfer formats are shown in figure 1.7 to 1.9.

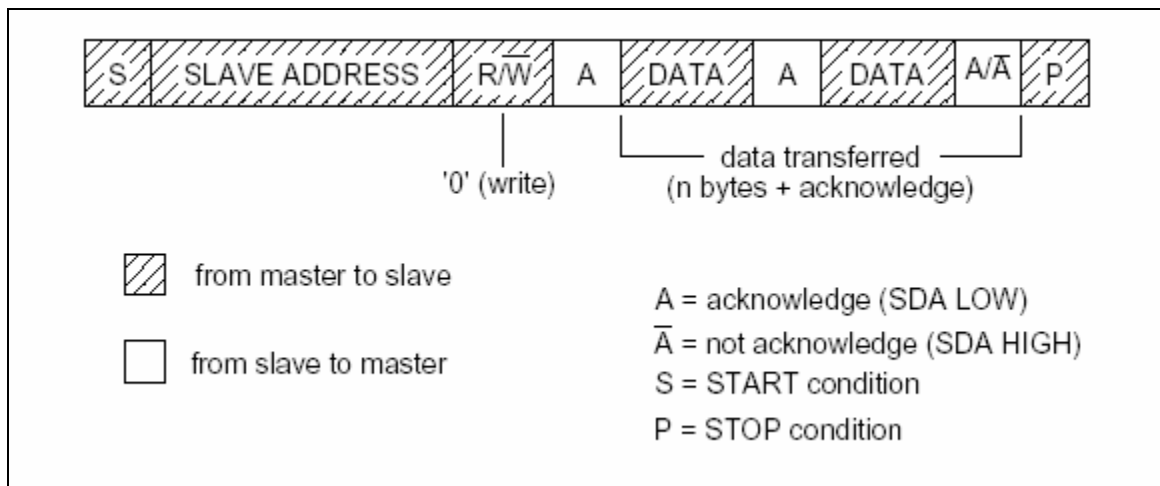


Fig. 1.7: A master-transmitter addressing a slave receiver with a 7-bit address. The transfer direction is not changed.

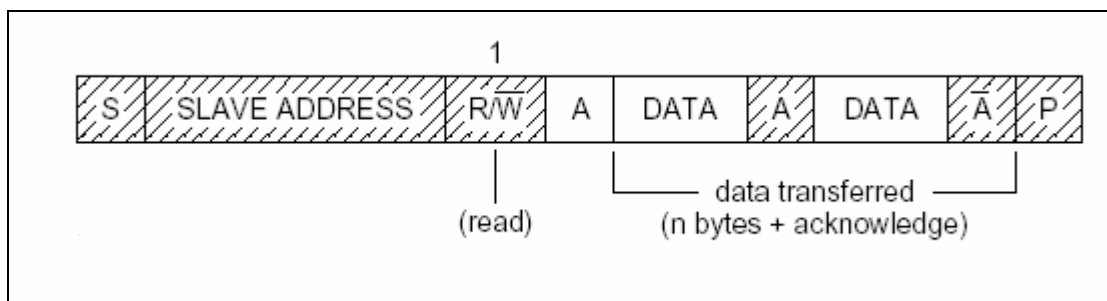


Fig. 1.8: A master reads a slave immediately after the first byte

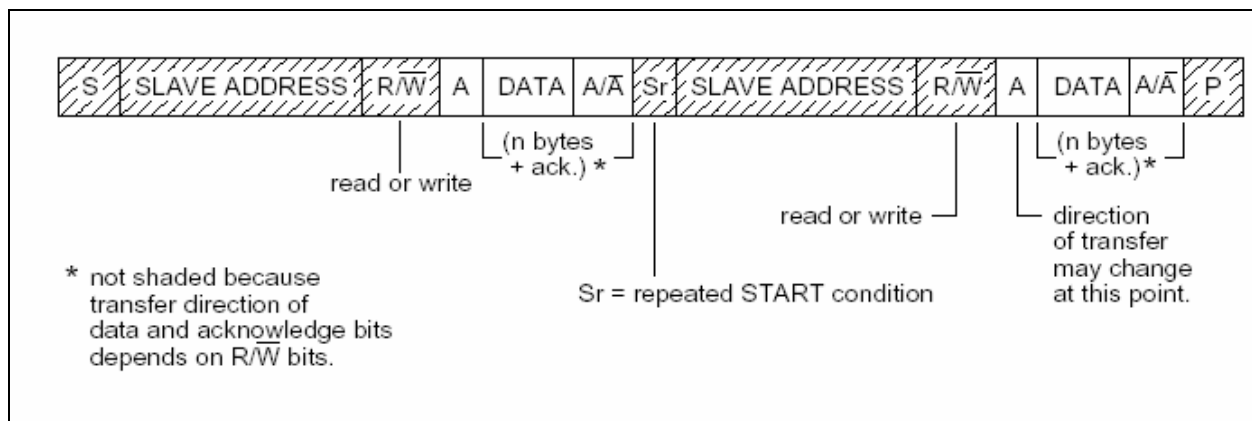


Fig. 1.9: Combined format

The I²C Bus concept bases on a wired-AND connection of all interfaces to the bus. Generally this can be considered as an advantage as components that have a malfunction and would pull the bus to ground could be switched off to solve the problem. In a situation where one of the CDHS components would fail completely, the EPS would turn of the CDHS and hence the bus would be cleared also.

There is no implementation for detecting errors during bus communication provided by the I²C Bus hardware. Thus the issue of error detection and correction has to be addressed by software solely.

1.1.4 Payload Interface Unit

The camera requires an **external clock generator**, which will be solved by a TTL logic that sits on the main board. The logic will have the following characteristics according to the camera requirements:

- frequency around 12MHz
- max. 5ns rise/fall times
- input duty cycle between 45..55%

The envisaged clock frequency will be around 12MHz. Even so, this value is settled at the lower half of possible frequencies, the constant data output of the camera is still way to fast for the Flash to handle it. Thus, a **FIFO** device is inserted to fetch up the images coming from the camera and buffers one at a time. The memory depth of the FIFO must be not less than about 300KByte in order to store one whole image. This requirement alone eliminates a majority of available FIFOs, because they don't have so much memory integrated in a single chip. By using the possibility to connect several devices in series increased power consumption would be the result. A component was found from IDT [10] that incorporates exactly the required features. It is the IDT72V2111 as shown in fig. 1.10.

Features:

- Memory organizations: 524,288 x 9
- 10ns read/write cycle time (6.5ns access time)
- Fixed, low first word data latency time
- 5V input tolerant
- Auto power down minimizes standby power consumption
- Master Reset clears entire FIFO
- Retransmit operation with fixed, low first word data latency time
- Empty, Full and Half-Full flags signal FIFO status
- Output enable puts data outputs into high impedance state
- Independent Read and Write clocks (permit reading and writing)
- Available in the 64-pin Thin Quad Flat Pack (TQFP)
- High-performance submicron CMOS technology

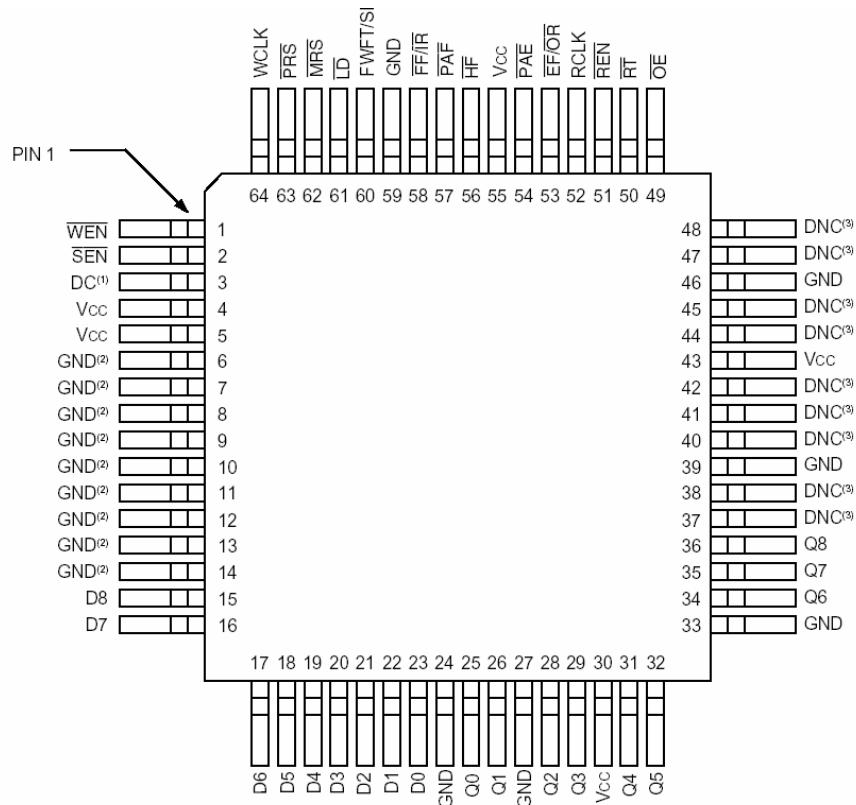


Fig. 1.10: Pinout of IDT72V2111 FIFO

A little drawback is that this component needs a stable power supply of 3V3. Since 5V and 3V are offered by the EPS it becomes necessary to set a voltage regulator ahead of it. The same is true for the camera module, which operates at 2V5. Two very low dropout voltage regulators from Zetex [11] are used, which are the ZLDO330 and the ZXCL250.

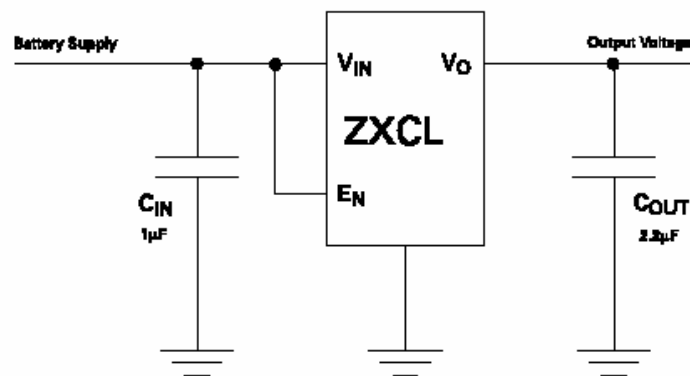


Fig. 1.15: Connection schematic of ZXCL devices

1.1.5 Main Board

All the above mentioned components (except the camera) will be mounted on a single PCB that is the main board. The upper side will hold the connectors for the subsystem boards whereas the devices are placed on the lower side. One of our projects goals will be to have the main parts of the satellite manufactured within our universities facilities, thus underlining its sovereignty. Of course this implements a number of restrictions on all levels of engineering and testing. The bottom line here is to find a compromise between performance level and time-keeping. As for the board the local facilities permit the in table 1.3 listed parameters.

Table 1.3: Manufacturing restrictions

		Shape Size	Hole Size
Pad Size	TO92-Package	61mil / 1.6mm	31mil / 0.8mm
	ICs	65mil / 1.7mm	31mil / 0.8mm
	Connectors	75mil / 1.9mm	39mil / 1mm
	High Power transistors	85mil / 2.2mm	51mil / 1.3mm
Via		50mil / 1.3mm	20mil / 0.5mm
Track	minimum	> 8mil / 0.2mm	-
	recommended signal	15mil / 0.4mm	-
	recommended power	> 15mil / 0.4mm	-
Track distance		10mil / 0.25mm	-

Moreover the following restrictions apply as well:

- Maximum of 4 different drill holes available (20/31/39/51mil)
- Board size up to 180mm x 240mm
- Two layer (top and bottom)
- Three pad layouts (round/rectangle/octagonal)

The circuits are going to be designed with CAD software tools and will finally be milled in-house accordingly. Next, the components are soldered onto the board by hand. (This step will require skilled students with lot of practice in soldering). Finally the board may be covered with protective varnish to better withstand ESD and radiation. Additional protective methods are not considered to be implemented.

As mentioned before, there are connectors placed on the upper side in order to attach the subsystem boards. Even intensive research could not offer a solution for the initial idea to use SMD slots, in which the other boards can be inserted (like the ISA slots). Therefore an alternative connection was chosen, which would moreover supply a better solidity against launch loads as well. With connectors of JST [3] a conceptual solution evolved by refining the idea behind the board-to-board connection. Instead of one long slot per board, two small edge connectors will be implemented. The plug and receptacle are both through-hole mounted and illustrated in fig. 1.11. They will furnish a great and reliable way to interconnect the boards, though the only concern is about their functionality in vacuum. A test campaign has to prove their resistance to out-gassing.

As indicated from the drawing the plugs will be placed next to the corners of the subsystem boards, thus leaving a rectangle of free space around the center of the main board for mounting the electrical components. Each plug allows up to 9 circuits.

There will be a total of three subsystem boards, one for ADCS, one for COM and one for EPS together with TCS, which yields in a total amount of 6 plug/receptacle pairs. The arrangement of the boards is going to be defined by the **structure group** and based upon volume requirements and mass distribution.

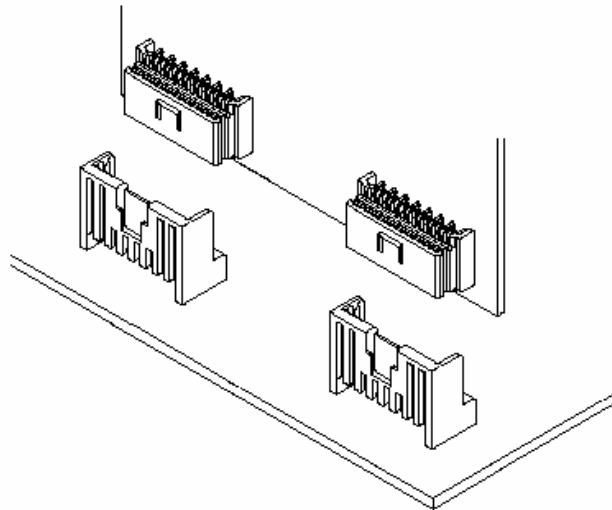


Fig. 1.11: Conceptual board-to-board interconnection using JET Connectors

Two other types of plugs are located on the bottom side of the CDHS main board, which are the JTAG header and the camera connector. The JTAG connector is a simple 10 pin header with 2.54mm pitch. The connection to the camera is going to be designed in the subsequent phase.

1.2 Integration

As said, the top side of the main boards accommodates the subsystem boards and the underside all the electrical devices as illustrated in the following figures.

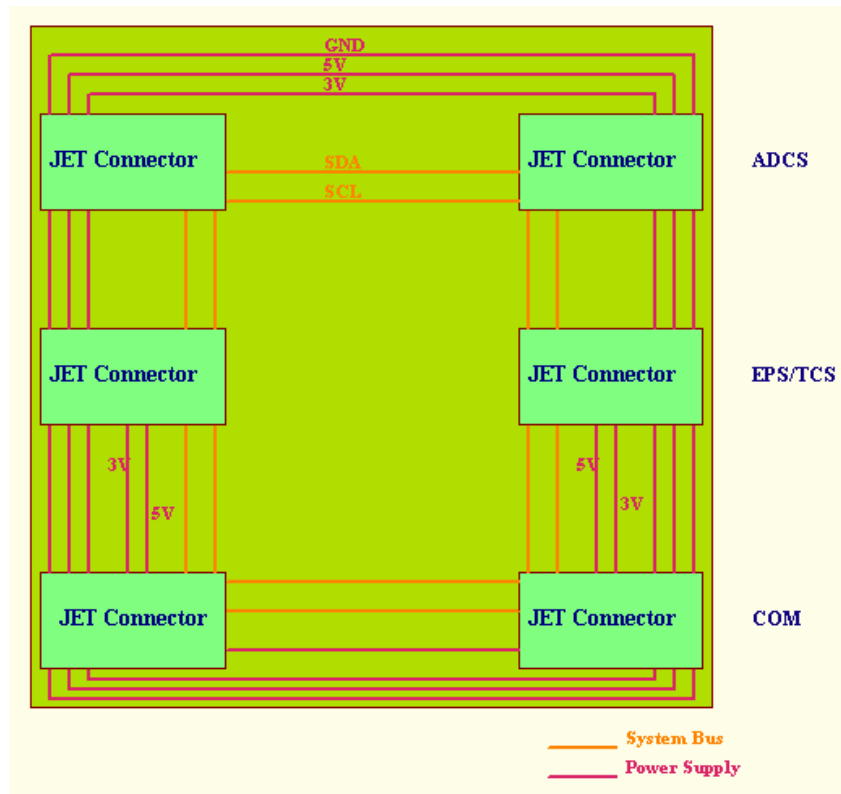


Fig. 1.12: Conceptual layout of main board up side

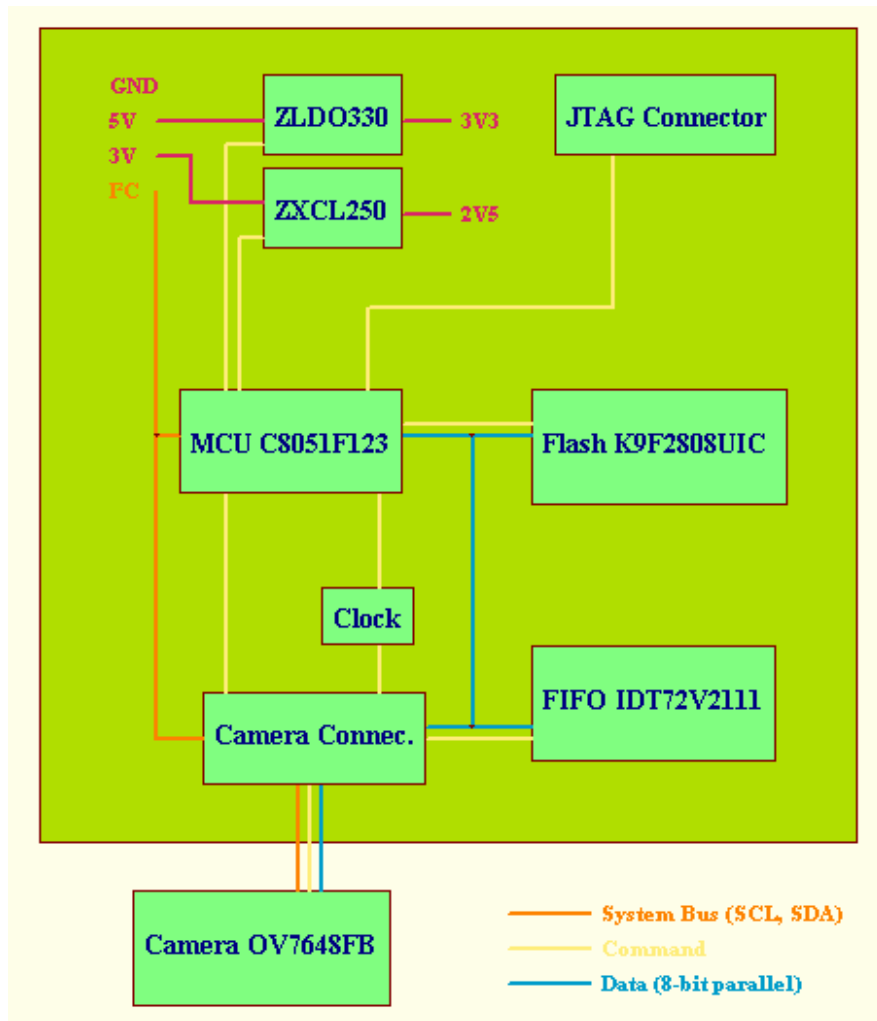
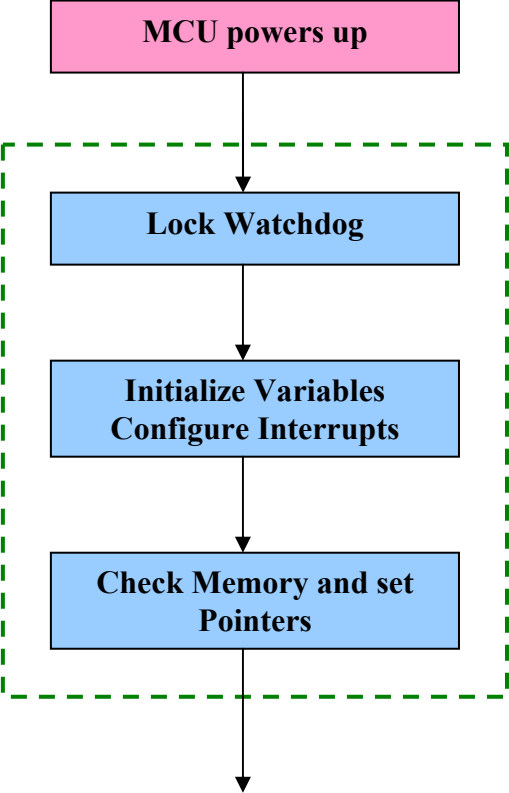


Fig. 1.13: Conceptual layout of main board underside

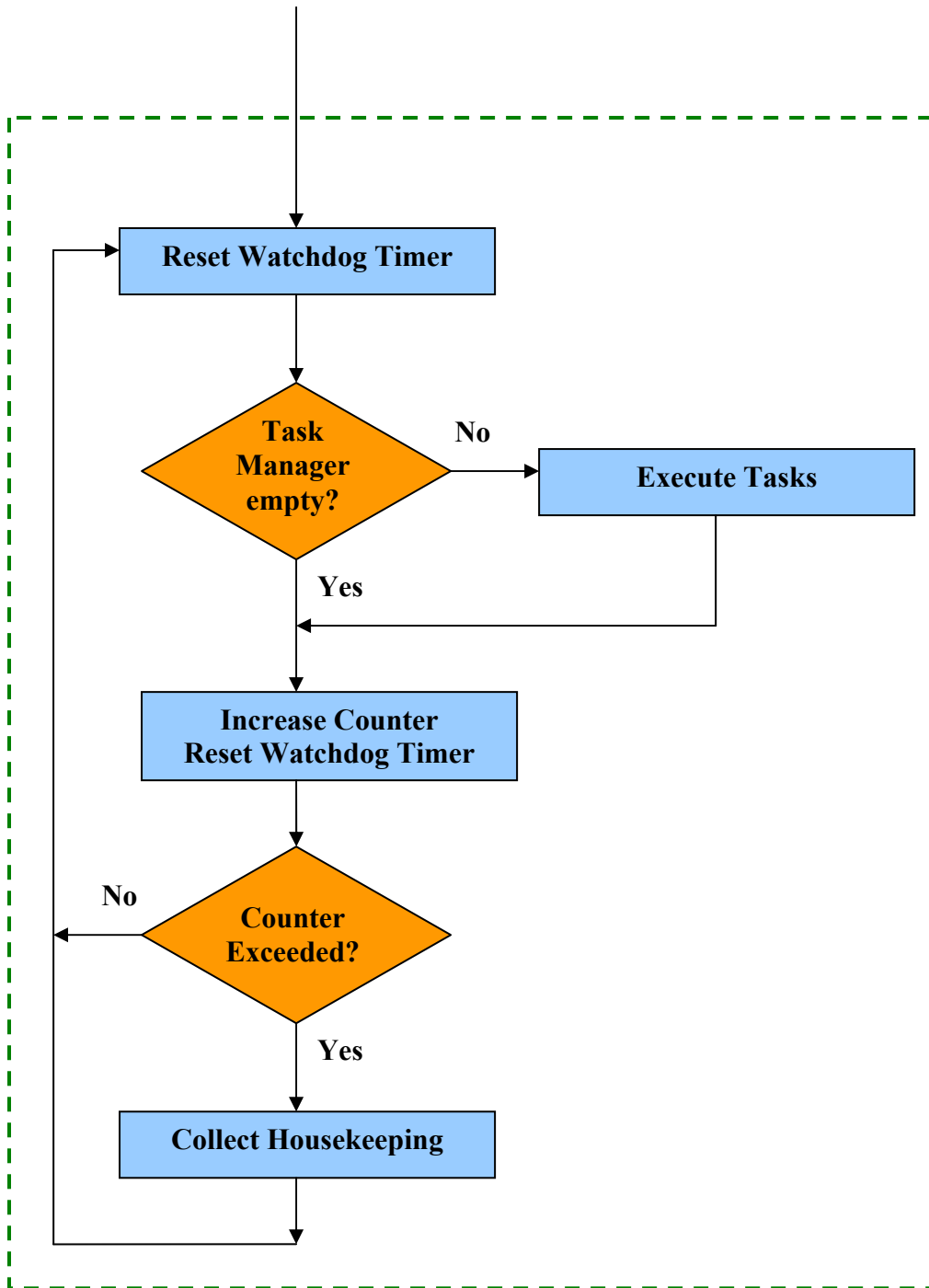
2. Software Definition

The software definition is straight-forward by following the requirements set up in the previous phase. There are two main procedures that are the boot procedure for the CDHS, which is triggered by the EPS. The boot routine does some basic checks and all required setup. Then it goes over to the main loop, which carries out the flight schedule.

2.1 Boot Procedure



2.2 Main Loop



2.3 Task Manager

The flight agenda is updated by commands, submitted by the other subsystems and carried out by the CDHS. This way the satellite is re-acting on extern commands, mainly those coming from ground. Each command holds a certain priority, in this way the system provides necessary power and time management.

Table 2.1: Task Manager

Priority	Item	Description
----------	------	-------------

Highest	Program ADCS parameters	Slew
	Transmit housekeeping data	Send housekeeping from memory to ground
	Transmit image	Send a stored image to ground
	Take picture	Capture image, store with user text and send to ground
Lowest	Control ADCS	Switch ADCS on or off

2.4 List of Commands

There exists a set of commands provided by the CDHS in order to control the interaction between CDHS and the other subsystems. Commands are made up of a singly byte command code (CC) and additional data if applicable. Commands are submitted via I²C Bus interrupts and always sent as master to slave. According to I²C rules the transfer is initiated by a START condition, followed by the slave address (component-specific) and a WRITE. After the slave acknowledges (A) the command code is send.

S	Slave Address	W	A	CC	A	Additional data...	A	P
----------	----------------------	----------	----------	-----------	----------	---------------------------	----------	----------

S = START

P = STOP

A = ACK

W = WRITE

CC = command code

Table 2.2: Command list

From	To	CC	Additional Data	Description
CDHS	ADCS	0x00	-	Request housekeeping data
ADCS	CDHS	0x01	13 Bytes	Send housekeeping data
ADCS	CDHS	0x02	-	Request for activation
CDHS	ADCS	0x03	-	ADCS on
CDHS	ADCS	0x04	-	ADCS off
ADCS	CDHS	0x05	-	Urgent Request for activation
CDHS	ADCS	0x06	3 Bytes	Slew into new attitude
ADCS	CDHS	0x07	-	ADCS control finished
CDHS	EPS	0x30	-	Request housekeeping data
EPS	CDHS	0x31	25 Bytes	Send housekeeping data
CDHS	COM	0x51	256 Bytes	Send housekeeping to ground
CDHS	COM	0x52	640x480 Bytes	Send image to ground
COM	CDHS	0x53	-	Request for image capturing
COM	CDHS	0x54	1Byte	Request for image number X
COM	CDHS	0x55	3 Byte	Send slew command to ADCS
COM	CDHS	0x56	-	Request housekeeping data

3. Budgets

The budgets were established to share the restricted resources among the subsystems. With the chosen technical solution in mind, it is now possible to draft the estimated amount of mass, power and volume consumption.

3.1 Mass

Table 2.3: Projected mass budget

Item	Unit Mass (g)	Quantity	Mass (g)
MCU	1	1	1
Flash	1	1	1
FIFO	1	1	1
Regulators	1	2	2
JET Connectors	1,25	12	15
JTAG Connector	1,5	1	1,5
PCB	30	1	30
others	10	1	10
TOTAL			61,5
Margin			8,5

Still there is a margin of more than 10% from the assigned 70g.

3.2 Power

Table 2.4: Projected Power consumption

Item	Voltage [V]	Standby current [mA]	Active current [mA]	Active times [%]	Consumption [mW]
MCU	3	0	2	100	6
Flash	3	1,05	20	10	9
FIFO	3,3	0	55	10	18
Regulators	5	0	1	10	0
others	3	5	10	50	22,5
TOTAL					56
Margin					4

The requirement was 60mW maximum. It shall be noted that those values strongly depend on the satellites activities. For the figures it was assumed that an image is requested once every orbit.

3.3 Volume

The board shape is 94mm x 94mm and has is about 5mm high with components. The six connectors for the Subsystem boards are each 10mm x 15mm x 15mm. Thus the total volume yields into about 57680 mm³, which is 5.8% of the satellites total volume. The requirements were set to 100mmx100mmx20mm, thus having a margin of more than 50%!

4. Conclusion

The end of the detailed definition of the CDHS on components level allows the design and development process to begin. The selected devices correspond to the requirements and have the capability to fulfill the mission objectives when properly designed. The interconnections and interfaces were established on a logical level and have to be translated onto physical level in the next phase. Careful and iterative testing of software and hardware will ensure a reliable system for the satellite.

5. References

- [4] CubeSat Team Aachen. (2003) *Phase A Study of COMPASS-1*. www.raumfahrt.fh-aachen.de
- [5] Calpoly and Stanford University. (2003). *CUBESAT Design Specifications Document, Revision VIII*. <http://cubesat.calpoly.edu/>
- [6] www.silabs.com
- [7] www.samsung.com
- [8] www.semiconductors.philips.com/
- [9] www.jst.com
- [10] www.idt.com
- [11] www.zetex.com



2004-06-06

WBS450: EPS

Electrical Power System

Phase B: Detailed Definition

Author

Georg Kinzy

FH Aachen, Germany



Scope

This document describes the definition of the Electrical Power System for the COMPASS-1 spacecraft regarding the phase A results.

Contents

1. Hardware Definition	120
1.1 Components	120
1.1.1 MCU	120
1.1.2 Clock	121
1.1.3 DC-DC converter	122
1.1.4 Voltage regulator	123
1.1.5 Charging control	123
1.1.6 Temperature sensors	124
1.1.7 FET	125
1.1.8 TCS Hardware / Antenna Deployment Hardware	126
1.1.9 Solar cells	126
1.1.10 Batteries	127
1.2 Integration	127
2. Software Definition	129
3. Appendix	130
3.1 Abbreviations	130
3.2 References	130

1. Hardware Definition

The EPS hardware is based on an 8-bit MCU which controls the entire system. The energy generated by means of the solar cells will be stored in modern Lithium Polymer (LiPo) cells. Because the LiPo voltage could not satisfy the requirements of the other subsystems, it will be conditioned by two DC-DC step-up converters to 5 Volts and two Low Drop voltage regulators to 3 Volts. To generate a real-time base for time critical tasks, an external crystal oscillator is used to trigger the MCU. To ensure low power consumption in Emergency Mode, every component which is not in use could be switched off by the MCU. In addition to the components needed for the EPS functions, three MOS FETs for the Thermal Control System (TCS) are mounted on the Printed Circuit Board (PCB) and connected to the EPS MCU.

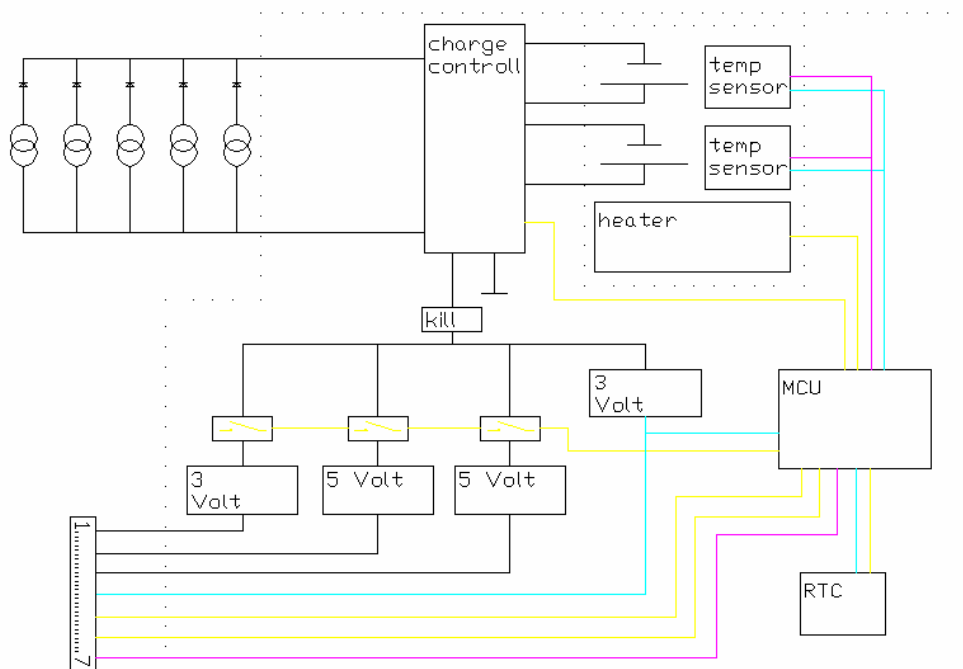


Fig.1.1: EPS architecture

1.1 Components

1.1.1 MCU

The MCU is the most important part of the EPS. It controls all hardware functions and communicates with the other subsystems. The required MCU peripherals needed are determined by the EPS hardware.

For the charging circuit, two Pulse-Width-Modulated PWM outputs with high speed and four A/D converters are required. A hardware I²C bus module and some hardware interrupts will significantly simplify programming task. To switch the voltage regulators, DC-DC converters and the TCS hardware, at least six general purpose I/Os are needed.

The timer for the Real-Time-Clock (RTC) function and its input is also needed.

The Silabs 8051 core MCUs are a good choice; they provide a lot more features than the EPS needs and are available in very small packages. The selected C8051F311 is only 5mm * 5mm square without any drawback in functionality.

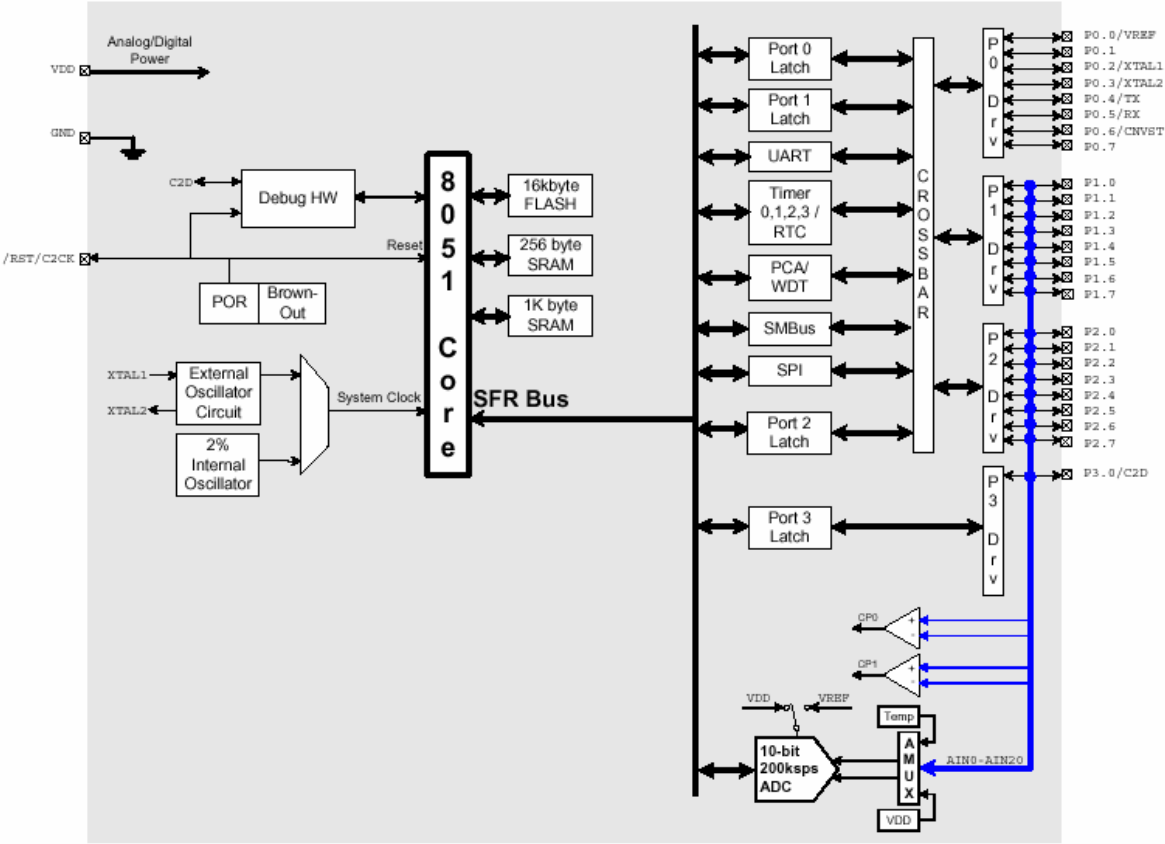


Fig.1.2: block diagram of C8051F311

The block diagram shows the features of the C8051F311. Additional ADC pins enable to easily measure the solar cell temperature with simple analog thermometers. These temperatures are a part of the house keeping data.

The Cygnal two wire system simplifies the development because an in-system programming is possible.

1.1.2 Clock

Although the MCU has its own oscillator, the system needs a crystal clock to deliver a time signal without temperature drift and offset. The MCU RC oscillator could not fulfill this and there would be no possibility to save energy by changing the MCU clock frequency.

For the clock the CD4060 CMOS logic chip with an external clock crystal has been selected. The CD4060 divides the crystal frequency in 14 stages, resulting in a logic signal with a frequency of 2 Hz for the MCU timer input. This signal is used to drive a MCU interrupt with a high priority to ensure proper software timing. An integrated hardware module, the PCA, simplifies the real-time clock operation by hardware support and comprehensive documentation.

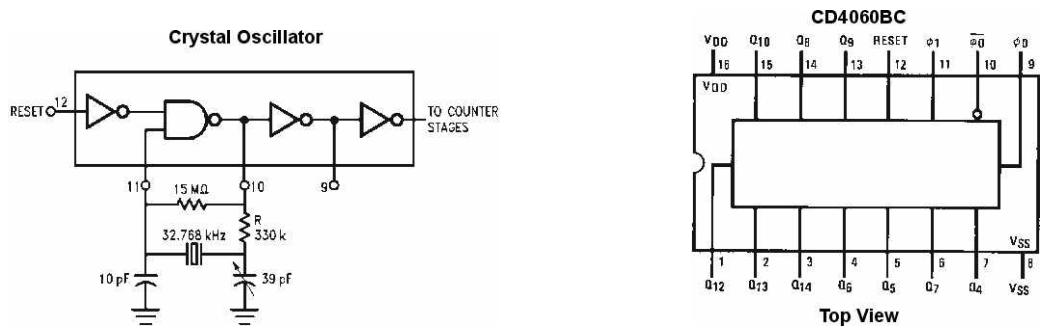


Fig.1.3: clock oscillator

Although no absolute time is available, the relative time is enough to trigger real time software for the measurement of housekeeping data, in particular the battery voltage.

An alternative approach would be the extraction of absolute time information from the GPS as part of the ADCS. However, this would result in significantly higher system complexity. Hence, the hardware solution discussed above is more adequate.

1.1.3 DC-DC converter

To provide a 5 volt voltage, a step up DC-DC converter is used. Thanks to modern Hand-Held Devices, this technology is available as compact single chip solution. There are a lot of different manufactures and devices. The Maxim MAX1675 is able to reach an efficiency of about 94% at 200mA output and industrial temperature range. Its reliability has been verified during independent previous testing. The IC is also used in model aircrafts at the same voltage ratio and alternating and inductive loads, as we could expect during the Compass-1 mission. To save power, the converter could be switched off. The Shutdown function does not satisfy our needs because the battery voltage remains present at the output of the voltage regulator, so a MOS FET will be used to solve this problem.

There are only a few external parts needed: tree capacitors and a coil.

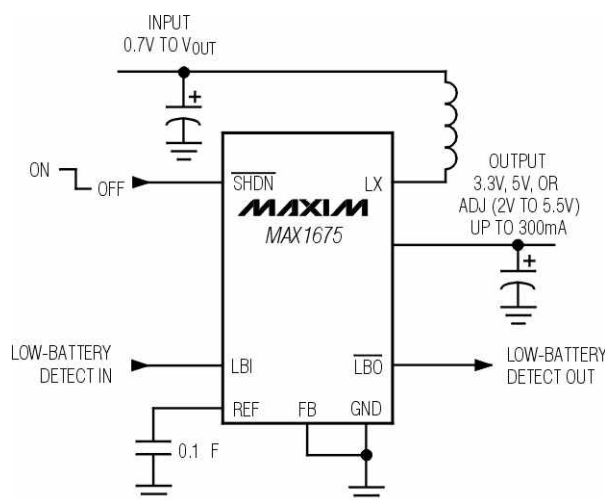


Fig.1.4: DC-DC converter IC

In emergency mode, only the COM system converter is switched on to save power, the other converter is switched of by the MCU.

1.1.4 Voltage regulator

Because the Lithium Polymer battery could fall below 3.3 volts, it has been decided to use 3 volts as second supply voltage. This is sufficient for the most parts and a lot less work to do. To stabilize the second voltage, an ultra-low-drop-out voltage regulator is needed to ensure stable output with nearly discharged batteries. With the Zetex ZLDO300, a suitable solution with only 100mV dropout at 300mA output and Shutdown function has been found. As for the DC-DC converter, the Shutdown is needed to save power where ever possible. The operating temperature ranges from $-40\text{ }^{\circ}\text{C}$ to $85\text{ }^{\circ}\text{C}$.

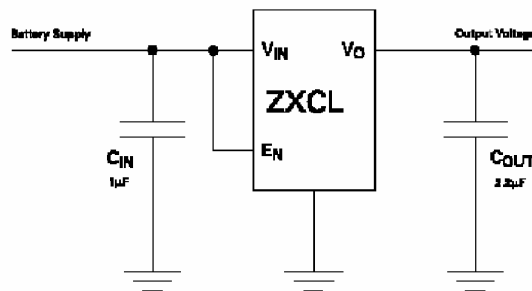


Fig.1.5: Voltage regulator

There are two voltage regulators used, one for the EPS, the temperature sensors and the COM subsystem, the other for the ADCS and the CDHS, which are switched off in emergency mode. The input and output is stabilized by two surface-mounted tantalium capacitors.

1.1.5 Charging control

As charging device two different solutions have been considered: An external single-chip solution with few external devices but less control or an integrated solution with the EPS MCU and additional hardware. To save space and weight, the MCU controlled charger was selected. The block diagram below shows the required hardware to charge a battery with the MCU.

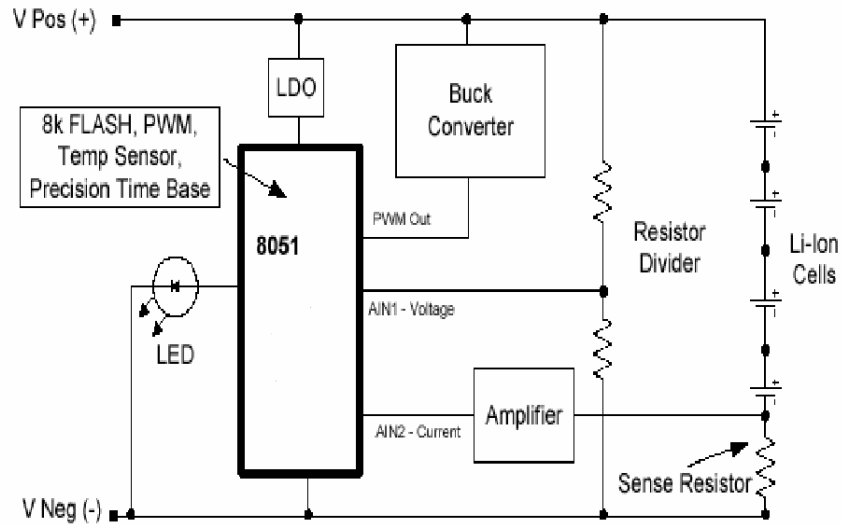


Fig.1.6: charging circuit

The buck converter is a switching regulator that uses an inductor as an energy storage element to create a linear charger. The converter is driven by a PWM signal from the MCU. The duty cycle controls the charging process.

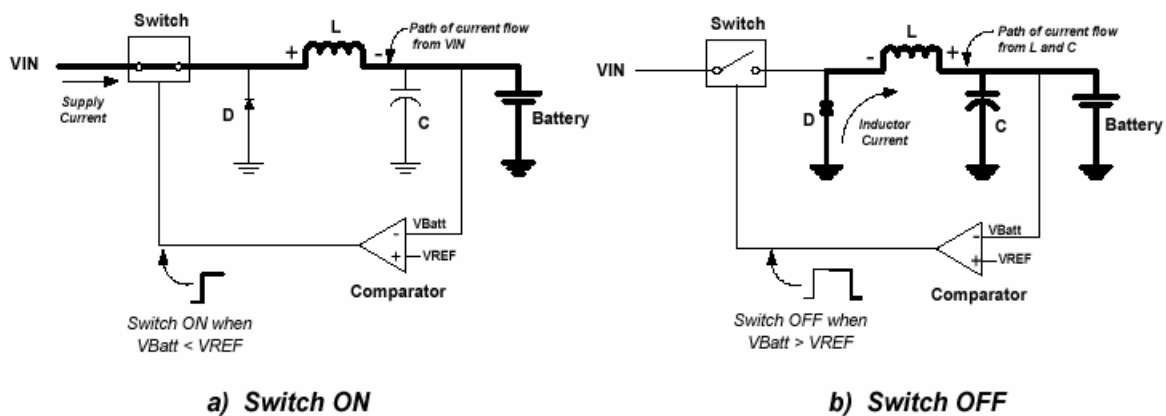


Fig.1.7: buck converter

The solar cells deliver enough voltage to charge the LiPo battery without an additional DC-DC converter.

1.1.6 Temperature sensors

There are two different types of temperature sensors to measure temperatures for the EPS. The temperature sensor LM75 was chosen because of its I²C two-wire interface and low power consumption. Up to eight sensors can be connected to one bus; this is a sufficient number. This sensor is used for PCB temperature surveillance. One additional temperature sensor is built in the EPS MCU, another one in the CDHS MCU. The mechanical link for the sensors is important, so the sensors for the batteries are also put into the battery box.

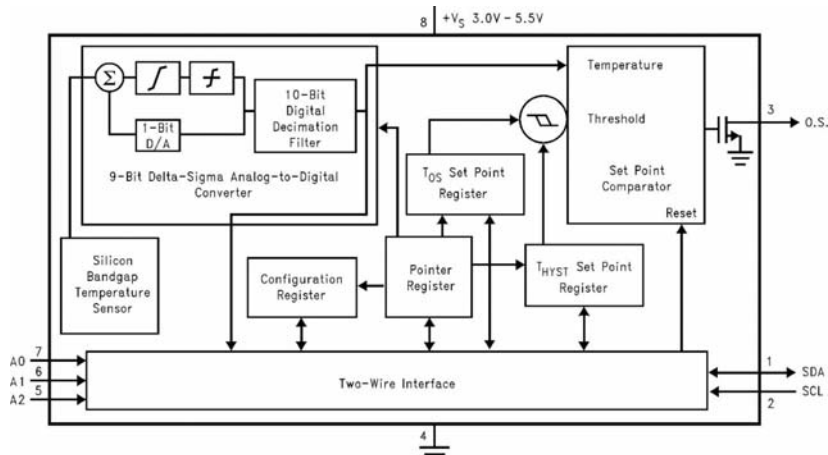


Fig.1.8:LM 75 block diagram

The address of the temperature sensor can be set by pins A0, A1, A2. The temperature could be read by any I²C device on the bus, not only the EPS MCU.

The second temperature sensor is used to determine the Solar Cell temperature on each side of the spacecraft. This platinum thin-film sensor is small and light and can be used within a temperature range from -70°C to 500°C . It is very long-term stable with a drift of 0.04% after 1000h at 500°C .

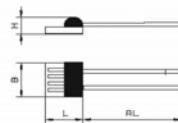
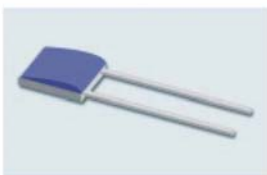
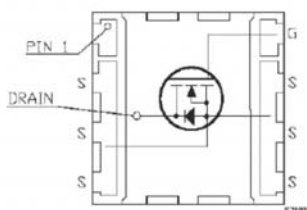


Fig.1.9: clock oscillator

1.1.7 FET

The Field Effect Transistors are used to switch on and off loads which are too high for the MCU. Especially for the power supply, a low loss and therefore a low internal resistance is important. Normal values of the FETs resistance is about 0.003-0.016 Ohms.

INTERNAL SCHEMATIC DIAGRAM



**PowerFLAT™ (5x5)
(Chip Scale Package)**

Fig.1.10: FET schematic and package

Available in a surface mountable package, the STL28NF03LL is a suitable choice with only 0.0065 Ohms resistance and a small 5x5 mm² package. The FETs are driven by the MCU. External pull down resistors reliably switch them off when the MCU is powered down during reset.

1.1.8 TCS Hardware / Antenna Deployment Hardware

The TCS Hardware and Software is also integrated on the EPS board. To toggle the heaters, the same logic level MOS FETs are used as for the EPS. With the low internal resistance they provide minimal losses and maximal power for the heaters. The transistors are controlled with a PWM signal from the EPS MCU. To control the deployment of the antenna, one of the FETs delivers energy to the wire to melt the nylon wire and activate the antenna deployment mechanism.

1.1.9 Solar cells

The selected cells are RWE ultra-triple-junction cells based on a Ge substrate with an average efficiency of 26.6%. The solar cell panel will be delivered by Astrium and RWE.

The output voltage at maximum power is 2.258 Volt (at 28°C), so two cells have enough voltage to charge the Lithium Polymer Cell with its maximal voltage of 4.2 volts including the losses in the charging circuit which are a result of resistance. To provide additional solar cell data, a temperature sensor is mounted on each solar cell panel. Because of the mentioned address restrictions of the I²C temperature sensors, analog sensors will be used and connected to the analog-digital-converter function of the MCU.

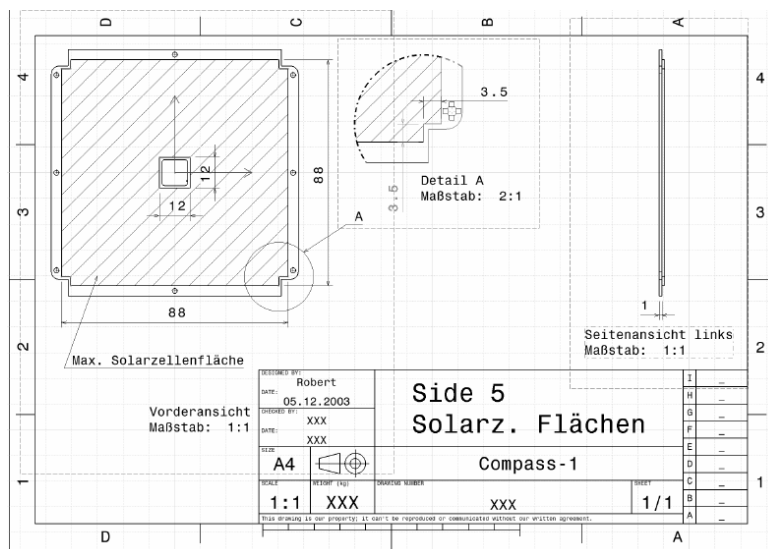


Fig.1.11: solar cell area

The final configuration depends on the method that the cells are connected with. The multi-junction cell has four pads to connect. Because no suitable alignment was found yet, the cells may be connected directly to the EPS board.

A cover glass for the solar panel is needed to protect them from UV light and small low-energy particles.

1.1.10 Batteries

The comparison between different types of energy storage in phase A led to a LiPo cell system because of its low weight and a good cell voltage. There are a lot of different cells with different shapes, unfortunately not intended to be used in CubeSats. Two of the market leaders E-Tech and Kokam are widely spread in the model market, so it was no problem to find a distributor. Finally, the E-Tech cell wins the challenge because of its higher energy density and its shape.

A common problem with this type of battery cells is that they may rapidly lose performance and eventually entirely cease function when subjected to a high vacuum. Typically this effect is related to a physical expansion of the battery block. To counteract this effect on Compass-1, it is enclosed in a stiff milled aluminum box. The gap between this box and the LiPo cell is filled with epoxy resin. Besides the need to protect the cell from the harsh environment, this is also a solution to provide mechanical interface between the cell and the satellite structure.

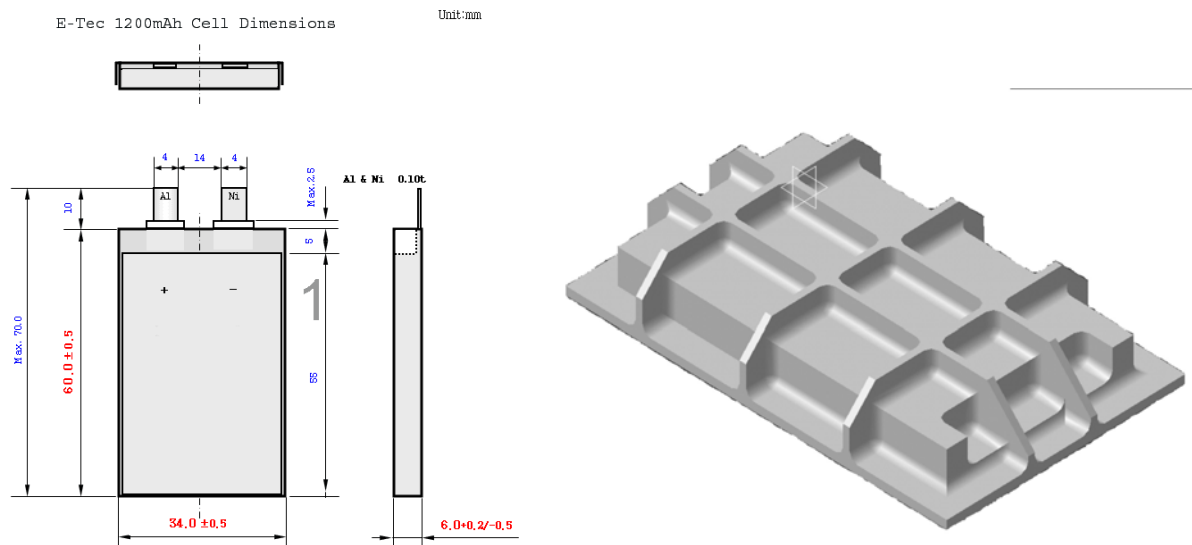


Fig.1.12: LiPo cell and aluminum box

1.2 Integration

All parts are mounted and connected on a typical epoxy printed circuit board with a thickness of 1.5mm. A major advantage of surface mount technologies is the possibility to use both sides of the board. Because of the small part count, a multilayer board is not needed.

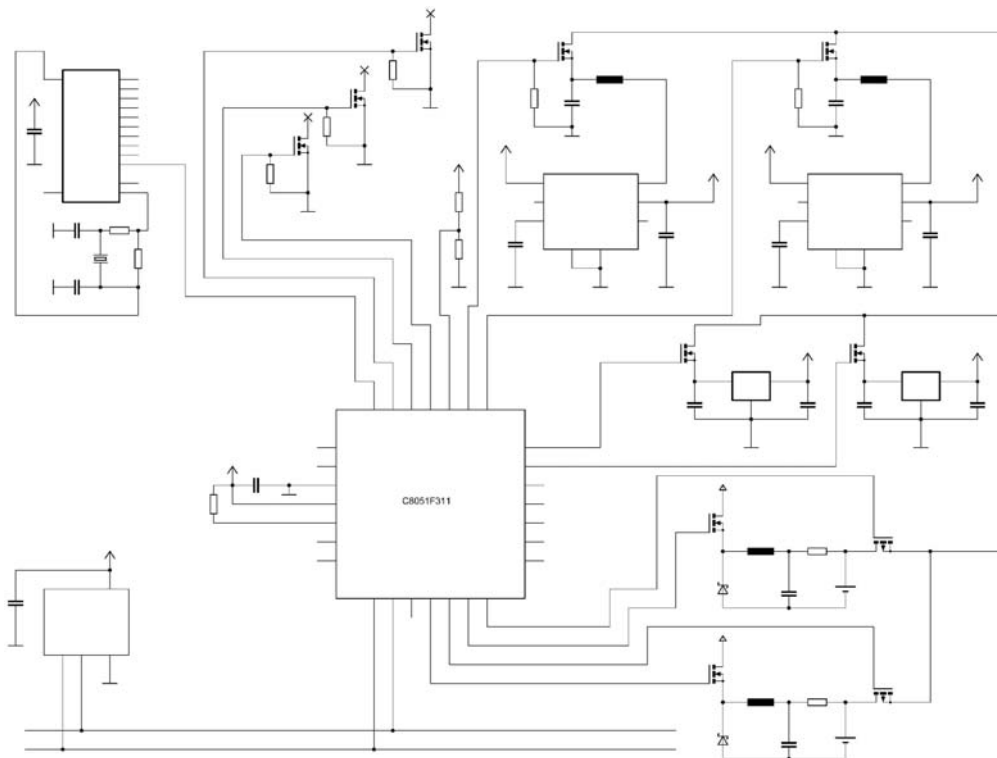


Fig.1.13: EPS preliminary schematic

The EPS communicates with two other subsystems, the CDHS and, in emergency mode, the COM subsystem. Because of the multiple I²C bus participants, the CC value is used to identify the requested operation.

From	To	CC	Additional Data	Description
CDHS	EPS	0x30	-	Request housekeeping data
EPS	CDHS	0x31	25 Bytes	Send housekeeping data

Fig.1.14: I²C commands

The 25 bytes of house keeping data is enough for all important values, including the solar cell voltage and temperature to record the solar cell behavior as requested.

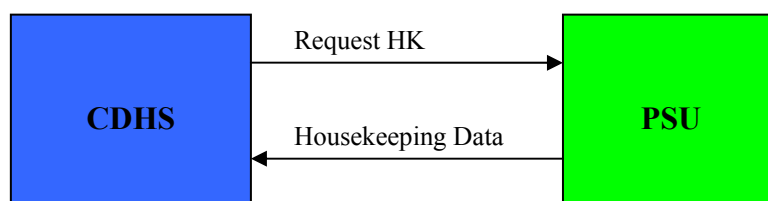


Fig.1.15: Communication CDHS - EPS

Beside the data send trough the spacecraft bus, there is another connection between the power subsystem and the COM subsystem to the transfer house keeping data directly to the Morse encoder if the satellite operates in emergency mode. Although this connection uses CHDS tracks and connectors, it is completely independent of all other subsystems.

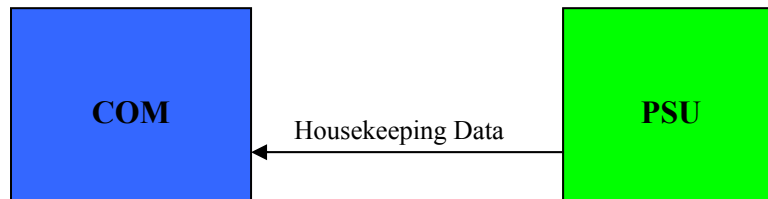
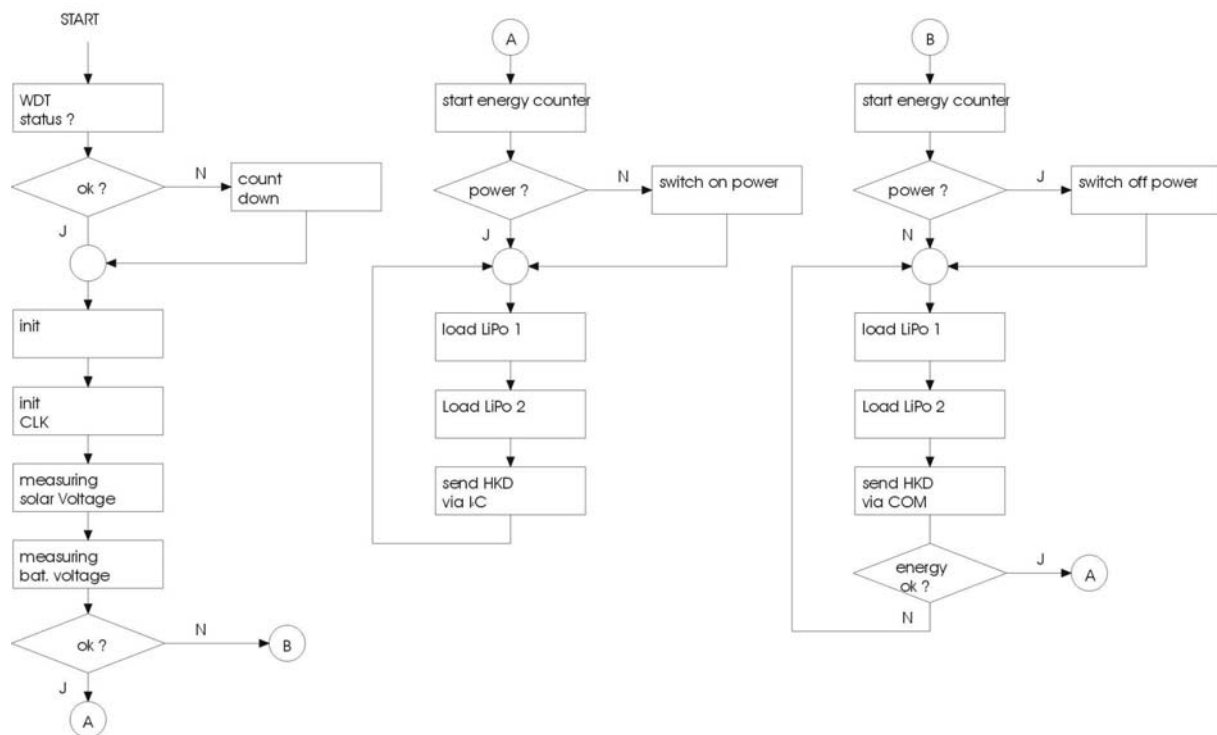


Fig.1.16: Communication COM - EPS

2. Software Definition

The software for the EPS consists of four major parts, at first the boot procedure where all hardware modules are initialized and registers loaded with default values. After the boot procedure, the MCU decides if it is necessary to change to Emergency Mode or if Normal Mode could be started. In Normal Mode every subsystem is powered up and then coordinated by the CDHS. The housekeeping data from the EPS can be read via the I²C bus. In Emergency Mode only the EPS, TCS and COM systems are working and the COM system is fed with the house keeping data from EPS via an additional one wire bus system. The flow chart represents the three different operating modes: on the left side is the boot procedure illustrated. During the boot procedure the WDT status monitors if the power up delay after deployment is needed. Then the software decides between Normal Mode (A) and Emergency Mode (B) depending on the energy stored in the two LiPo cells.



The next steps to write suitable software are tests with the hardware. That will give more information about the need for interrupts and other hardware modules to save time in the subroutines. In the name of saving energy, the MCU should be clocked as slow as possible.

To increase the hardware control, the MCU clock needs to run fast, so a suitable compromise has to be found. Some functions require a real time response, i.e. the real time clock or the LiPo charging function, so the use of assembly language seems to be an advantage.

3. Appendix

3.1 Abbreviations

ADCS	Attitude Determination and Control System
CDHS	Command and Data Handling System
FET	Field effect transistor
LiPo	Lithium Polymer battery
MCU	Micro control unit
PWM	Pulse Width Modulation
TCS	Thermal Control System
WDT	Watch Dog Timer

3.2 References

- [12] CubeSat Team Aachen. (2003) *Phase A Study of COMPASS-1*. www.raumfahrt.fh-aachen.de
- [13] www.silabs.com
- [14] www.zetex.com
- [15] www.maxim-ic.com
- [16] www.semiconductors.philips.com
- [17] www.national.com
- [18] www.rwespace.com



2004-06-08

WBS460: TCS

Thermal Control System

Phase B: Detailed Definition

Author

Sylwia Czernik

FH Aachen, Germany



Scope

This paper documents the detailed definition of the Thermal Control System of the COMPASS-1 CubeSat.

Contents

Introduction.....	134
Nomenclature	135
TCS Requirements	136
1 Thermal Environment	137
1.2 Basic Laws	139
1.3 Orbital parameters	142
1.4 Heat transfer	146
1.4.1 Convection	146
1.4.2 Conduction	146
1.4.3 Radiation	147
2 Calculations.....	149
2.1 Energy balance of Compass-1	149
2.2 Temperature equilibrium	150
2.2.1 Cold case eclipse	150
2.2.2 Hot case	151
2.2.3 View Factor	152
2.4 Properties of materials	154
2.5 Instationary calculation	157
2.6 Results of instationary calculation	159
3 3D model of satellite.....	160
3.1 Thermal model	160
3.2 Analysis	162
3.3 Nodal network modeling results	164
4. Thermal control	165
4.1 System optimisation	170
References	172

Introduction

Unlike terrestrial or airborne vehicles, spacecraft in general and satellites in particular are subject to an extreme thermal environment. Body temperatures ranging from -100°C to $+100^{\circ}\text{C}$ are not uncommon in astronautically engineering applications. Sometimes these extreme temperatures are present at the same time at different locations of the spacecraft. Fairly straightforward analytical and numerical methods are available to compute the thermal states for a given geometrical body in Earth orbit. The thermal control engineer must derive essential conclusions from these results and design thermal management solutions that satisfy the operational temperature limits of all components installed on the spacecraft. Numerical simulation is the most important tool for the thermal control engineer. Considerable effort must be spent in determining the thermal behaviour of a body; the derived system solutions often seem trivial on first sight but in fact they are highly optimized solutions emerging from a comprehensive and sophisticated design preparation.

Nomenclature

Background temperature T_{space}	$3[K]$
Earth Radius R_E	$6370[km]$
IR Radiation I_E	$260\left[\frac{W}{m^2}\right]$
Albedo	$470\left[\frac{W}{m^2}\right]$
Heat flux sun I_S	$1378\left[\frac{W}{m^2}\right]$
Altitude of Compass-1 H	$600[km]$
Gravity constant γ	$6,67 \cdot 10^{-11}\left[\frac{Nm^2}{kg^2}\right]$
Stefan-Boltzman-Constant σ	$5.67 \cdot 10^{-8}\left[\frac{W}{m^2 K^4}\right]$

TCS Requirements

1 Thermal Environment

Compass-1 will be exposed to physical conditions and terms, which are differ from the conditions on Earth.

Sunlight is the greatest source of environmental heating incident on most spacecraft. The emitted radiation from the sun is constant within a fraction of 1% at all times. However, due to the Earth's elliptical orbit, the intensity of sunlight reaching the Earth varies approximately $\pm 3.5\%$ depending on the Earth's distance from the sun. At summer (northern hemisphere) the intensity is at a minimum of $1327W/m^2$ and at a maximum of $1471W/m^2$ at winter solstice.

Sunlight that is reflected off of a planet or his atmosphere is known as Albedo. The Earth's Albedo is usually expressed as a percentage of incident sunlight that is reflected back out to space and is highly variable. As a first approximation one can assume a value of about 34%; however, reflectivity is generally greater over continental as compared to oceanic regions and generally increase with decreasing local solar regions elevation angles and increasing cloud coverage.

The Earth not only reflects sunlight, it also emits long-wave IR radiation. The Earth, like a satellite, achieves thermal equilibrium by balancing the energy received (absorbed) from the sun with the energy re-emitted as long-wavelength IR radiation into space. This balance is maintained fairly well on a global annual average basis. As a first approximation one can use a value of around $237 \pm 21W/m^2$ emitted from the Earth's surface

At satellite altitudes the background of the sky is black. Radiation (gamma, X, ultraviolet, visible, infrared and radio) from deep space represents a very small amount of energy.

The temperature surrounding the satellite in space is 2.7K and the pressure surrounding is very close to vacuum.

This radiative environment causes extreme temperature variations in the satellite's outer skin. Thus the outside layers of insulating blankets can reach temperatures of $100^\circ C$ when turned towards to the sun and drop to $-100^\circ C$ when in the shadow of the satellite or Earth.

Radiation balance of Compass1 in LEO

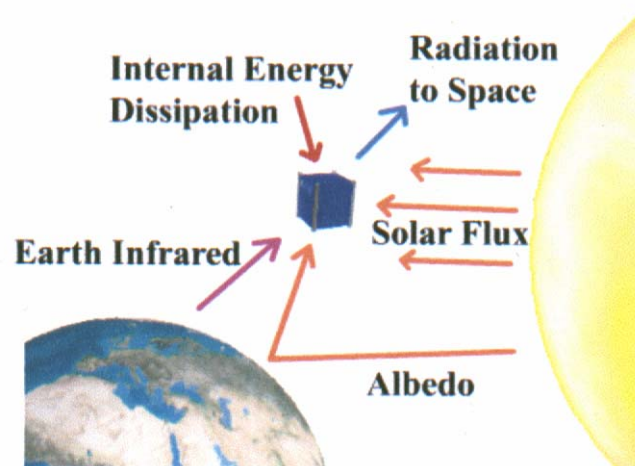


Figure1 Space environment for Compass1 in LEO

The following is a Table of constrains for the thermal control system

Constraints
<ul style="list-style-type: none">- Peak power < 1W- Average power < 80mW- Mass below 30g

Table1 TCS constrains

1.2 Basic Laws

Spectrum of solar radiation

Solar intensity varies as a function of wavelength. The energy distribution is approximately 7% ultraviolet, 46% visible and 47% near infrared with the total integrated energy being equal to the $1327W/mm^2$ to $1471W/mm^2$ values mentioned above.

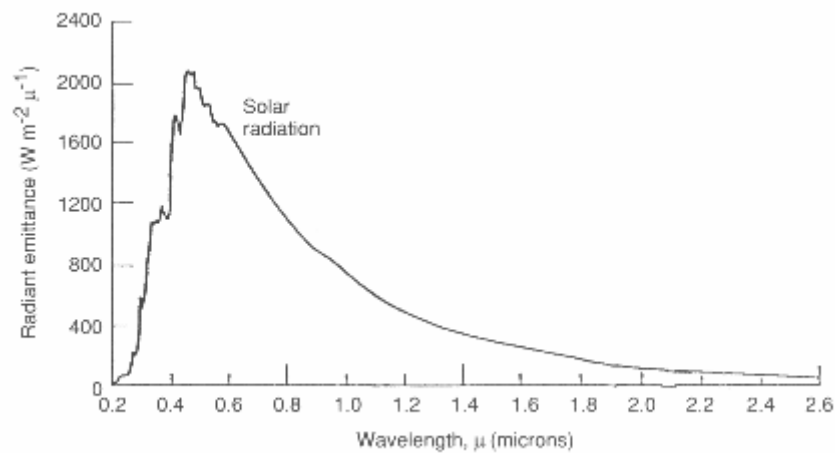


Figure 2. Spectral distribution of sun radiation on LEO

Black body

An ideal black body is a theoretical object that absorbs all the radiant energy falling upon it and emits it in the form of thermal radiation. Planck's radiation law gives the power radiated by a unit area of black body and the Stefan-Boltzman law expresses the total power radiated.

Black body radiation

Black body radiation is the radiation emitted by a perfect black body, i.e., a body which absorbs all radiation incidents on it and reflects none. The wavelength dependence of the radiated energy density ρ (energy per unit volume per unit wavelength range) is given by the Planck law.

Stefan-Boltzman Law

The rate at which a blackbody radiates energy is given by:

$$I = \sigma T^4 \left[\frac{W}{m^2} \right] \quad (1)$$

$$\sigma = 5.67 \cdot 10^{-8} \left[\frac{W}{m^2 K^4} \right] \text{ Stefan-Boltzman-Constant}$$

Planck's law

The Planck law gives the hemispheric (2α) intensity radiated by a blackbody as a function of frequency (or wavelength)

$$E_{b\lambda} = \frac{2\pi hc^2}{\lambda^5} \cdot \frac{1}{e^{ch/k\lambda T} - 1} \left[\frac{W}{m^3} \right] \quad (2)$$

where

λ = Wavelength [m]

h = Planck's constant $6.6261 \cdot 10^{-34} \text{Ws}^2$

T = Temperature [K]

c = speed of light $\approx 3 \cdot 10^8 \frac{m}{s}$

k = Boltzman constant $1.380 \cdot 10^{-23} \frac{Ws}{K}$

If the emissivity is a constant, independent of wavelength, the integration of equation (2) over all wavelengths results in the Stefan-Boltzman-Equation (1).

Wien's displacement law

The wavelength λ_{\max} , for which the radiated power per unit of wavelength is maximal, is related to the temperature T of the thermal emitter.

$$\lambda_{\max} T = \text{const.} = C_3 \quad (3)$$

$$C_3 = \text{constant in Wien's displacement law } 0.28978 \left[\frac{\text{cm}}{\text{K}} \right]$$

Thus the hotter an object is the lower the wavelength at which the intensity peaks. An object that glows bluish is hotter and brighter than an object that glows red (the wavelength of blue light is smaller than that of red light).

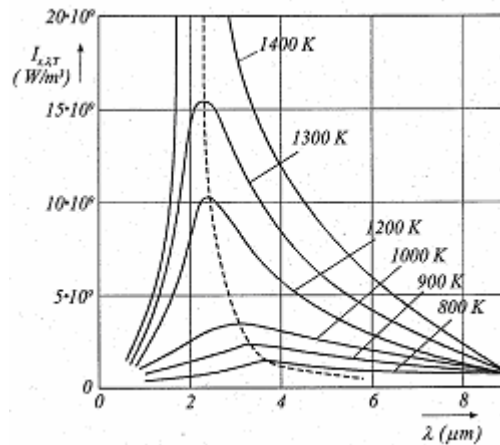


Figure3 . Wien's displacement law

1.3 Orbital parameters

The Compass-1 is designed for a sun synchronous low earth orbit at an altitude of 600 km with an inclination of 98deg. The sun synchronous orbit has the characteristic of maintaining the orbit plane at a nearly fixed angle relative to the sun. The result of this is that, on every orbit, the satellite passes over points on the Earth that has the same local time. Because the Earth rotates beneath the orbit, the satellite sees a different swatch of the Earth's surface on each revolution and can cover nearly the entire globe over the course of a day.

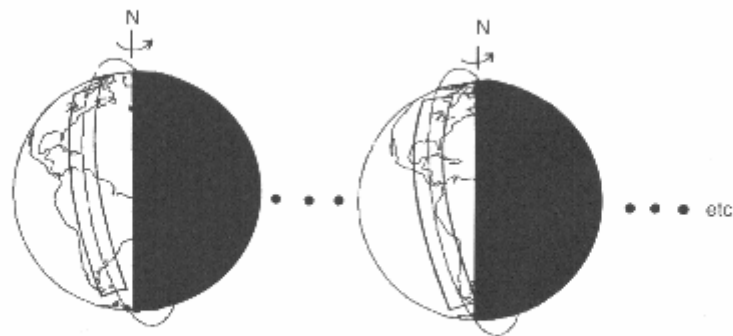


Figure4. Sun synchronous orbit

In Low Earth Orbit (LEO), there is another parameter, known as the orbit beta angle β , which is very useful in visualizing the orbital thermal environment, particularly for the low Earth orbits. The beta angle is defined as the minimum angle between the orbit plane and the solar vector and can vary from -90deg to +90deg, as illustrated in Figure5. The beta angle is defined mathematically as

$$\beta = \arcsin(\cos \delta_s \sin RI \cdot \sin(\Omega - \Omega_s) + \sin \delta_s \cos RI) \quad (4)$$

where

- δ_s = declination of the sun
- RI = orbit inclination
- Ω = right ascension of the ascending node
- Ω_s = right ascension of the sun
- β = beta angle

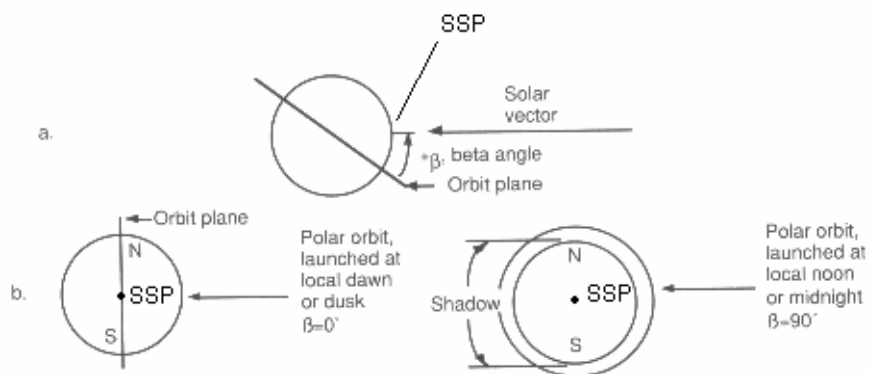


Figure5 Orbital beta angle

As viewed from the sun, a $\beta=0\text{deg}$ orbit would appear edgewise SSP, as shown in *Figure5.b*. A satellite in such an orbit would pass over the sub-solar point on the Earth (the point on the Earth where the sun is directly overhead). Where Albedo loads are the highest, but it would also have the longest eclipse time due to shadowing by the full diameter of the Earth. As the β angle increases, the satellite passes over areas of the Earth further from the sub-solar point, thereby reducing Albedo loads; however, the satellite will also be in the sun for a larger percentage of each orbit due to decreasing eclipse times. At some point, which varies depending on the altitude of the orbit, eclipse time drops to zero. At a beta angle of 90deg a circular orbit appears as a circle as seen from the sun there are no eclipses no matter what the altitude, and Albedo loads are near zero. It should also be noted here that beta angles are often expressed as positive or negative positive if the satellite appears to be going counter-clockwise around the orbit as seen from the sun, negative if clockwise.

The eclipse fraction of a circular orbit can be calculated from following equation

$$t_E = \frac{1}{180^\circ} \cos^{-1} \left(\frac{(h^2 + 2Rh)^{0.5}}{(R + h) \cos \beta} \right) \quad \text{if } |\beta| < \beta^* \quad (5)$$

where

- R = Earth's radius
- h = orbit altitude
- β = orbit beta angle
- β^* = beta angle at which eclipses begin

β^* may be calculated using:

$$\beta^* = \sin^{-1}\left(\frac{R}{R+h}\right) \quad (6)$$

Equations (5) and (6) assume that the Earth's shadow is cylindrical, which is valid for low orbits where there is no appreciable difference between the umbra and penumbral regions of total and partial eclipsing, respectively.

Orbital revolution of Compass-1

$$t_u = \sqrt{\frac{4\pi^2}{\gamma \cdot M_E} \cdot a^3} = 96.30 \text{ min} \quad (7)$$

Time of eclipse

$$\frac{t_{shadow}}{t_u} = \frac{2 \cdot \alpha}{360^\circ} \quad (8)$$

where

$$\alpha = \arcsin \left(\frac{\sqrt{\left(\frac{R_E}{r}\right)^2 - \sin^2 \beta}}{\cos \beta} \right) \quad (8.1)$$

$$a = \frac{r_a + r_p}{2} = \frac{(R_E + h_a) + (R_E + h_p)}{2} \quad (8.2)$$

a = Orbit semi-major axis

M_E = Mass of Earth = $5.97 \cdot 10^{24} \text{ kg}$

R_E = Earth's radius

$h_a = h_p = 600 \text{ km}$, circular

For a 600km orbit with $\beta = 0$ Compass-1 completes one orbital revolution t_u in 96.30 minutes. For two-third of the orbital period, i.e. 60.52 minutes, the satellite is in sunshine and its surfaces goes hot, while for 35.38 minutes it is in the Earth's shadow and cools down.

1.4 Heat transfer

There are three mechanisms by which thermal energy is transported:

1. Convection
2. Conduction
3. Radiation

For each of the three transfer mechanisms, thermal energy flow is always directed from regions of higher to lower temperature.

1.4.1 Convection

Due to the extremely low density of the atmosphere at the orbital altitude and because of the microgravity environment, there are no mass or particles for convection process. The surrounding background temperature in space is 3 K, very close to absolute zero. Then there is no transfer between hot and cold areas due to convection.

1.4.2 Conduction

When there exists a temperature gradient within a continuum (gas or rigid mass), thermal energy will flow from the region of high temperature to the region of low temperature. This is known as conduction heat transfer, and is described by Fourier's Law

$$Q_{cond} = \frac{\lambda \cdot A \cdot \Delta T}{L} \quad (9)$$

Replacing the expression of Q_{cond} the geometrical and materials values by a resistance factor $R_{th,cond}$, it yields:

$$R_{th,cond} = \frac{L}{\lambda \cdot A} \left[\frac{K}{W} \right] \quad (10)$$

equation (9) can be written as:

$$Q_{cond} = \frac{1}{R_{th.cond}} \cdot \Delta T \quad (11)$$

where

L = Length of the conduction path [m]
 λ = thermal conductivity coefficient
 A = cross sectional area [m²]

Conduction will apply only for components on the same board and R_{jc} (thermal resistance junction case) can be assumed as a thermal resistance for this transfer.

1.4.3 Radiation

Radiation is the only mechanism of heat transfer for which no medium is required in order to transport heat between two elements. Energy is transferred from one body to another in the form of electromagnetic waves. Matter with a temperature above 0 K emits a certain amount of radiation. The radiation energy an object emits is affected by its geometry, surface properties, relative position with respect to other thermally significant objects and its surface temperature.

$$Q_{rad} = \varepsilon \cdot \sigma \cdot F_{ij} \cdot A \cdot T^4 \quad (12)$$

where

ε = emissivity (value between 0-1) [÷]
 A = surface area of object [m²]
 T = temperature [K]
 F_{ij} = View factor [÷]

Radiative heat transfer must be account for both *incoming* and *outgoing* radiation. By stating that a body's surface emissivity is equal to its absorption fraction, Kirchhoff's Identity binds incoming and outgoing thermal radiation into a useful dependent relationship

$$\varepsilon = \alpha_{thermal.absorb.}$$

Incoming solar radiation can be absorbed, reflected or transmitted.

$$1 = \alpha + \tau + r \quad (13)$$

Since most solid bodies used on Compass-1 are opaque to thermal radiation, transmissivity can be neglected:

$$1 = \alpha + r \quad (13.1)$$

2 Calculations

In this chapter a preliminary thermal calculations will be done in order to have an idea of the temperature Compass-1 will have to withstand during an orbit.

2.1 Energy balance of Compass-1

Thermal heat balance happens when the amount of heat coming into the spacecraft equals the amount of heat leaving the spacecraft.

$$\dot{Q}_{in} = \dot{Q}_{out} \quad (14)$$

$$\dot{Q}_{sun} + \dot{Q}_{albedo} + \dot{Q}_{earth} + \dot{Q}_{space} + \dot{Q}_P = \dot{Q}_{sat \rightarrow earth} + \dot{Q}_{sat \rightarrow space} \quad (14.1)$$

where

$$\dot{Q}_{sun} = \alpha_s A_{sat,proj} I_{sun}$$

$$\dot{Q}_{albedo} = \alpha_s A_{sat} F_{earth \rightarrow sat} 0.34 \cdot I_{sun}$$

$$\dot{Q}_{earth} = \alpha_{IR} A_{sat} F_{earth \rightarrow sat} I_{earth}$$

$$\dot{Q}_{space} = \alpha_{IR} A_{sat} F_{space \rightarrow sat} \sigma T_{space}^4$$

$$\dot{Q}_{sat \rightarrow earth} = \epsilon_{IR} A_{earth} F_{sat \rightarrow earth} \sigma T_{sat}^4$$

$$\dot{Q}_{sat \rightarrow space} = \epsilon_{IR} A_{space} F_{sat \rightarrow space} \sigma T$$

$$A_{sat} F_{earth \rightarrow sat} = A_p$$

$$A_{sat} F_{space \rightarrow sat} = 1 - (A_{sat} F_{space \rightarrow sat}) = 5 \cdot A_p$$

$$A_{sat} F_{sat \rightarrow earth} = A_p$$

$$A_{sat} F_{sat \rightarrow space} = 1 - (A_{sat} F_{sat \rightarrow earth}) = 5 \cdot A_p$$

$$\alpha_{IR} = \epsilon_{IR}$$

$$F_{i \rightarrow j} = \text{view factor}$$

$$\dot{Q} = \text{electrical power dissipation}$$

2.2 Temperature equilibrium

The objective is the computation of the equilibrium temperature for Compass-1, considering no internal heat sources at this stage, such that

$$\dot{Q}_p = 0$$

Radiation balance

The calculation of the steady-state temperatures uses a basic energy balance (see chapter 2.1). The effects included in the calculation are solar radiation, albedo, terrestrial radiation and radiation from the body to space. The equation after solving for equilibrium temperature is:

$$T = \sqrt[4]{\frac{\alpha}{\varepsilon} \cdot \frac{I_s}{\sigma} \cdot \frac{A_p}{A} + \frac{\alpha}{\varepsilon} \cdot \frac{0.34I_s}{\sigma} \cdot \frac{A_p}{A} + \frac{\alpha_E}{\varepsilon} \cdot \frac{A_p}{A} \cdot \frac{I_E}{\sigma} + \frac{\alpha_{IR}}{\varepsilon \cdot \sigma} \cdot \frac{5A_p}{A} \cdot T_{space}^4} \quad (15)$$

2.2.1 Cold case eclipse

If the spacecraft is in the shadow of the Earth and is not in view of any portion of the sunlit parts of the Earth, this condition is called 'a worst-case cold condition'. For this condition there is no direct solar, albedo energy intake, which also means, that no electric power can be generated. The equation which defines the temperature for this condition is Kirchhoff's law for a rigid body:

$$T_{\min} = \left[T_{space}^4 + \frac{I_E}{\sigma} \cdot \frac{\alpha_{IR}}{\varepsilon_{IR}} \cdot \frac{A_p}{A} \right]^{1/4} \quad (16)$$

where

$$\begin{aligned} \alpha_s &= \text{IR absorbtivity} \\ \varepsilon_{IR} &= \text{IR emissivity} \end{aligned}$$

2.2.2 Hot case

For a solar array covered body of a spacecraft, the energy balance equation includes a power generation term since the solar cells convert solar energy directly to electrical energy. There is some dissipation associated with solar arrays; however, these losses are accounted for in the array efficiency term. The solar array efficiency, η , is defined as the ratio of electrical power output to incident solar radiation.

The worst-case hot temperature for the flat plate or solar array is defined as:

$$T_{\max} = \left[T_{space}^4 + \frac{I_s}{\sigma} \cdot \frac{A_p}{A} \cdot \frac{\alpha_s}{\epsilon_s} + \frac{I_E}{\sigma} \cdot \frac{A_p}{A} \cdot \frac{\alpha_E}{\epsilon_E} + \frac{0.34 \cdot I_s}{\sigma} \cdot \frac{A_p}{A} \cdot \frac{\alpha_s}{\epsilon_s} \right]^{1/4} \quad (17)$$

Where

A	=	surface area (thermal radiation), total surface area of the spacecraft
A_p	=	proj. surface area area that is exposed to earthshine/sunshine
α_s	=	solar absorbtivity
ϵ_{IR}	=	emissivity

The results:

$T_{\min} = 180.23K = -92.77^\circ C$ for worst cold case at the end of eclipse and

$T_{\max} = 295.85K = 22.85^\circ C$ for worst hot case.

2.2.3 View Factor

The view factor between two objects F_{12} is used to parameterize the fraction of thermal power leaving object 1 and reaching object 2. Specifically, this quantity is equal to:

$$Q_{1 \rightarrow 2} = A_1 F_{12} \varepsilon_1 \sigma T_1^4 \quad (18)$$

Likewise, the fraction of thermal power leaving object 2 and reaching object 1 is given by:

$$Q_{2 \rightarrow 1} = A_2 F_{21} \varepsilon_2 \sigma T_2^4 \quad (19)$$

The case of two blackbodies in thermal equilibrium can be used to derive the following reciprocity relationship for view factors

$$A_1 F_{12} = A_2 F_{21} \quad (20)$$

Another important Property of the view factor is the summation rule. For a complete enclosure with n surfaces the rule states:

$$\sum_{j=1}^n F_{ij} = 1 \quad (21)$$

The view factor for two surfaces is a function of area, orientation and distance. In its general form the view factor follows equation (22).

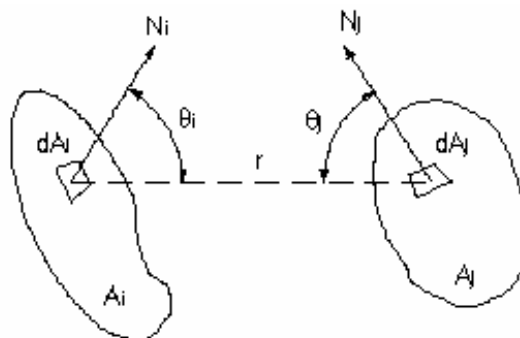


Figure6 View factor

$$F_{12} = \frac{1}{\pi A_1} \int_{A_1} \int_{A_2} \frac{\cos \theta_1 \cdot \cos \theta_2}{r^2} \cdot dA_1 dA_2 \tag{22}$$

where

A_1, A_2 = area of surface 1 and surface 2

r = distance between differential surfaces 1 and 2

θ_1 = angle between N_1 and the radius line to surface $d(A_1)$

θ_2 = angle between N_2 and the radius line to surface $d(A_2)$

N_1, N_2 = surface normal of $d(A_1)$ and $d(A_2)$

Compass-1 can be consider like a flat plate, with its surface normal parallel to the solar vector and passing through the centre of the Earth (*Figure7*)

$$F_{sat \rightarrow Earth} = \frac{1}{2} \left(1 - \frac{1}{\sqrt{1 + \left(\frac{R_2}{H}\right)^2}} \right) \tag{23}$$

where

H = the altitude of the cube, 600km

R_2 = the Radius of the Earth, 6370km

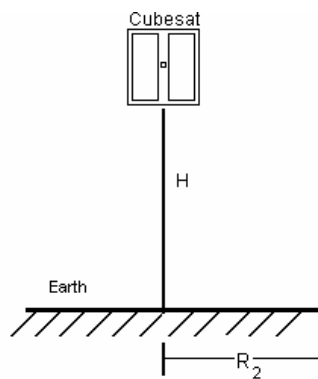


Figure7 View factor Cubesat→Earth

2.4 Properties of materials

Surface

The external surfaces of a spacecraft radiatively couple the spacecraft to space. Because these surfaces are also exposed to external sources of energy such as sunlight and Earth-emitted IR, their radiative properties must be selected to achieve an energy balance at the desired temperature between spacecraft internal dissipation, external sources of heat, and reradiation to space.

For Compass-1 the used materials with their properties as are shown in the following table.

Satellite structure

The basis structure is made from Al 6061-T6. The optical surface properties shown in *Table2* are based on an uncoated surface.

Solar cells

Due to their high absorptance, high emittance, and low weight, solar arrays typically cycle over wide temperature ranges as they go from sunlight to eclipse. The most advanced are from RWE/Germany with a poor efficiency of 28.0%. They are Ultra Triple Junction Solar Cells.

	Al 6061-T6	Solar cells	Black paint
Density [kg/m ³]	2700	2100	-
Conductivity [W/(m*K)]	166.9	200	-
Specific Heat [J/(kg*K)]	1000	1600	-
Emissivity (thermal)	0.379	0.85	0.90
Absorptivity (solar)	0.0346	0.92	0.95

Table2. Material properties of Compass1 [9]

The surface of Compass-1 is made up of about 30% aluminium alloy and 70% solar cells. Hence, it is necessary to calculate an average material property for the thermal analysis.

$$Q_{A_p} = Q_{sc} + Q_{Al} \tag{24}$$

where

$$Q_{sc} = \epsilon_{sc} \cdot A_{sc} \cdot \sigma \cdot T_{sc}^4$$

$$Q_{Al} = \epsilon_{Al} \cdot A_{Al} \cdot \sigma \cdot T_{Al}^4$$

$$T_{Al} = T_{sc}$$

using the equation (24)

$$\epsilon_m \cdot A_p \cdot \sigma \cdot T^4 = \sigma \cdot T^4 (\epsilon_{sc} \cdot A_{sc} + \epsilon_{Al} \cdot A_{Al})$$

$$\epsilon_m = \epsilon_{sc} \cdot \frac{A_{sc}}{A_p} + \epsilon_{Al} \cdot \frac{A_{Al}}{A_p}$$

it follows that:

$$\alpha_m = 0.7 \cdot 0.92 + 0.3 \cdot 0.0346 = 0.654$$

$$\epsilon_m = 0.7 \cdot 0.85 + 0.3 \cdot 0.379 = 0.7087$$

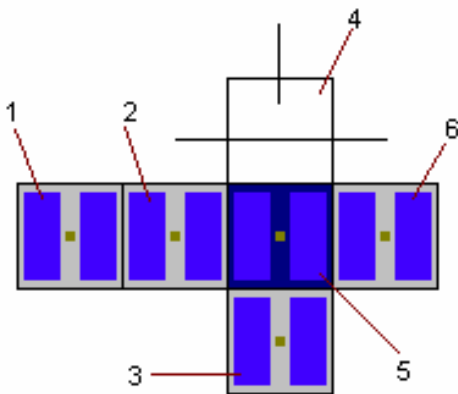


Figure8 Structure of Compass-1

Cube surface	ϵ_m	α_m	Coverage
1	0.7087	0.654	70% Sc, 30% Al
2	0.7087	0.654	70% Sc, 30% Al
3	0.7087	0.654	70% Sc, 30% Al
4	0,379	0.0346	100% Al
5	-	-	70% Sc, 30% Bp
6	0.7087	0.654	70% Sc, 30% Al

Table3. Average of optical surface properties for partial

Sc = Solar cells
 Al = Aluminium
 Bp = black paint

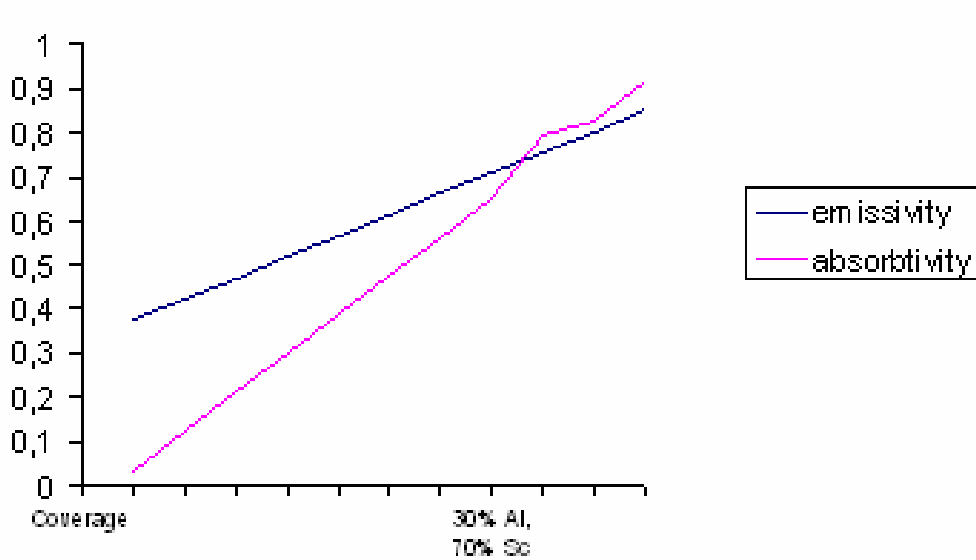


Diagram1 Average material properties for various Solar cell and aluminium construction

2.5 Instationary calculation

Using the equations in 2.2.1 and 2.2.2 the equilibrium temperatures are:

* For the cold case in the eclipse: $T_{\min} = 180.23K$

* For the hot case in sun: $T_{\max} = 295.85K$

Instationary calculation [2],[5]:

The temperature extremes for Compass-1 as a one mass thermal node have been calculated in the previous sections. The analytical means discussed in these sections do not allow for the computation of the temperature varying with time between the two steady-state boundary conditions. In order to be able to calculate the transient thermal behaviour of Compass-1, a basic instationary equation has to be considered:

$$m \cdot c_w \cdot \frac{dT}{dt} = \dot{Q}_{in} - \dot{Q}_{out} \quad (25)$$

This equation can be solved in a first step for the equilibrium conditions $\frac{dT}{dt} = 0$,

$$\dot{Q}_{in} = \dot{Q}_{out}$$

Using the general formulation of the resulting equilibrium temperature (T_{\max}, T_{\min}) for solving the instationary basic equation a nonlinear differential equation emerges which can be easily solved by separating the variables and integration.

In case of no internal energy dissipation, the separated differential equation is:

$$\frac{m \cdot c_w}{\varepsilon \cdot A \cdot \sigma} \cdot \int_{T=T_0}^T \frac{dT}{T_S^4 - T_{space}^4} = \int_{t=0}^t dt \quad (26)$$

Integrating this equation for the heating up phase ($T > T_0$) the result is

$$\Delta t_{up} = c \cdot \left[\left(\arctan h \left(\frac{T}{T_S} \right) + \arctan \left(\frac{T}{T_S} \right) \right) - \left(\arctan \left(\frac{T_0}{T_S} \right) + \arctan \left(\frac{T_0}{T_S} \right) \right) \right] \quad (27)$$

where

$$T_S = T_{\max} = 295.25K$$

$$T_o = \text{starting temperature of calculation} = 180.23K$$

$$T = \text{actual temperature}$$

In case of down cooling the satellite the integration results in

$$\Delta t_{down} = c \cdot \left[\left(\operatorname{arc\,coth}\left(\frac{T}{T_E}\right) + \arctan\left(\frac{T}{T_E}\right) \right) - \left(\operatorname{arc\,coth}\left(\frac{T_o}{T_E}\right) + \arctan\left(\frac{T_o}{T_E}\right) \right) \right] \quad (28)$$

where

$$T_E = T_{\min} = 295.25K$$

$$T_o = \text{starting temperature of calculation} = 180.23K$$

$$T = \text{actual temperature}$$

The constant c is given by:

$$c = \frac{\sum m_i \cdot c_{w_i}}{2 \cdot T_{E,sun}^3 \cdot \varepsilon \cdot A \cdot \sigma}$$

Using the parameters of Compass-1 the value of c=5109.98s

where

$$m_{Al} = 270g \quad \text{and} \quad c_{w_{Al}} = 1000 \frac{Nm}{kg \cdot K}$$

$$m_{SC} = 27g \quad \text{and} \quad c_{w_{SC}} = 1600 \frac{Nm}{kg \cdot K}$$

$$\varepsilon = 0.7$$

$$T_E^3 = 295.85K$$

2.6 Results of instationary calculation

Starting with the equilibrium temperatures in hot and cold phase, the temperature behaviour during the circulation on orbit can now be calculated.

If the starting point is assumed at the end of the shadow phase and use the calculated (chapter 1.3) time span of the sun phase of 60.52min is used, the temperature just before entering the shadow is

$$\Delta t_{sun} = 60.52 \text{ min} \quad \rightarrow \quad \begin{aligned} t_0 &= t_{min} \\ t_{sun1} &= 295.85K \end{aligned}$$

This is the start temperature for the cooling phase calculation in the earth shadow (30.38min).

$$\Delta t_{shadow} = 35.38 \text{ min} \quad \rightarrow \quad \begin{aligned} t_0 &= t_{sun1} \\ t_{shadow} &= 180.23K \end{aligned}$$

This calculation can be done several times up to a point where the sun and shadow end temperatures does not change more, i.e. an abort condition of $\epsilon \leq \pm 1K$ is reached. *Table4* shows the results for a period of 3 orbits, to determine which temperature values will be reached.

Stationary calculations	Temperature Sun T=295.85K	Temperature eclipse T=180.23K
1. Orbit	282.93K	193.91K
2. Orbit	285.36K	194.07K
3. Orbit	285.39K	194.07K

Table 4 Results of the transient temperature calculation

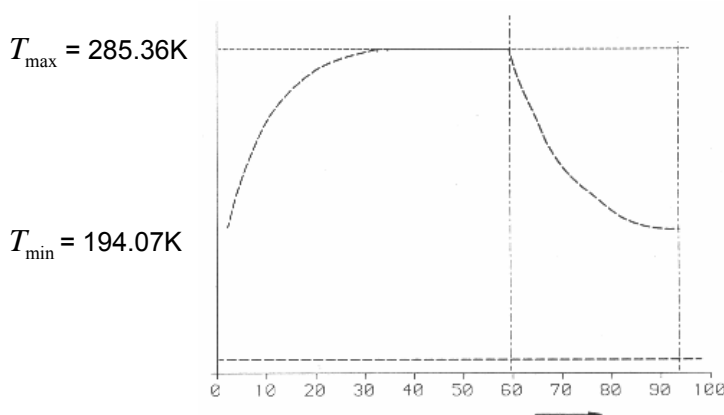


Figure9 Temperature distribution during one Earth orbit

3 3D model of satellite

The purpose of this chapter is to develop a thermal model which will simulate the Compass-1 orbiter during its normal orbit.

The nodal network modeling method first divides the satellite for thermal analysis into a finite number of nodes and connects between node and node by using thermal resistance. This method has advantages of simplicity and fast calculation.

3.1 Thermal model

In this analysis the ANSYS software has been chosen as a most suitable for our application. Its biggest advantage is that it considers the material properties accurately and it works in three dimensions.

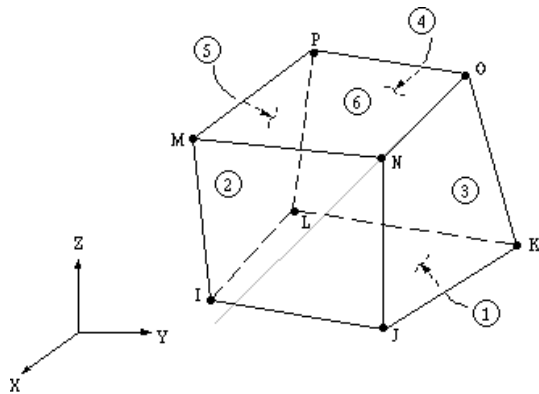
Because the heat flow that radiation causes varies with the fourth power of the body's absolute temperature, radiation analyses are highly nonlinear, such that an iterative solution is required to reach a converged solution.

The basis for thermal analysis in ANSYS is a heat balance equation obtained from the principle of conservation of energy. The finite element solution you perform via ANSYS calculates nodal temperatures, then uses the nodal temperatures to obtain other thermal quantities.

For a 3D analysis was chosen a SHELL157 element with AUX12 Radiation Matrix Method. For the AUX12 method must be SHELL157 superimposed by superelement "MATRIX50" on which must be defined conditions for radiation. This method works for generalized radiation problems involving several surfaces receiving and emitting radiation. The method involves generating a matrix of form factors (view factors) between radiating surfaces and using the matrix as a superelement in the thermal analysis.

The thermal model was build with the Solid70 element. Solid70 has a three-dimensional thermal conduction capability. The element has eight nodes with a single degree of freedom, temperature, at each node. The element is applicable to a three-dimensional, steady-state or transient thermal analysis. The element also can compensate for mass transport heat flow from a constant velocity field.

The geometry, node locations, and the coordinate system for this element are shown in *Figure10*. The element is defined by eight nodes and the orthotropic material properties. Orthotropic material directions correspond to the element coordinate directions.



FIGUR10 Solid-element

SHELL157 (Figure11) is a 3-D element having in-plane thermal and electrical conduction capability. The element has four nodes with two degrees of freedom, temperature and voltage, at each node. The element applies to a 3-D, steady-state or transient thermal analysis, although the element includes no transient electrical capacitance or inductance effects. The element requires an iterative solution to include the Joule heating effect in the thermal solution.

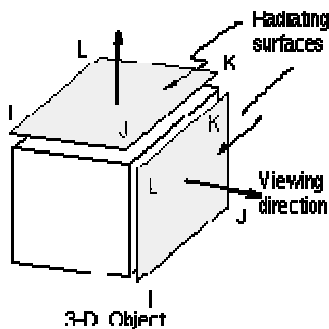


Figure11 SHELL157 Thermal Shell

Matrix50 is a group of previously assembled ANSYS elements that is treated as a single element. The superelement, once generated, may be included in any ANSYS model and used in any analysis type for which it is applicable. The superelement can greatly decrease the cost of many analyses. Once the superelement matrices have been formed, they are stored in a file and can be used in other analyses the same way any other ANSYS elements are used. Multiple load vectors may also be stored with the superelement matrices, thereby allowing various loading options.

The major heat input is the solar flux. Earth IR radiation and sunlight reflected by the Earth (Albedo) will also have a significant contribution to the thermal behaviour. There is also dissipation from the electronics. Inside the satellite the energy output is only by radiation to dark space background. The amount of absorbed and emitted heat will be regulated by the optical surface properties.

3.2 Analysis

The aim of the thermal analysis is to determine with a good accuracy the temperature mapping of Compass-1 and then develop a thermal solution to maintain all components within their allowable temperature limits for all operating modes (*Table7*).

ANSYS supports two types of thermal analysis:

1. A steady-state thermal analysis determines the temperature distribution and other thermal quantities under steady-state loading conditions. A steady-state loading condition is a situation where heat storage effects varying over a period of time can be ignored.
2. A transient thermal analysis determines the temperature distribution and other thermal quantities under conditions that vary over a period of time.

The model was created as a cube of aluminium with a wall thickness of 0.001m with the optical surface properties of our Cubesat project.

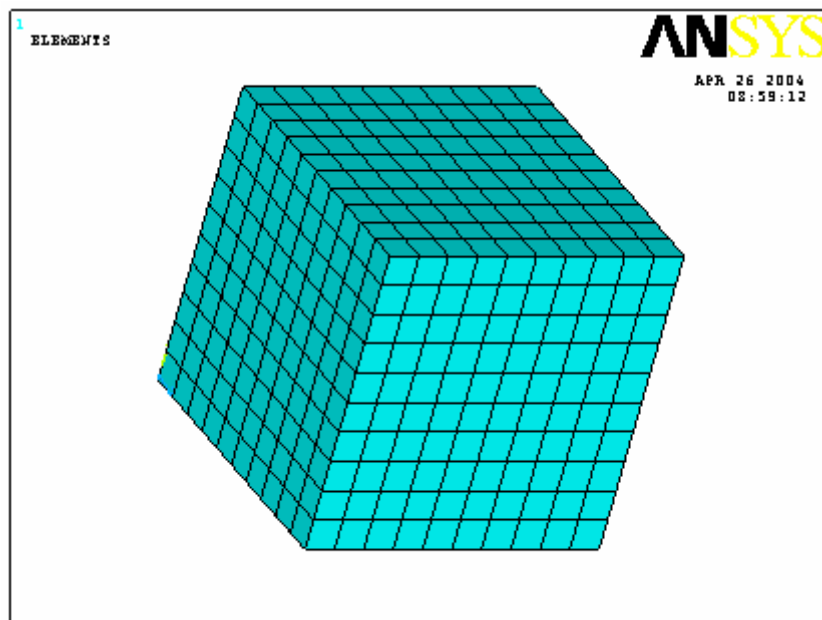


Figure12 Ansys FEM Model

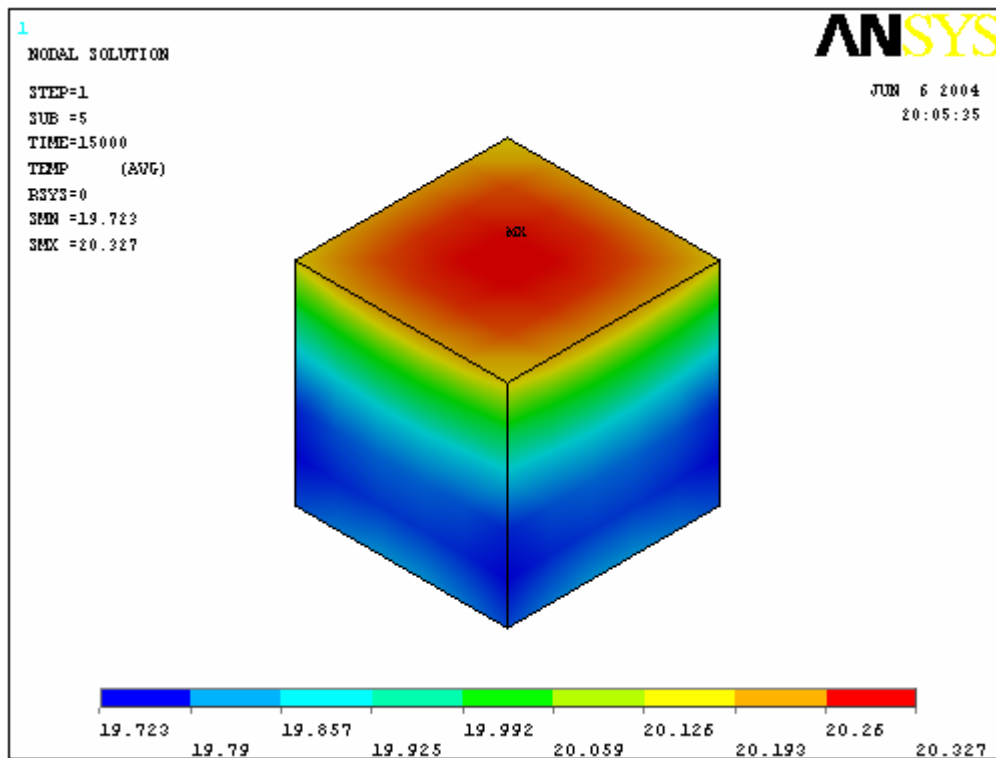


Figure13 Temperature distribution

In Figure13 can be seen the temperature distribution of Compass-1 over the sun period.

Input parameters

Heat flux sun	1370 W/m ²
Albedo	470 W/m ²
IR radiation	260 W/m ²
Conductivity	167 W/m°K
Specific Heat	1000 J/kg°K
Density	30,000 kg/m ³
Emissivity	0.707
Time (per orbit)	3600 s

Table5 Input parameters

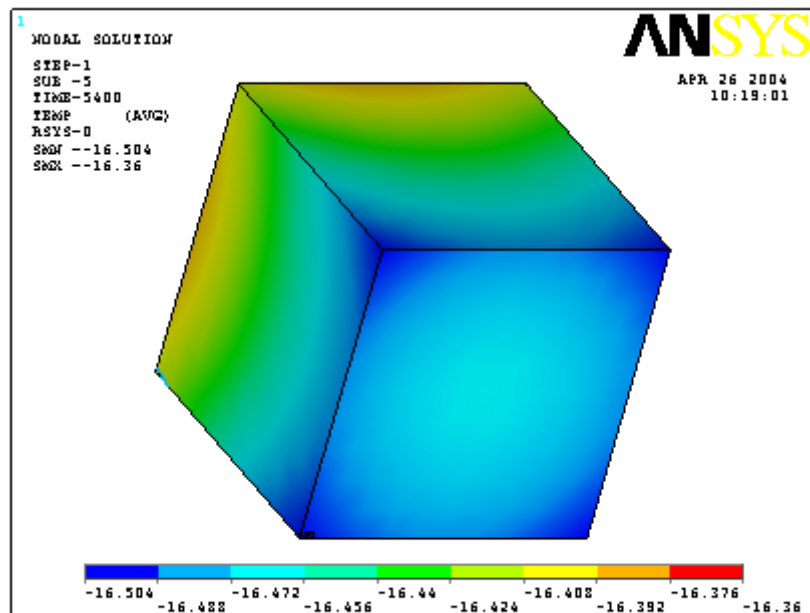


Figure14 Temperature distribution

In *Figure14* can be seen the temperature distribution of Compass-1 in eclipse.

Input parameters

IR radiation	190 W/m ²
Conductivity	167 W/m ^{°K}
Specific Heat	1000 J/kg ^{°K}
Density	30,000 kg/m ³
Emissivity	0.707
Time (per orbit)	2160 s

Table6 Input parameters

3.3 Nodal network modeling results

From the analysis results of the nodal network modeling, it was obtained that the maximum temperature is 20.3°C during the sun period. The temperature contour which resulted from the thermal analysis is shown in *Figure13*. The temperature distribution during eclipse is shown in *Figure14*. The average temperature value is -16.5°C. Because of the allowable temperature ranges it is necessary to control the temperature during the eclipse period.

4. Thermal control

It is necessary to keep the temperature of Compass-1 in a define temperature range during its entire mission, because all electronic devices are designed to operate in this temperature range. Basically, the allowable temperature range is defined by the “weakest” subsystem component, i.e. the component with the smallest temperature range.

Components	Temperature Range [°C]
Camera	-10...+70
Electronics	-40 +85
Battery	+5...+20
Solar cells	-100...+100
Structures	-45...+65

Table7. Subsystem temperature limits

The thermal control system is composed of two different types of systems the passive and active. The passive is generally lighter, requires less electrical power and is less costly then an active design. The active systems are used for manned spacecraft, for situations requiring very close tolerance temperature control or for components that dissipate a large amount of waste energy. A completely passive system is not sufficient for Compass-1. The spacecraft will carry a combination of passive and active solutions.

Active thermal control system

The active thermal control of a spacecraft may require the use of heaters, cooler, shutters, louvers or cryogenic materials. The heaters are usually wire-wound resistance heaters that may be controlled by a thermostat. Shutters and louvers are the most common active thermal control devices. The louvers open when heat needs to be radiated and close when the temperature is lowered. For long term cooling to low temperatures, the best approach it to use the cryogenic fluid because it uses less energy and it is more effective.

A comparison between the analysis results above and the temperature limits listed in table 3 shows that the thermal environment is not suitable for the battery and camera components without thermal management efforts. In the worst cold case the components will excessively cool and perhaps cease to function. To prevent that, one heater will be attached to the battery and activated each time, the temperature drops below a certain threshold level. A new analysis is in process to calculate the new temperature distribution in Compass-1, accounting for the active management measures.

Passive thermal control system

The techniques applied for passive thermal control include the use of spacecraft coatings, insulation blankets (MLI), sun shields, radiating fins and heat pipes. Due to the volume and power constraints of Compass-1, passive control methods in the form of thermal coatings and insulation are preferred.

The operating ranges of different components of Compass-1 drive the thermal requirements, as well as the power dissipated and exposure to the external environment. *Table 2* above shows the thermal operating ranges for the vital components on Compass-1. Out of these components, the camera and the battery are the most thermally constrained.

The bottom side of the satellite will be painted black, because of the high absorptivity. There are also two solar cells on the bottom panel, which convert the albedo (after all 35% of the solar flux) radiation to electrical energy. The top of the satellite and the side plates are made from aluminum (6061-T6) and are covered with two solar cells each, apart from the antenna side.

Hardware

To avoid the low temperatures during the eclipse the implementation of heaters has been found an adequate solution. The heaters can be hard or flexible. Flexible heaters are the most common in the satellite because they can conform to various shapes. Heater from Minco Products, Inc offers a wide range of different heaters, but some are not suitable for our constraints. Wire-wound rubber heaters are more economical in larger size, oversized for our size requirements. Silicone heaters are not suitable for radiation and vacuum. Mica heaters consist of an etched foil element sandwiched between layers of mica and they are not flexible. A Kapton has been selected. Kapton is a thin, semitransparent material with excellent dielectric strength. Kapton heaters are ideal for applications with space and weight limitations, or where the heater will be exposed to vacuum.

The heater shall heat the battery to within the required temperature range for that component.

Heater:

Minco Products, Inc – Strip heater with Kapton Insulation

Product number	HK 5276 R71.7 L12 E
Mass	0.4g
Resistance	68 Ω
Max. power	2.01 W
Volume	1.9 x 7.6 x 127cm
Location	inside top of battery box

Table8 Heater characteristics

The heater shall be connected to the power subsystem.

Temperature Sensors:

Temperature sensors are used to relay relevant thermal information to EPS, which toggles the thermal controls. The heater shall be turned on or off based on the instruction from EPS.

The LM75 is a temperature sensor, Delta-Sigma analog-to-digital converter, and digital over-temperature detector with I²C® interface. The host can query the LM75 at any time to read temperature. The open-drain Overtemperature Shutdown (O.S.) output becomes active when the temperature exceeds a programmable limit. This pin can operate in either “Comparator” or “Interrupt” mode.

The LM75 sensors will be installed on all boards inside of the satellite, to the camera and to the battery of the power subsystem. The purpose is to measure the temperature of each board of the satellite and to measure the temperature of the battery and send the information to EPS to make sure the temperatures are within their survival limits.

Temperature sensors shall be connected to a 2-wire bus.

LM75 Temperature sensor

Supply voltage	3.0V to 5.5V
Supply current	operating 250µA (typ); 1mA (max) shutdown 4µA (typ)
Temperature	-25°C to +100°C
Accuracy	± 2°C (max)
Temperature	-55°C to +125°C
Accuracy	± 3°C (max)
Interface	I ² C Bus

Table9 Temperature sensor LM75 characteristics

The M-FK 222 temperature sensors will be mounted to all panels of the satellites.

LM75 Temperature sensor

Insulation resistance	> 10 M Ω at 20°C > 1M Ω at 500°C
Temperature range	-70°C to +500°C
Temperature coefficient	TCR=3850 ppmK
Leads	Nickel platinum-clad wire
Measuring current	100 Ω : 0.1 to 0.3mA

Table 10 Temperature sensor M-FK 222 characteristics

You can find more details at Electrical Power System.

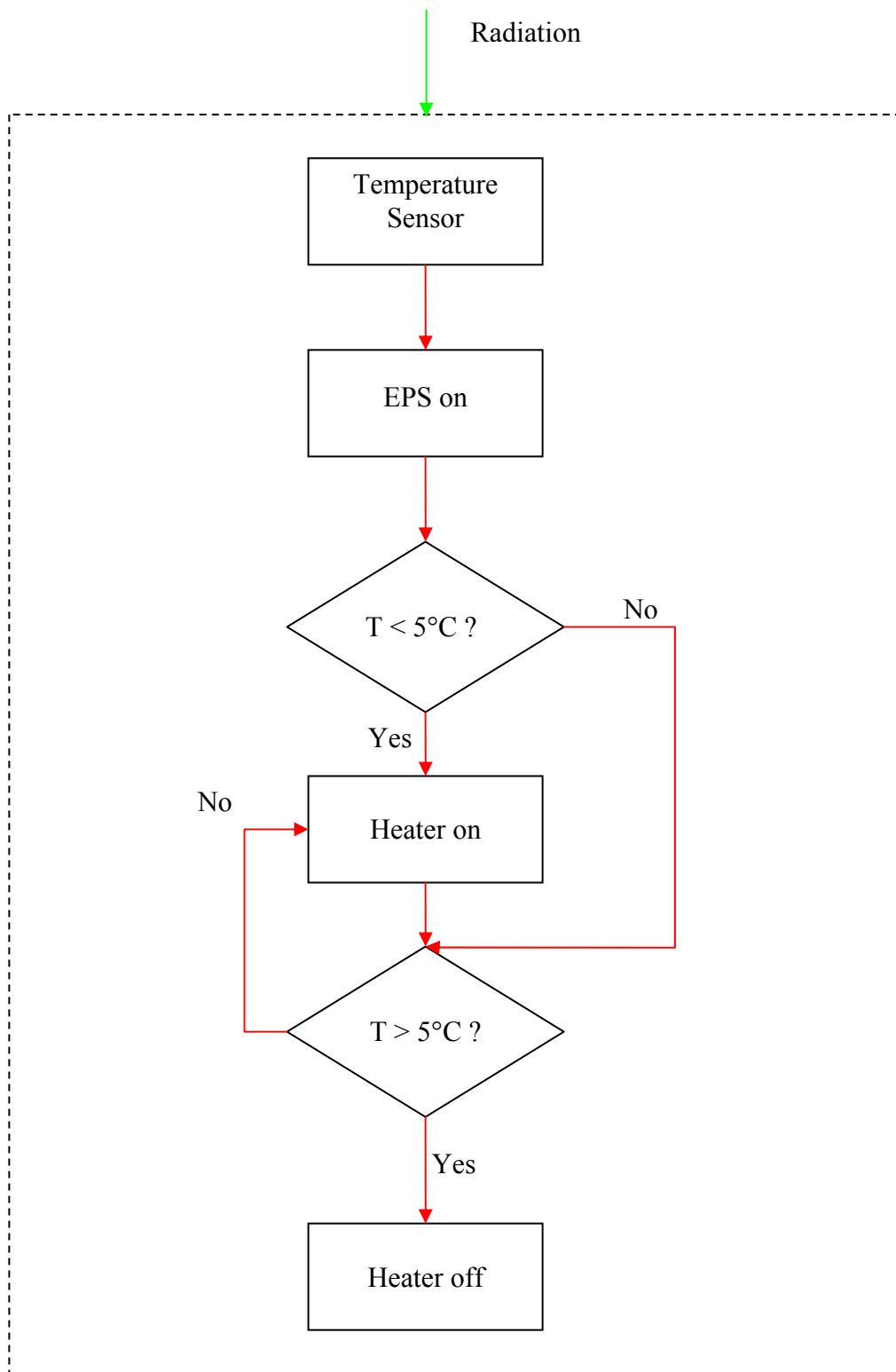


Figure15 Thermal subsystem block diagram

4.1 System optimisation

The results of the previous calculations and the analysis show (*Table 4*), the overall temperature of Compass-1 is too low to fulfil the requirements. From the numbers it can be derived that Compass-1 tends towards lower temperatures rather than higher. To maintain the satellite at a mean temperature close to 20°C, a satisfactory balance has to be achieved between heat sources and cold sinks. There is a variety of engineering parameters that can be adjusted in order to achieve this goal. However, only few of those are open for change. As an example, changing the geometry of the spacecraft can have a positive effect on the temperatures of Compass-1. For obvious reasons, changing the geometrical configuration is not an option.

Another way of passively improving the thermal behaviour of the spacecraft, is to influence its radiation characteristics. These are governed by its surface properties, in particular ϵ and α . As has been discussed earlier, a black paint coating of exposed aluminium parts has been assumed during the calculations. This coating generally leads to higher temperatures. The selection of coating is an optimum solution and will not be adjusted.

The bottom line problem is that the satellite will cool down to exceedingly low temperatures during cold mission phases, i.e. phases without significant energy intake. The active solution is to keep Compass-1 warm by electrical heaters during these phases. The EPS manages the thermal control system. Temperature measurements recorded by a network of temperature sensors are compared to reference values.

References

- [19] CubeSat Team Aachen. (2003) *Phase A Study of COMPASS-1*. www.raumfahrt.fh-aachen.de
- [20] Willi Hallmann, Wilfried Ley (1999) *Handbuch Raumfahrttechnik*, Hanser
- [21] Gilmore, David G. (1994) *Thermal Control Handbook*, The Aerospace Corporation Press, El Segundo, California
- [22] Larson, W.J. and Wertz, J.R. (1996) *Space Mission Analysis and Design*. Kluwer Academic Publishers, Dordrecht, The Netherlands
- [23] Prof. Dr. rer. nat. H-J. Blome, *Vorlesungsumdruck*, FH-Aachen, Stand 2003



2004-05-31

WBS470: STR

Structures & Mechanisms System

Phase B: Detailed Definition

Author

Marco Hammer
Structure & Mechanism Supervisor
&
Robert Klotz

FH Aachen, Germany



Scope

This paper documents the detailed definition of the STR subsystem of the Compass-1 CubeSat under development at the University of Applied Sciences Aachen, Germany.

Phase B deals with the following tasks:

- Hardware definition
- Test and analysis

A structural lay-out has been designed in the preliminary design phase already. The main objective of the definition phase B is to refine the structure to achieve a compromise between parameters like stiffness, weight, stability, connection points, accessibility, etc. Most of the structural members will be manufactured in-house, but some part will have to be ordered from outside whenever the manufacture is infeasible. Examples are the separation springs, which have to be selected. The same is true for the 'kill switches'. The most suitable solution for all structural components must be found. The STR group has structural interfaces with all other subsystems of Compass-1. As part of the interface definition between the EPS and STR, mounting solutions for the solar cells have to be investigated. Apart from the kill switches, Compass-1 will carry a second mechanism: the antenna deployment mechanism. This mechanism must fulfill all requirements and must have a small packaging configuration for the launch within the P-POD deployer.

The test and analysis deals with the validation of the strength of the structure. It has to be determined if the structure is capable to withstand the worst case loads and frequencies during launch. Also, as an interface effort between STR and TCS, a thermal analysis of the satellite structure has been conducted (refer to the TCS section), to identify the thermal distribution over the structure and, more importantly, subsystem components.

This documentation describes the results of the above considerations and will present a detailed structural layout that satisfies the needs of all subsystems. The manufacturing drawings of each part of the structure and finally the satellite emerge from this CAD model and will be the basis for manufacture.

Contents

1. Material Definition	176
1.1 Anodizing.....	176
2. Structural Members	178
2.1 The Frames.....	178
2.2 The Beams	178
2.3 Side Plates.....	179
2.4 The PCB Holder.....	181
2.4.1 Mainboard PCB.....	181
2.4.2 ADCS PCB.....	181
2.4.3 COM PCB	181
2.4.4 EPS PCB	182
2.5 Camera Assembly	182
2.6 Magnetorquer Fitting	183
2.6 Sun Sensors.....	184
2.7 GPS Antenna.....	184
2.8 COM Antennas	185
4. Mechanisms	185
4.1 Antenna Deployment Mechanism.....	185
4.2 Kill Switches	185
4.3 Separation Springs	186
5. Integration	186
6. Properties	187
6.1 Center of Mass	187
6.2 Mass Budget.....	188
6.3 Moment of Inertia	188
7. Dynamic Analysis and Simulation	189
7.1 Scope.....	189
7.2 Input Data.....	190
7.3 Modal Frequencies.....	190
8. Conclusions	202
9. References	202

1. Material Definition

For the structural members, Stanford [2] proposed the use either aluminum 7075-T6 or 6061-T6. It would also be possible to use a different material, provided that its thermal expansion factor equals them of the P-POD material (7075-T73). To evaluate the suitable material for Compass-1, a comparison between the two aluminum alloys, has been conducted, which is shown in the table 1.

Table 17: Frame Material Comparison ^[1]

	7075-T6	6061-T6
Density	2.81 g/cm ³	2.7 g/cm ³
CTE, linear 20°C	23.6 μm/m°C	23.6 μm/m°C
Modulus of Elasticity	72 GPa	69 GPa
Heat Capacity	0.96 J/g°C	0.896 J/g°C
Tensile Strength, yield	505 MPa	275 MPa
Costs	Expensive	Cheap

As table 1 shows there are not many discrepancies between those two aluminum types. The main advantage of 7075 is its very high tensile strength, optimized for highly stressed structural parts.

In general 6061-T6 provides excellent joining characteristics, good acceptance of applied coatings and combines relatively high strength, good workability, and high resistance to corrosion. Moreover it is widely available and much cheaper than the 7075-T6. For these reasons, the aluminum alloy 6061-T6 has been selected.

1.1 Anodizing

To achieve anti-friction properties, it is required that parts, which are in direct contact with the deployer, will be hard-anodized. Hard-anodizing is a term used to describe the production of anodic coatings with film hardness or abrasion resistance as their primary characteristic. These anodic coatings are usually thick by normal anodizing standards, and they are produced using special anodizing conditions. The thicknesses are usually between 25 and 250 μm, and the anodizing time can be up to 240 minutes. Most hard anodizing processes are based on sulphuric acid, and the parameters are commonly within the following limits:

Electrolyte concentration: 5..15%(vol.) sulphuric acid

Current density: 2..5 A/dm² (DC) or 2..10 A/dm² (DC and pulse)

Voltage: 23..120 volts

Temperature: -5 to +5°C

The reason why anodic oxide coatings produced under hard anodizing conditions have high hardness values and very good abrasion resistance, is due to the low anodizing temperature the low electrolyte concentration, and the high current density compared to normal sulphuric acid anodizing. To keep the temperature on the low level, good cooling and agitation are of great importance. At these temperatures water cooling is not possible, and some type of refrigerant must be used. Air agitation is sometimes not sufficient, but agitation can be

provided by pumping the electrolyte through an external heat exchanger which thus combines cooling with agitation.

Alloys with a very high copper or silicon content are less suitable for this process. The colour of the coatings depends on the alloy and the coating thickness. AW 6061 has a tan or grey colour which darkens to jet black at 75 μm .

After hard-anodizing, the profiles may be sealed in boiling distilled water, dichromate solution, dewatering oil or wax (80°C, 15..30 minutes). Dichromate sealing improves the fatigue properties, but decreases the abrasion resistance to some extent (in common with other aqueous sealing solutions). For this reason, aqueous sealing processes are not normally used where high wear resistance is required.

Hard-anodized coatings may be impregnated with oils, silicones or dry lubricants for the improvement of anti-friction properties. Corrosion resistance could be improved by PTFE impregnation. This treatment gives no reduction in abrasion resistance of the coating.

For the best resistance to wear and abrasion it is preferable to use pure aluminium or alloys with the lower values of alloying additions. It is usually necessary however to couple the hard surface with a higher mechanical strength and hardness in the basis metal than is possible with pure aluminium. The hardness should be greater than 350 HV to be called a hard anodized coating. Hardness values up to 1400 HV are reported to be obtained from a mixed electrolyte.

Hard-anodized aluminium shows a good **heat resistance**, and a hard anodic oxide coating of 75 μm withstands short exposures to temperatures of the order of 2000°C. The coatings give also very good **electrical insulation**. This property can be further improved by hot water sealing and waxing.

Hard-anodic oxide coatings find application in the engineering industry for components which require a very wear resistant surface such as pistons, cylinders, and hydraulic gear. Another application is in the coating for the production of flame and chemically resistant surfaces.

2. Structural Members

2.1 The Frames

The frames are the only parts of the satellite that will have contact with the P-POD. All contact surfaces must have rounded edges. CubeSats must have at least 75% of flat frame contact with the deployer to prevent cold-welding. All contact surfaces with the P-Pod and other CubeSats are not to be made of raw alloy material. Hard-Anodizing is recommended. Derlin inserts are an alternative.

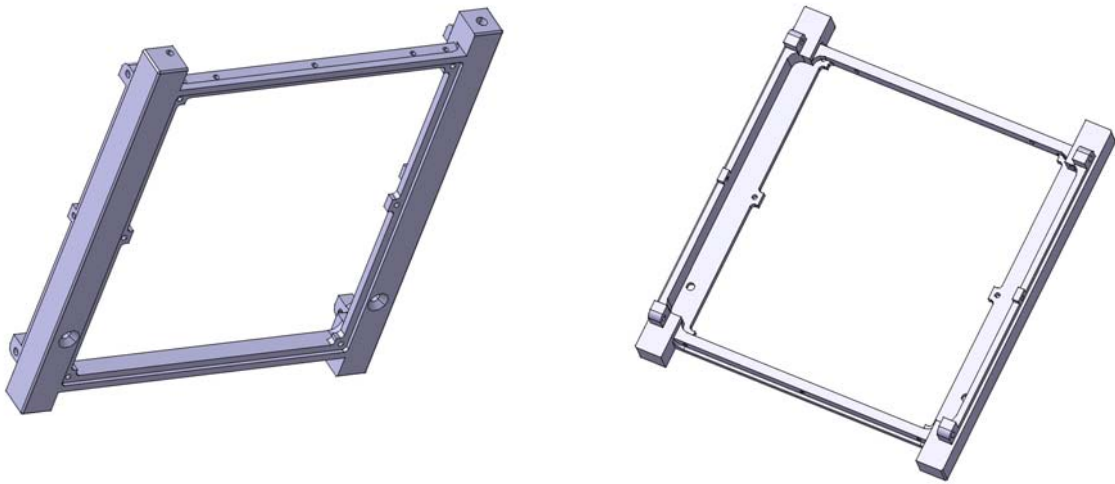


Figure 27: Compass-1 carries 2 frames

2.2 The Beams

4 beams constitute the main load-bearing connection between the two main frames.

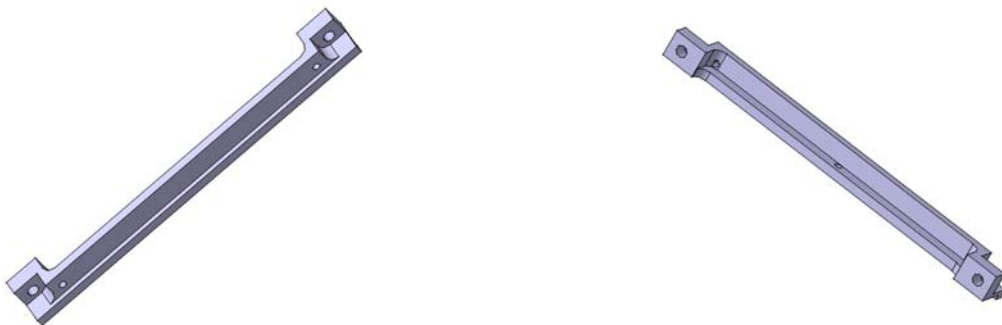
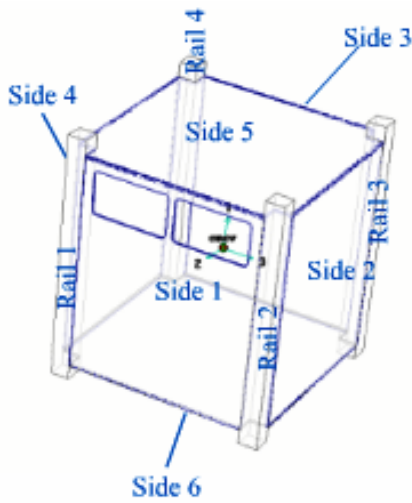


Figure 28: In total, Compass-1 carries 4 beams as main load path between the frames

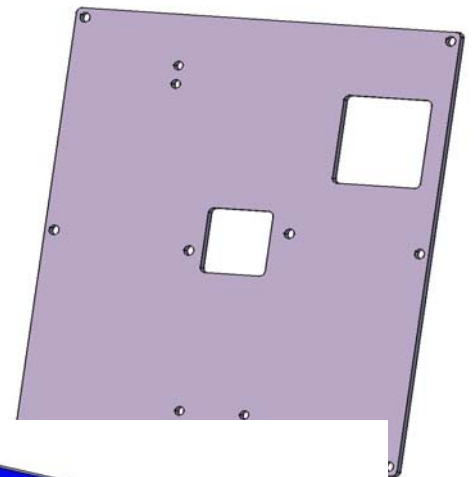
2.3 Side Plates



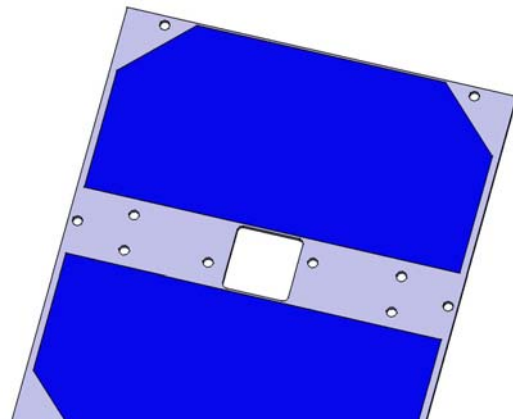
The cubic structural frame made up 2 frames and 4 beams holds the attachment points for 6 side panels of 1mm thickness. All panels are made from 6061-T6 alloy as is the main structure. The number convention for the side plates is shown in figure 3.

Figure 29: Nomenclature convention for the side panels

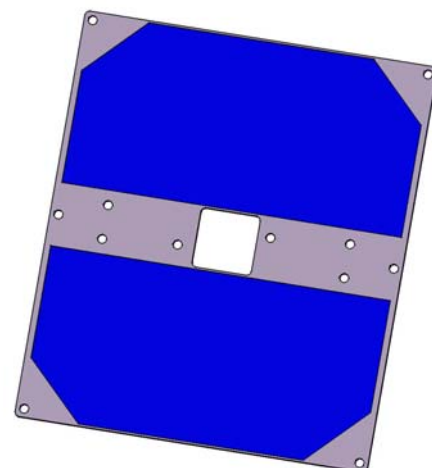
Side 1 includes the mounting points for an ADCS sun sensor which is positioned in the geometrical center, the COM antenna system with the monopole and the dipole antenna. Also, the remove-before-flight-pin, the antenna release mechanism and the mounting point for the GPS antenna. Side 1 is the only panel which does not hold solar cells for power generation.



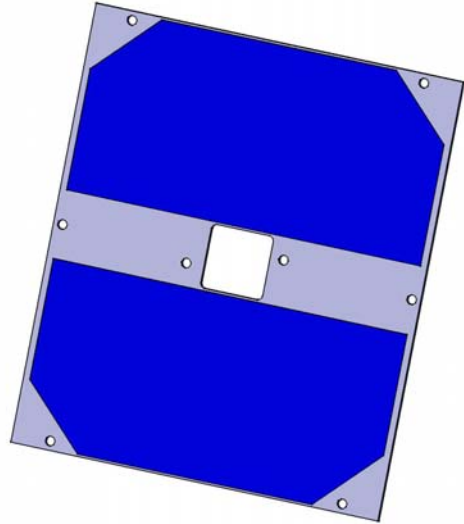
Side 2 includes the mounting points for an ADCS sun sensor which is positioned in the center and the magnetorquer clamps. There are two solar cells mounted on Side 2.



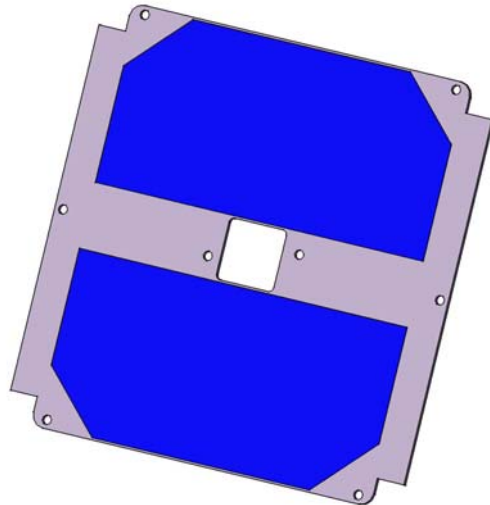
Side 3 includes the mounting points for an ADCS sun sensor which is positioned in the center and the magnetorquer clamps. There are two solar cells mounted on Side 3.



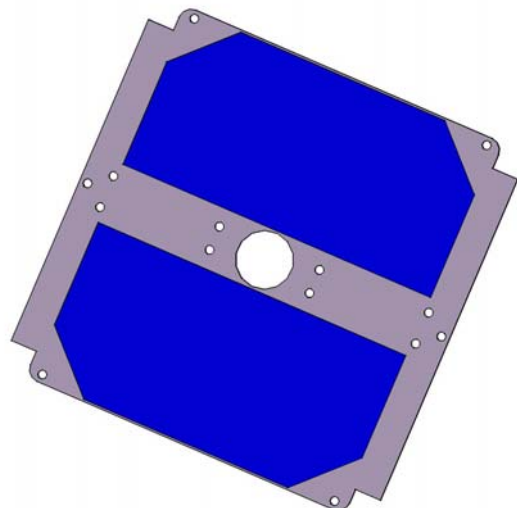
Side 4 includes the mounting points for an ADCS sun sensor which is positioned in the center. There are two solar cells mounted on Side 4.



Side 5 includes the mounting points for an ADCS sun sensor which is positioned in the center. There are two solar cells mounted on Side 5.



Side 6 includes the mounting points for the camera assembly which is positioned in the center and the magnetometer clamps. This panel does not carry provisions for sun sensor mounting. There are two solar cells mounted on Side 6.



2.4 The PCB Holder

All boards are additionally constrained on the top side by means of a board holder with aluminum-angles. This constraint will reduce the PCBs affinity for vibrational strain.

2.4.1 Mainboard PCB

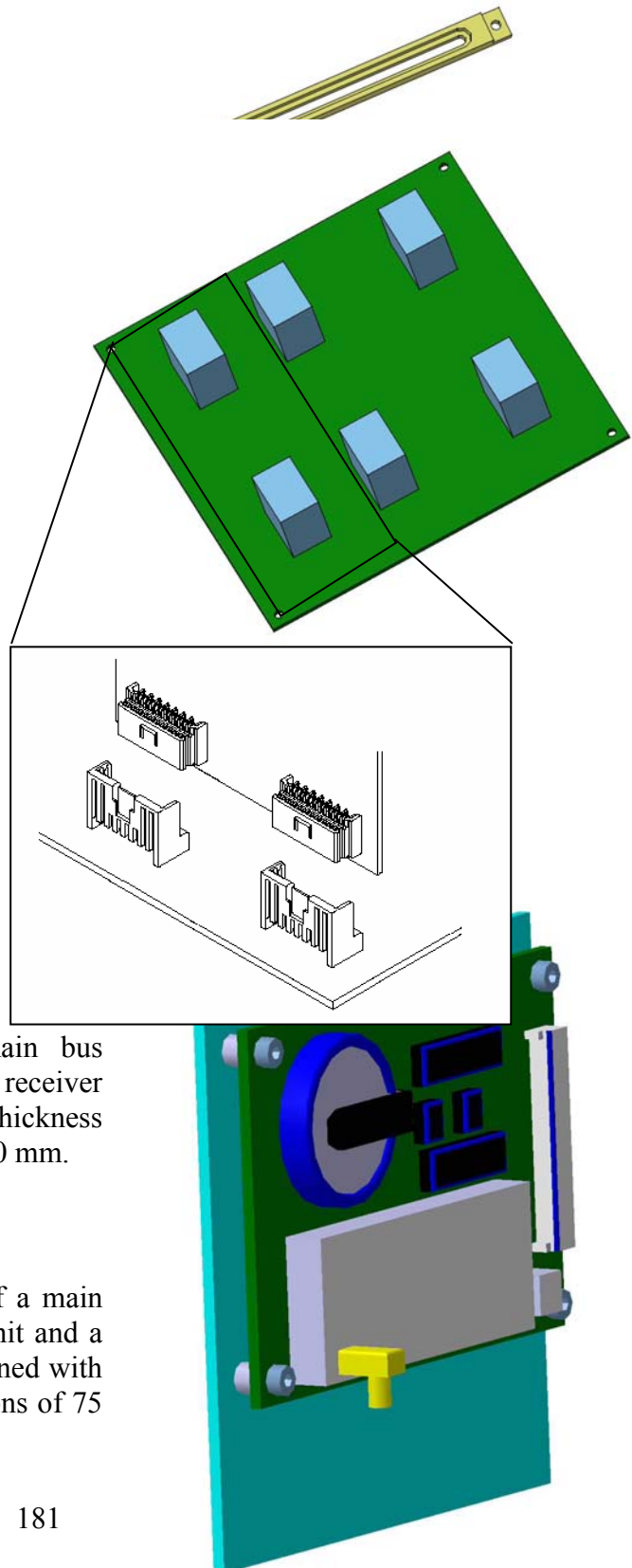
This PCB has a thickness of 1.5mm and surface dimensions of $(93.5\text{mm})^2$. It is the responsibility of the STR group to define the PCB drill points for physical mounting onto the structure. The connectors, as defined in the CDHS section, provide the electrical and mechanical interface. Hence, the subsystem boards are physically constrained on points at the top and bottom edge of the respective PCB.

2.4.2 ADCS PCB

The ADCS PCB will consist of a main bus compatible board plus the Phoenix GPS receiver board. The ADCS PCB is defined with a thickness of 1.5mm and surface dimensions of 75 x 70 mm.

2.4.3 COM PCB

The communication system will consist of a main bus compatible board with a transceiver unit and a Morse encoder unit. The COM PCB is defined with a thickness of 1.5mm and surface dimensions of 75 x 70 mm.

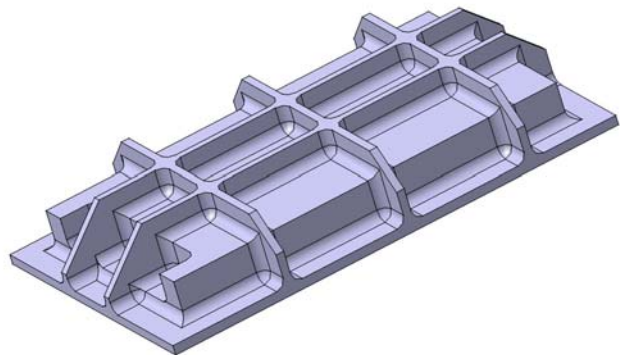


2.4.4 EPS PCB

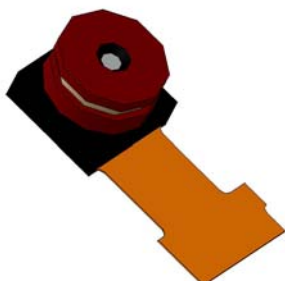
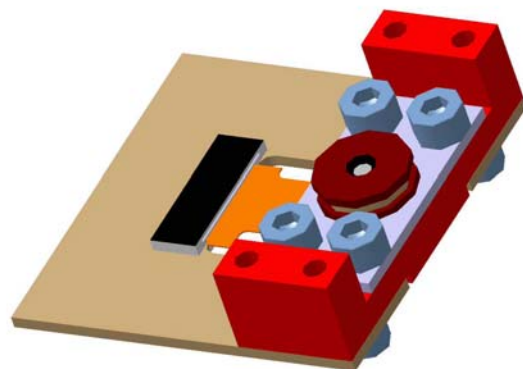
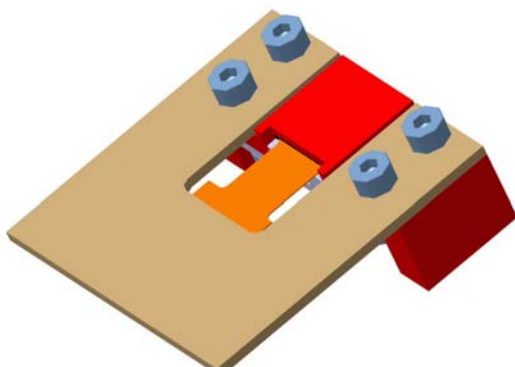
The power subsystem contains several solar arrays which provide the main power and a minimum of two batteries, which are used as buffer storage cells for providing sufficient power during shadow phases and current peaks. The best efficiency is obtained when the solar cells point directly towards the sun. The satellite constantly changes its attitude with respect to the sun during its mission. Mechanisms that would orient the solar cells as the position is changing are much too complicated for a spacecraft of this size. Therefore the solar generators will be mounted directly on each available surface of the spacecraft. Because of the difference of thermal expansion of the solar cells and the sides of the CubeSat they will be adhesively bonded to the aluminum panels. The definition of a detailed method how to fix the Solar cells on the Structure is kept to phase C/D.

The Lithium-Polymer batteries require protection against the high vacuum in LEO. Therefore a dedicated battery pressure box which is mounted on one side of the power PCB has been designed. This box will provide housing with sufficient stiffness to prevent the batteries from expanding under space environment conditions.

The EPS PCB is defined with a thickness of 1.5mm and surface dimensions of 75 x 70 mm.

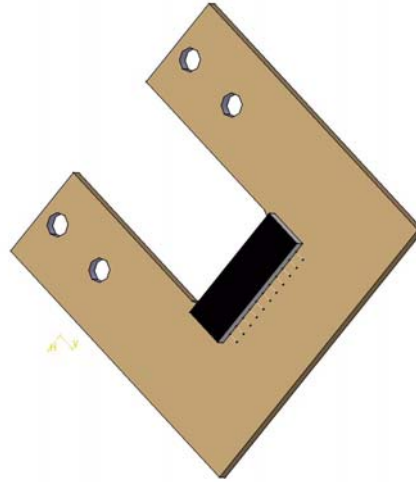


2.5 Camera Assembly



Camera Dummy

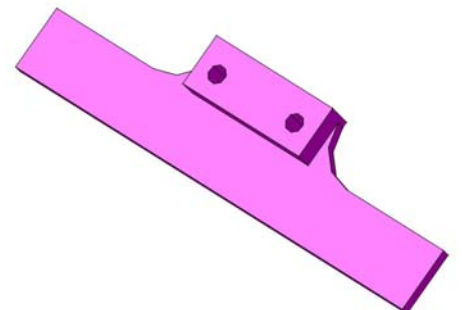
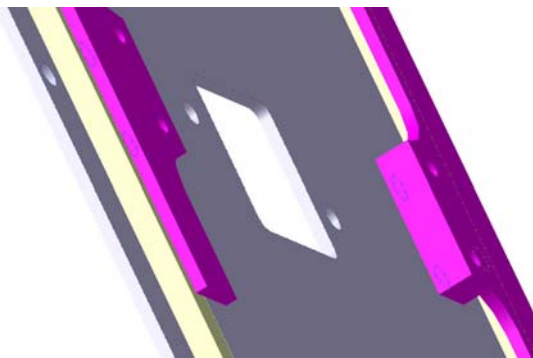
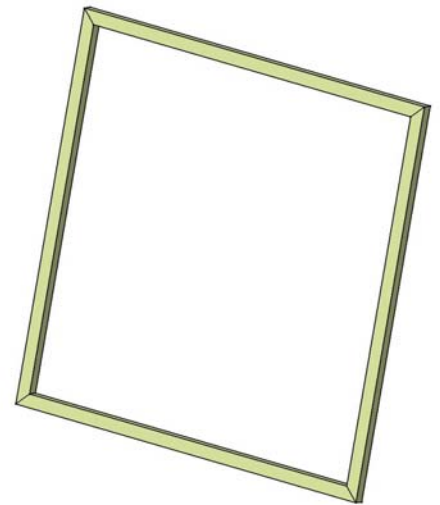
To avoid that the capton wire Camera will break through will use an Adapter PCB to



foil from the vibration we protect them.

2.6 Magnetorquer Fitting

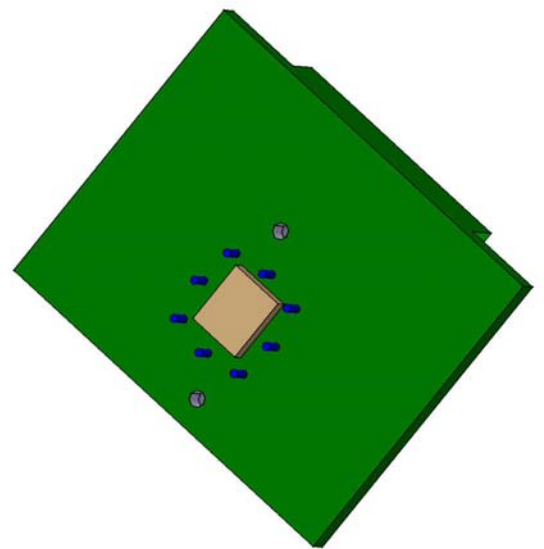
The bigger the included surface of the coils is the better is their efficiency. Therefore the coils will be of square shape. They are aligned at the edges of the side plates and will be mounted on them. This will avoid extra coil supporting parts. A minimum of 3 coils, 1 for each axis, is required. The outer dimensions are 74 x 74 mm, the thickness of the coils is 2mm (+0.05/-0) and the inner dimensions are 69 x 69 mm.



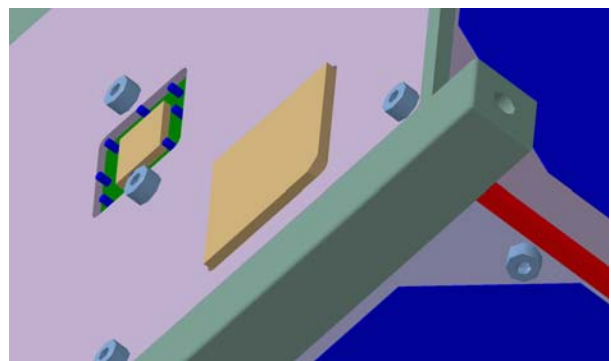
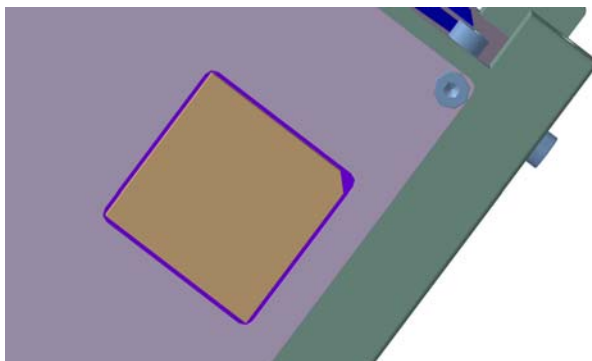
Magnet Torquer Holding Plates

2.6 Sun Sensors

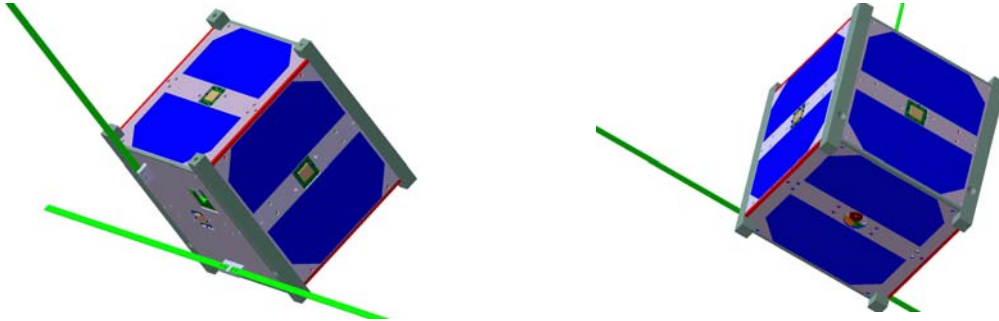
The sun sensors, which are located on five sides of the spacecraft, will be screw-mounted on the panels. All potential electrical contacts will be isolated from the structure with capton foil.



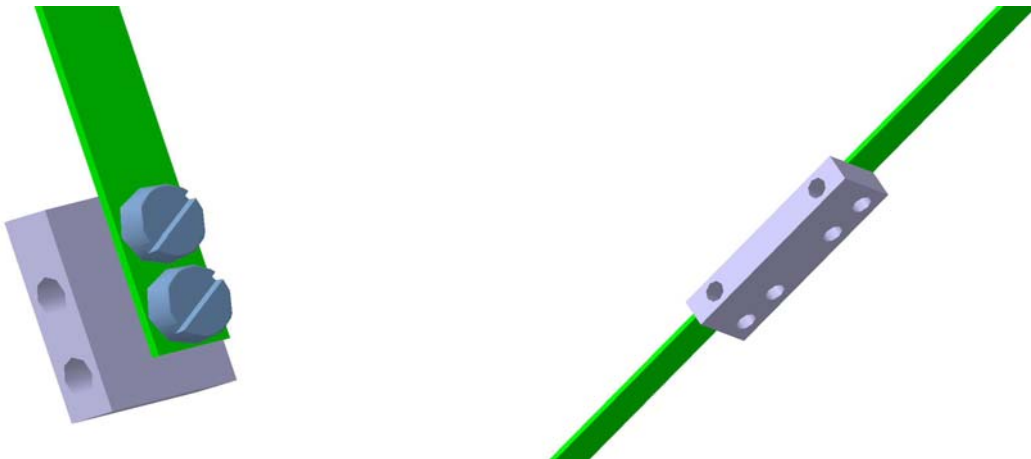
2.7 GPS Antenna



2.8 COM Antennas



The following figures show the mounting of the monopole and dipole antennas, respectively.



4. Mechanisms

4.1 Antenna Deployment Mechanism

A deploy mechanism for the two communication antennas will be used. It is intended to use polymer nylon threads which will be melted with electrical power. Once the nylon wire is broken, the antennas will be released by their inherent elastic properties. Further investigations on the deployment mechanism will be done in phase C/D.



4.2 Kill Switches

The main part of the Kill Switch assembly will be the Omron D2F-D1L micro switch.

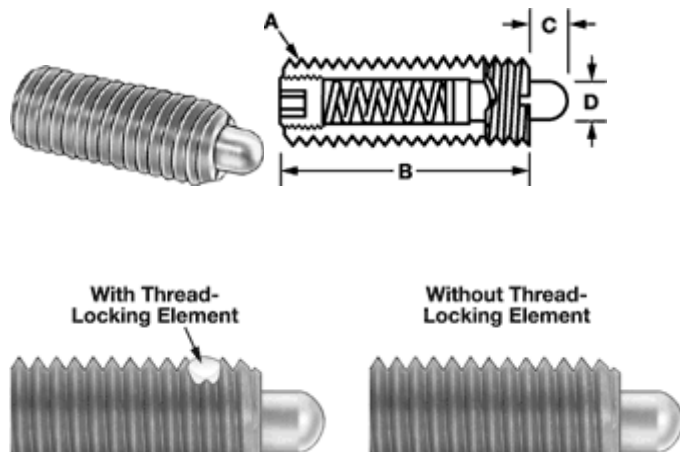
- Sub-miniature switch
(12.8 x 6.5 x 5.8 (W x H x D)) ideal for PCB mounting
- Incorporating a reverse mechanism made with two highly precise split springs which ensures a long service life (1,000,000 operations)
- Construction resistant to flux wicking
- PCB, self-standing, solder, and right angle terminals are available
- Superior contact wiping action

For the mechanism we will use the principle that Tokyo University has been verified space-proved already. The detailed system is to be defined in phase C/D.

4.3 Separation Springs

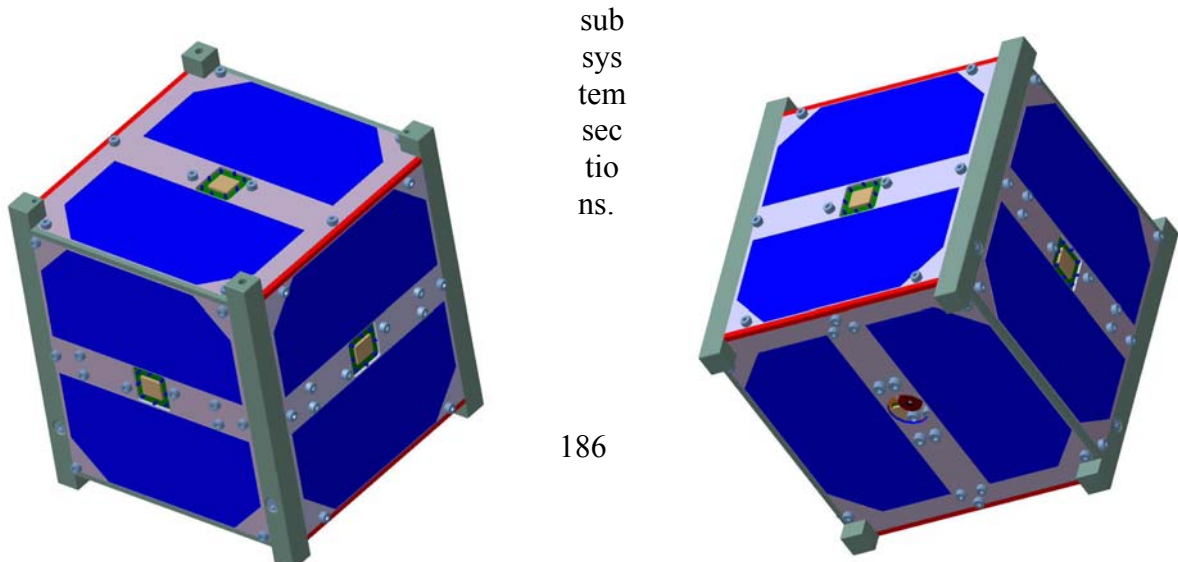
As recommended by Stanford University, separation spring plungers will be used.

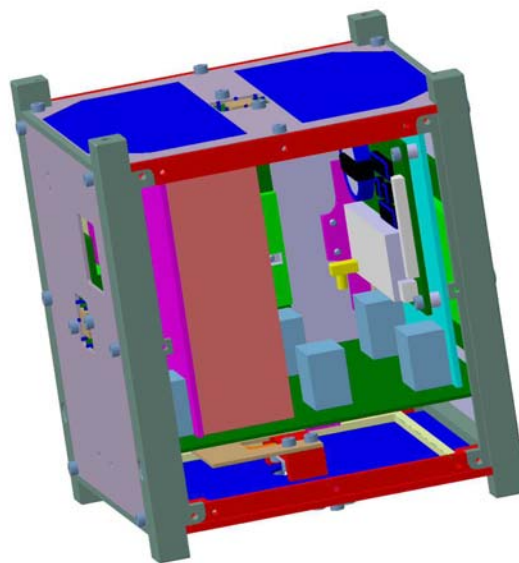
These plungers have a round, cylindrical nose that offers long travel and has a large bearing surface so it rides smoothly inside the plunger body.



5. Integration

This section gives an overview of how the mentioned elements will be fitted into the structural main frame. The electrical interfaces are subject of the C&DHS and the Power





6. Properties

6.1 Center of Mass

Table 18: Actual Center of mass coordinates without the Subsystem PCBs.

Axis	(mm) from geometrical Center
X =	- 1,002
Y =	+ 0,454
Z =	- 0,085

6.2 Mass Budget

Table 19: STR mass budget

Part	Weight in g	Quantity	Total in g
------	-------------	----------	------------

Frame	43	2	86
Beam	3.5	4	14
Coils Holder	1	6	6
Side 1	20	1	20
Side 2	21	1	21
Side 3	21	1	21
Side 4	21	1	21
Side 5	24	1	24
Side 6	24	1	24
Cam Holder	3	1	3
Cam Plate	0.93	1	0.93
Main Bus Board Holder	2	4	8
PCB Holder	3	2	6
PCB Fix	0.35	6	2.1
Dipole Antenna Holder	0.98	1	0.8
Monopoly Antenna Holder	0.45	1	0.5
Separation Spring	2	2	4
Screws	10	1	10
Kill Switch Mechanism	5	2	10
Total			282,33

6.3 Moment of Inertia

The following table lists the current tensor of inertia **without** consideration of the subsystem PCBs. This table will be updated as structural changes and refinements are conducted in phase C/D.

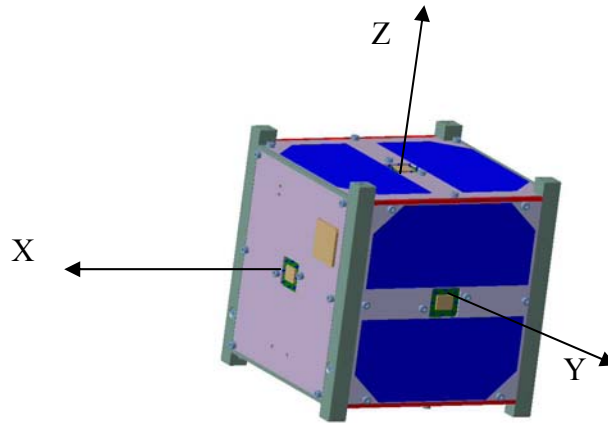


Table 20: Current tensor of inertia

$I_{xx} = 7,943e-004 \text{kgxm}^2$	$I_{xy} = 1,969e-006 \text{kgxm}^2$	$I_{xz} = 1,104e-006 \text{kgxm}^2$
$I_{yx} = 1,969e-006 \text{kgxm}^2$	$I_{yy} = 7,792e-004 \text{kgxm}^2$	$I_{yz} = 6,217e-007 \text{kgxm}^2$
$I_{zx} = 1,104e-006 \text{kgxm}^2$	$I_{zy} = 6,217e-007 \text{kgxm}^2$	$I_{zz} = 7,85e-004 \text{kgxm}^2$

7. Dynamic Analysis and Simulation

7.1 Scope

The scope of the dynamic analysis and simulation of the CubeSat structure is to verify the structural integrity and localize weak points in the structure at an early design stage to prevent major modifications later. The structure of the satellite must assure integrity during the whole life cycle. Especially the high loads acting during the launch must be considered. A software-based analysis and simulation with appropriate programs is able to compute stress values under static load and behavior of the structure under dynamic loads. These computed values have to be in accordance with the material properties and the launcher requirements. A simulation based on the CATIA V5 software was able to calculate the first modal frequencies of the parts and the assembled structure, and maximal deflection and stresses under static loads.

7.2 Input Data

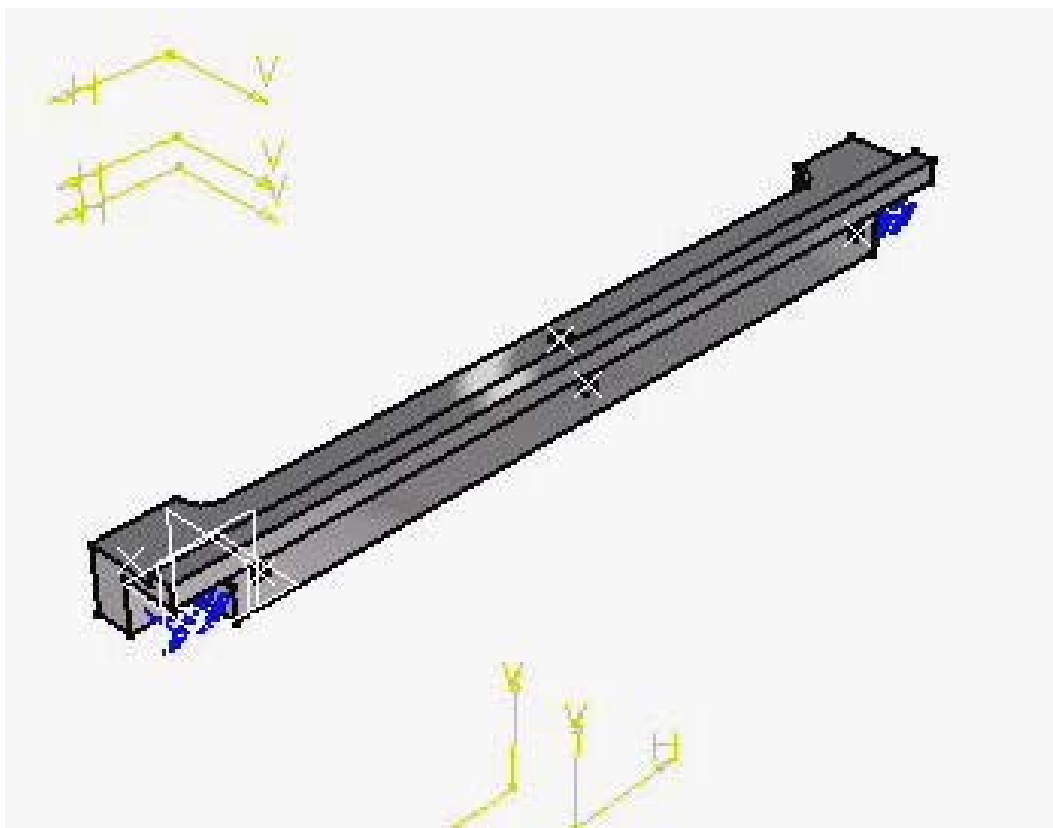
Since a CAD model of the structure in CATIA already exists, this one was also used for the simulation. Prior to the analysis, the exact material properties had to be assigned to each structural part.

Material	Aluminum 6061-T6
Young-Modulus	1e+009N/m ²
Poisson-Factor	0,33
Density	2710kg/m ³
Thermal expansion	23,6e-006/°C
Elasticity limit	2,4e+008N/m ²

Material	Epoxy
Young-Modulus	3e+009N/m ²
Poisson-Factor	0,37
Density	1300kg/m ³
Thermal expansion	6e-005/°C
Elasticity limit	8,5e+007N/m ²

7.3 Modal Frequencies

Beam: Constraints: Part is fixed at contact points (blue)
Load: frequency analysis



Modus	Frequency Hz	Tx (%)	Ty (%)	Tz (%)	Rx (%)	Ry (%)	Rz (%)
1	6.5971e+002	0.00	58.82	0.05	31.28	0.00	0.00
2	7.3130e+002	0.00	0.00	59.42	29.96	0.00	0.00
3	1.9037e+003	5.36	0.00	0.00	0.00	7.07	0.19
4	2.2144e+003	0.23	0.00	0.00	0.00	4.53	0.00
5	2.8488e+003	0.04	0.31	0.94	1.93	0.04	0.02
6	3.5599e+003	0.86	10.59	0.35	7.19	0.67	0.71
7	3.6069e+003	64.93	0.13	0.00	0.06	50.82	55.54



11.21	3.
0.00	0.
0.00	0.
71.97	7.

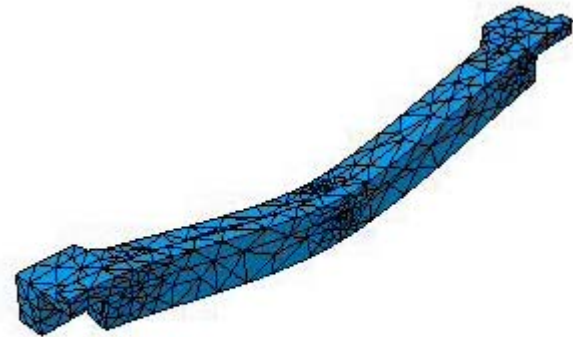


Figure 31: Mode 1 frequency: Figure 30: Mode 2 frequency: 731,302Hz

points (green)

Load: free frequency Analysis

Assembled: Constraints:
Parts are fixed at contact

Modus	Frequency Hz	Tx (%)	Ty (%)	Tz (%)	Rx (%)	Ry (%)	Rz (%)
1	0.0000e+000	1.18	5.58	39.36	42.48	8.45	3.35
2	0.0000e+000	2.56	8.94	13.69	1.89	10.40	62.26
3	0.0000e+000	1.52	38.82	27.86	18.42	0.08	13.98
4	4.9668e-005	0.37	38.70	15.21	17.05	29.88	1.31
5	1.8198e-004	0.01	7.94	3.27	23.11	48.22	16.66
6	3.5324e-004	93.65	0.03	0.46	0.05	2.97	2.44
7	4.5958e+002	0.00	0.00	0.00	0.00	0.00	0.00
8	5.9007e+002	0.00	0.00	0.00	0.00	0.00	0.00
9	6.2335e+002	0.00	0.00	0.00	0.00	0.00	0.00
10	6.2499e+002	0.00	0.00	0.00	0.00	0.00	0.00
	Total	100.00	100.00	100.00	100.00	100.00	100.00

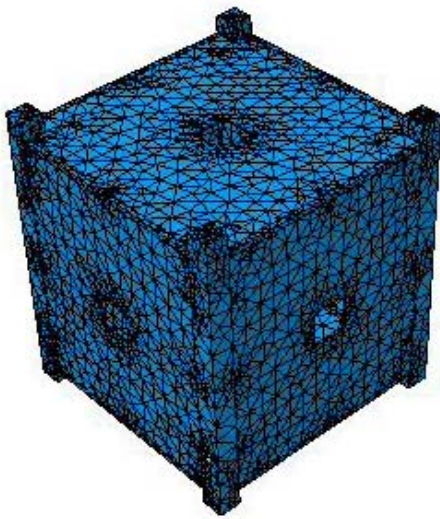


Figure 32: Mode 7 frequency: 459.576Hz; in this mode the inside parts (Mainboards and Subsystem boards) are in resonance

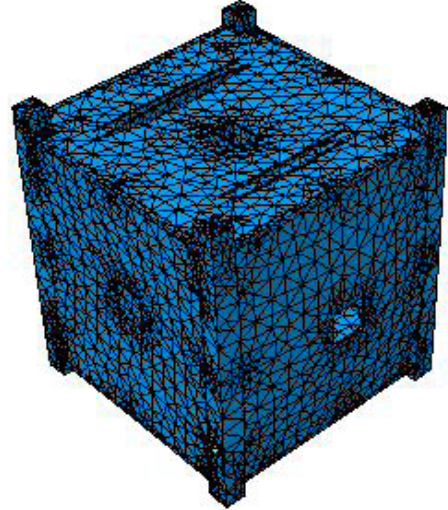


Figure 33: Mode 8 frequency: 590.068Hz; in this mode the side panels are in resonance

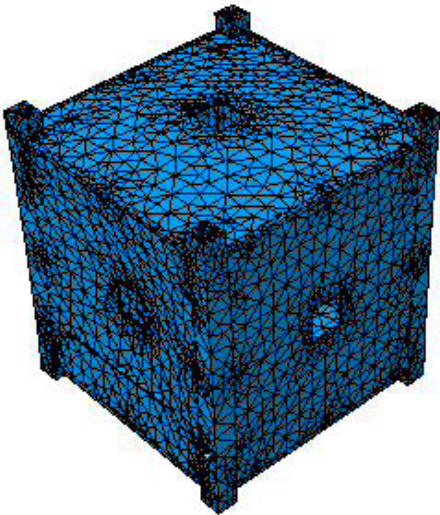


Figure 35: Mode 9 frequency: 623.352Hz; In this mode the side panels are in resonance

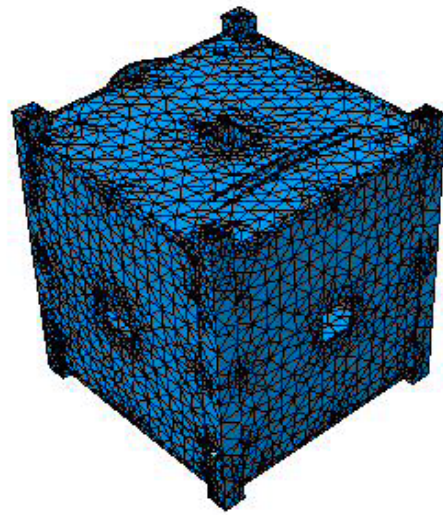


Figure 34: Mode 10 frequency: 624.986Hz; in this mode, the PCB holders are in resonance

Static

Panel:

D

Component	Applied Loads	Reaction	Left over	Relativ Error importance
F_x (N)	-3.0997e+000	3.0997e+000	8.2339e-012	2.0549e-011
F_y (N)	0.0000e+000	-3.0578e-013	-3.0578e-013	7.6315e-013
F_z (N)	0.0000e+000	2.4525e-013	2.4525e-013	6.1207e-013
M_x (Nxm)	0.0000e+000	8.3948e-015	8.3948e-015	4.1902e-013
M_y (Nxm)	-5.0042e-003	5.0042e-003	1.6346e-014	8.1591e-013
M_z (Nxm)	-6.6599e-006	6.6599e-006	-2.3545e-014	1.1752e-012

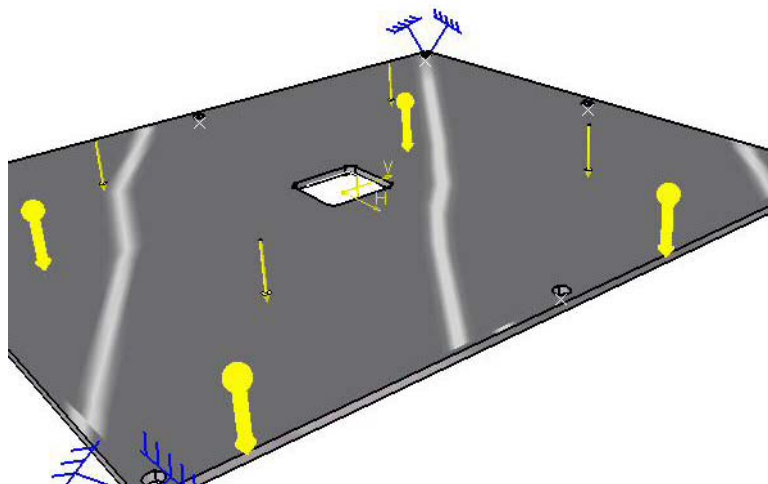
Due to similarity of geometry, constraints, only one panel was analyzed. The highest stresses and deformation occur when panel was simulated with loads in normal direction to the plate which is the worst case

Constraints: Panel is fixed on 4 edges

Load: Constant acceleration: -98.1 m/s^2 (10g) normal to the plate
(Represented by yellow arrows)

Solar cells represented by a distributed load of 0.9 N/m^2
(Total Mass of: 0.01Kg under 10 g)

Sun sensor represented by a force resulting of 0.01 kg at 10g acting at panel cut-out.



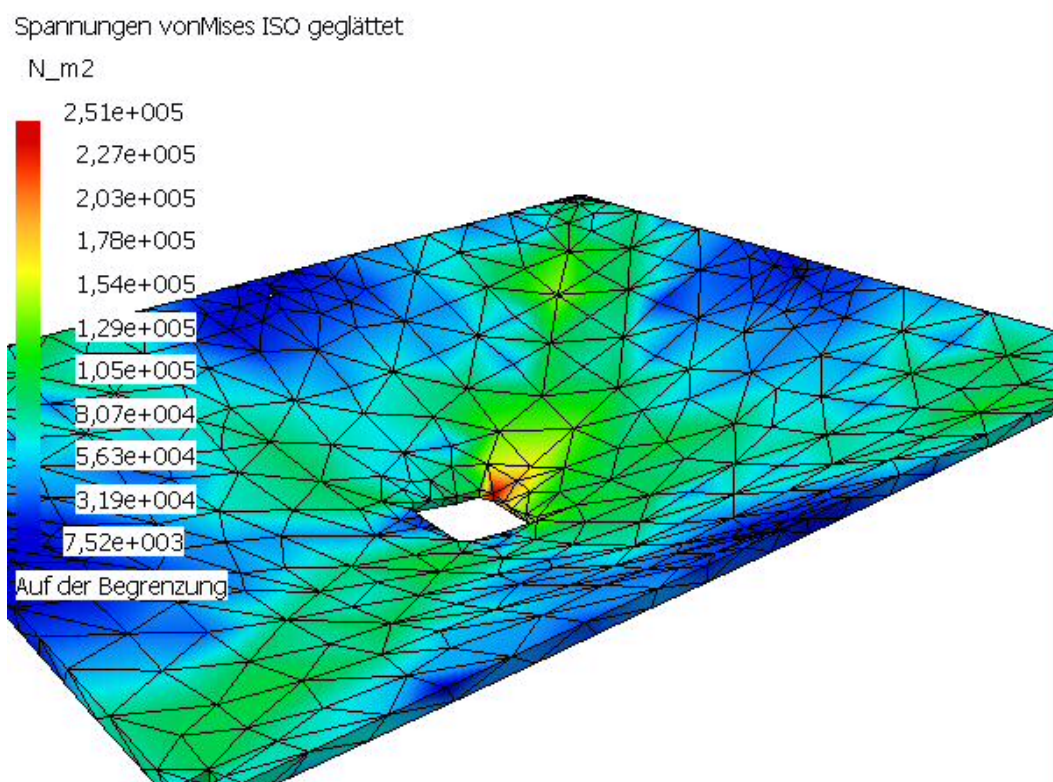


Figure 36: Stress distribution under acceleration loads in the top panel; High stresses appear where the extra load simulating the Sun-sensor was placed. In the final design the Sun sensor will be attached to the side panel with 2 screw-connections and lower stresses will be expected

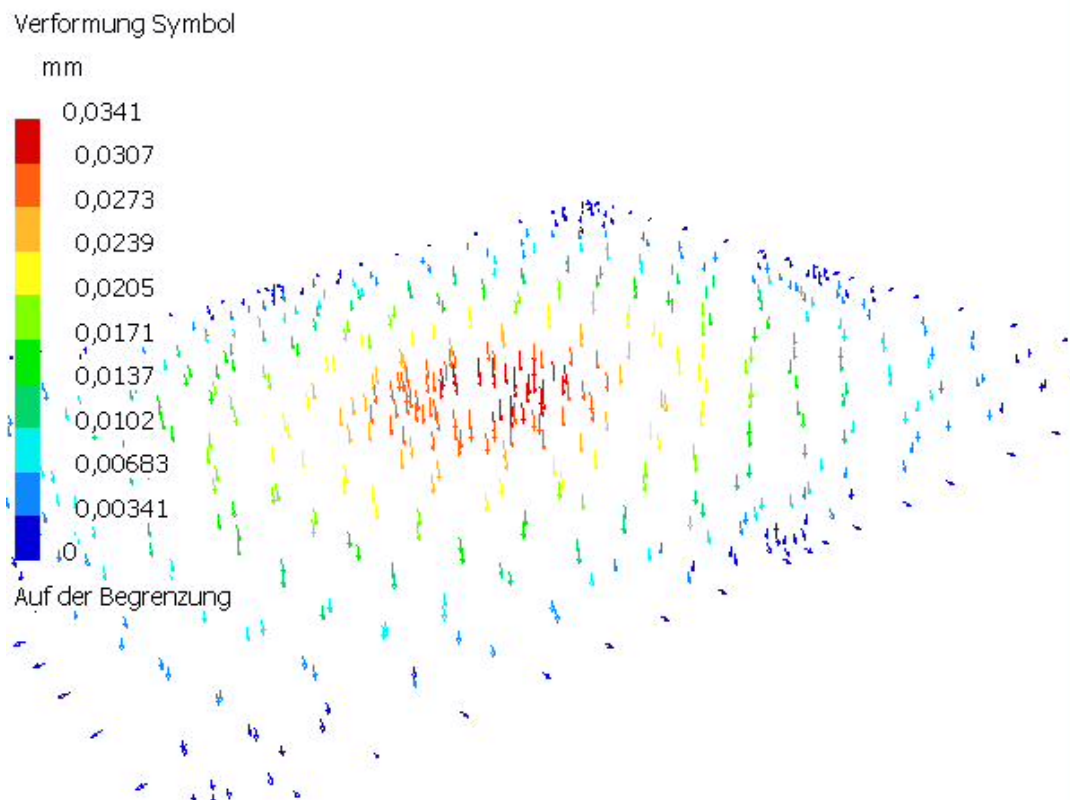
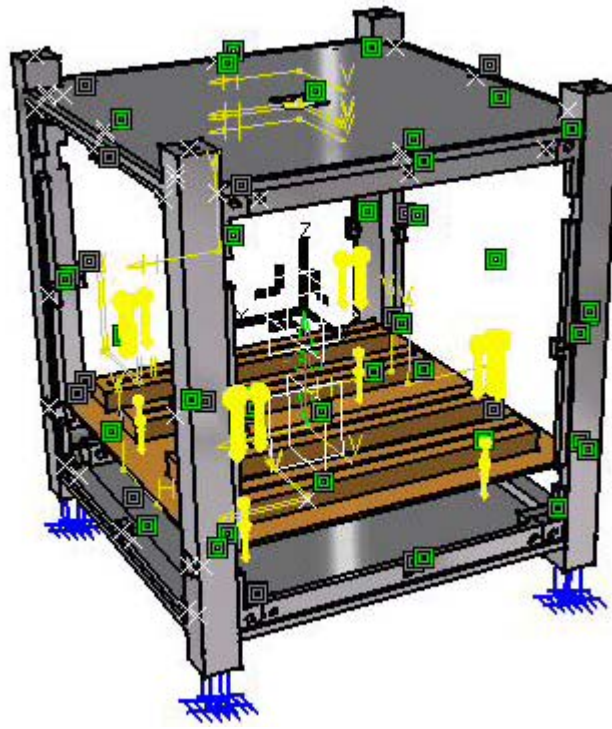


Figure 37: Deformation resulting from acceleration loads on top panel

Assembled

Constrains: fixed on bottom surface of the rails

Load: constant acceleration of -150m/s^2 in Z direction ($>15g$ represented by yellow arrows)



Components	Applied Loads	Reaction	Left over	Relative error importance
Fx (N)	0.0000e+000	-4.0054e-013	-4.0054e-013	2.1646e-013
Fy (N)	0.0000e+000	5.9508e-013	5.9508e-013	3.2159e-013
Fz (N)	-4.1184e+001	4.1184e+001	-8.1002e-013	4.3775e-013
Mx (Nxm)	3.8343e-004	-3.8343e-004	7.7330e-013	7.3317e-012
My (Nxm)	-2.3182e-004	2.3182e-004	-6.2447e-014	5.9206e-013
Mz (Nxm)	0.0000e+000	2.2412e-014	2.2412e-014	2.1249e-013

Spannungen vonMises ISO geglättet

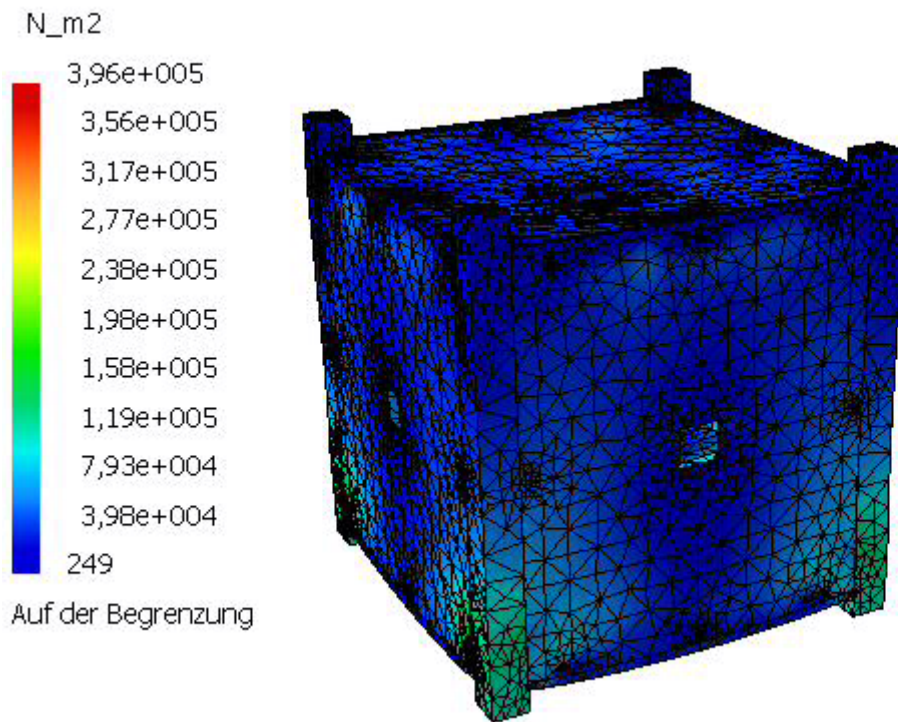


Figure 38: Stresses in the assembly under acceleration loads

Verformung Symbol

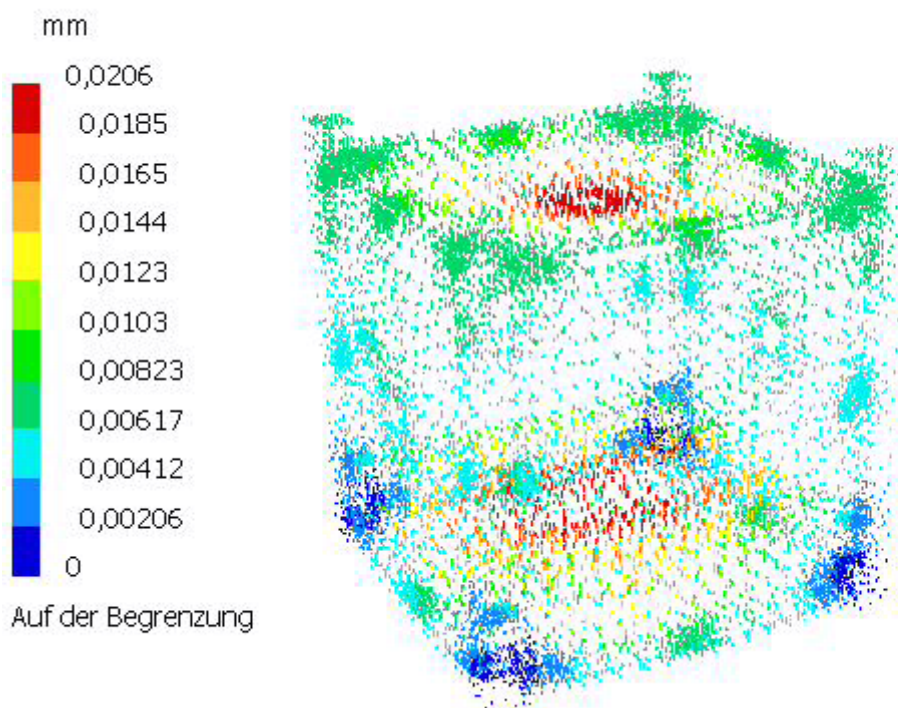


Figure 39: Assembly deformation under acceleration loads

Assembled with additional load:

This scenario simulates the satellite inside of the P-Pod with the load of 2 other CubeSats acting on the structure in the z-direction. This case must be examined if the satellite would be placed 1st in the deployer and the deployer aligned in z-direction during take-off.

Here the additional load was simulated by four additional masses on top of the rails. Two CubeSats having a weight of 2 kg, 0.5 kg are placed on each rail.

Constraints: Fixed on bottom surface of the rails

Loads: constant acceleration of -150m/s^2 in z-direction ($>15\text{g}$ represented by yellow arrows)

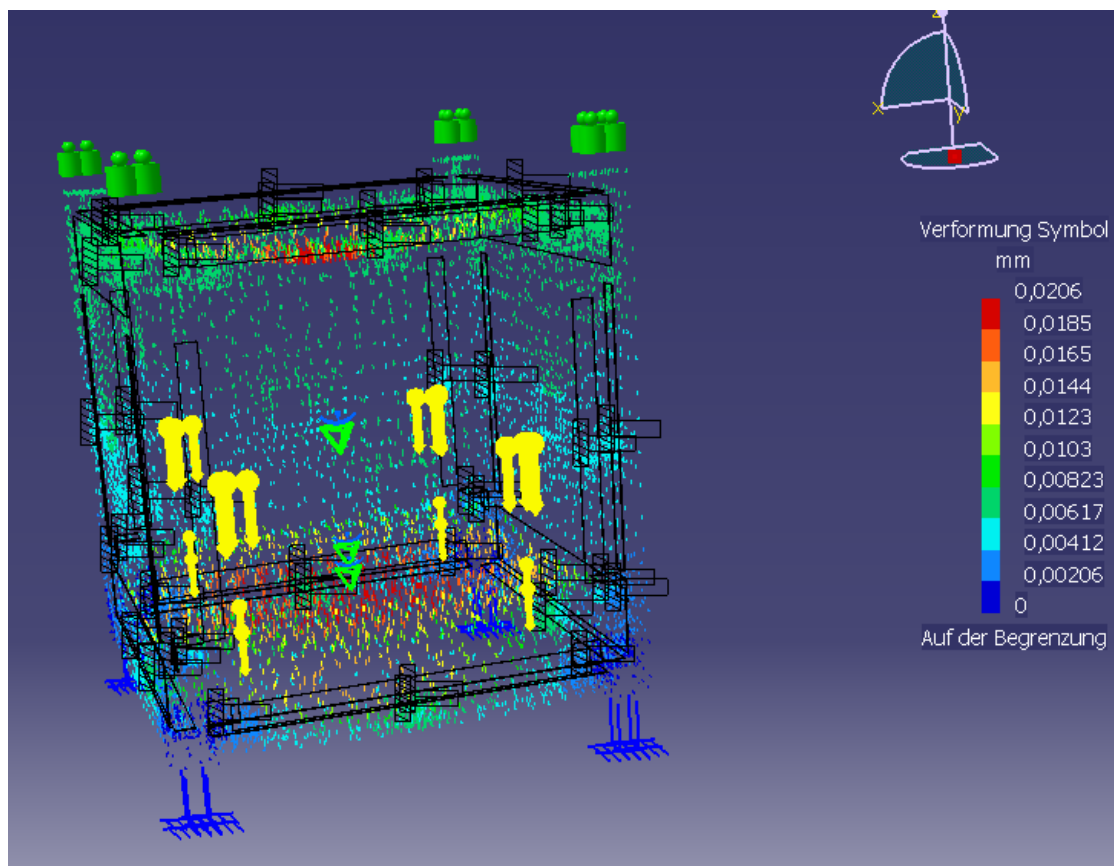


Figure 40: Deformations under acceleration loads plus 2 additional CubeSats

Dynamic Analysis

The first natural frequency of the parts and the assembled structure is much higher than the payload requirements for conventional launchers. The launcher is not contracted at this time the exact natural frequency of the launcher is assumed being roughly in the same range as those.

Example:

Launcher	Axial [Hz]	Lateral [Hz]
Space Shuttle	13	13
Proton	30	15
Scout	18	20

Fundamental Frequencies for Spacecraft Design

Source: Table18-9, page 688. Space Mission analysis and design [1]

In the assembled configuration, the first natural frequency is at 459,576Hz. In this mode mostly the main board and the subsystem boards are in resonance. Additional mass of components on the subsystem boards were not considered at this stage. The true frequency considering the mass of the components will be slightly lower than the from the simulation result. This is assumed according to the theory of dynamics that the natural frequency of a system decreases if the mass increases for constant stiffness.

$$f_{nat} = \frac{1}{2\pi} \sqrt{\frac{k}{m}}$$

The amplitude of the vibration at resonance could not be examined at this stage with the available software but is likely to be in an acceptable range since the satellite is unlikely to be excited at exact resonance frequency or harmonic, and if yes, then only for very brief length of time.

Under constant acceleration the maximum stress ($\leq 2.7 \cdot 10^5 N/m^2$) and the maximum deflection (0.02 mm) are acceptable. The elasticity limit of the structure material is $2.4 \cdot 10^8 N/m^2$. If necessary the structure could be optimized to decrease weight.

This would decrease the stiffness as well as the natural frequency and will therefore not be done at this stage. This option will be considered again after exact frequency determination through tests. The second natural frequency of the assembled configuration corresponds to the resonance of the side panels and is at 590.068Hz. When a side panel is analyzed separately with 4 fixed edges the natural frequency lies at 581.21 Hz. The difference between the two results is because of the slightly different constraints. Similar to the subsystem boards the real natural frequency will be lower when the sun sensor and solar cells will be mounted.

Under constant acceleration the maximum stress and maximum deflection are acceptable and a breaking of the solar cells is unlikely if these are mounted with a ductile adhesive providing bonding but also compensating small deformation of the plate.

The results from the analysis have been compared to the results of the Hausat CubeSat [4] that has a similar structure. The values are similar and can therefore be considered as trustworthy. (Hausat simulation: 900Hz, test: 800Hz)

8. Conclusions

It was discussed the secondary layout of the Compass-1 structure. 6061-T6 aluminum alloy has been selected for the principal structural members. A reference model was established to provide an orientation for other subsystem groups as well. Then the several elements that make up the spacecraft were examined and solutions for their design were presented.

In the analysis section, a computational analysis of the top panel and the complete assembly has been conducted to determine stresses in and deflections of structural members under various static and dynamic load conditions.

9. References

- [24] CubeSat Team Aachen. (2003) *Phase A Study of COMPASS-1*.
www.raumfahrt.fh-aachen.de
- [25] Calpoly and Stanford University. (2003). *CUBESAT Design Specifications Document, Revision VIII*. <http://cubesat.calpoly.edu/>
- [26] Wiley J. Larson and James R. Wertz 1992, *Space Mission Analysis and Design*, Second Edition
- [27] System design review, Subsystem Structure Hausat-1, Hankuk aviation university
- [28] S. Wernick, R. Pinner and P.G. Sheasby, *The Surface Treatment and Finishing of Aluminium and its alloys*, Finishing Publications Ltd., England (1987), ISBN 0-904477-09-6